SYSTEMATIC SYNTHESIS OF HEPTANUCLEAR OSMIUM CLUSTERS

by

Christine Wilcox

B.Sc., Simon Fraser University, 2001

THESIS SUBMITTED IN PARTIAL FULFILLMENT OF
THE REQUIREMENTS FOR THE DEGREE OF

MASTER OF SCIENCE

In the Department
of
Chemistry

SIMON FRASER UNIVERSITY

Spring 2007

APPROVAL

Name:	Christine Wilcox
Degree:	Master of Science
Title of Thesis:	Systematic Synthesis of Heptanuclear Osmium Clusters
Examining Committee:	Dr. George R. Agnes Chair Professor, Department of Chemistry
	Dr. Andrew J. Bennet (Chair) for Dr. Roland K. Pomeroy Senior Supervisor Professor, Department of Chemistry
	Dr. Daniel B. Leznoff Interim Senior Supervisor Associate Professor, Department of Chemistry
	Dr. Byron D. Gates Supervisor Assistant Professor, Department of Chemistry
	Dr. Peter D. Wilson Supervisor Associate Professor, Department of Chemistry
	Dr. Andrew R. Lewis Internal Examiner Adjunct Professor, Department of Chemistry
Date Approved:	December 14, 2006

ABSTRACT

Heptanuclear osmium clusters, $Os_7(CO)_{20}(L)$ (L = $CNBu^t$, PMe_3, PEt_3, $P(OMe)_3$, $P(OCH_2)_3CMe$, PPh_3), have been systematically synthesized by reacting $Os_6(CO)_{18}$ with Me_3NO and $Os(CO)_4(L)$ at -78 °C; as the cone angle of the ligand increased, the yields decreased. Crystal structures of $Os_7(CO)_{20}(L)$ (L = $CNBu^t$, PMe_3, $P(OCH_2)_3CMe$) revealed a monocapped octahedral arrangement of metal atoms, with the ligand attached to the capping osmium group. As the ligand becomes a better π–acceptor, the Os–Os bond *trans* to the ligand shortens, while an increase in the steric properties lengthened the two *cis*–Os–Os bonds.

Carbonyl exchange in the $Os_7(CO)_{20}(L)$ clusters were investigated by variable temperature $^{13}C\{^1H\}$ NMR spectroscopy. Room temperature spectra were consistent with rotation about the individual $Os(CO)_2(L)$ (L = CO, $CNBu^t$, PR_3) units. At low temperatures, collapse of the resonances at different temperatures indicates slowed rotation of the $Os(CO)_3$ groups of the octahedral core, while the capping osmium group continues to exchange rapidly on the NMR timescale.

For my parents, Marie and Don,
for their love, support and encouragement.

ACKNOWLEDGEMENTS

I am grateful to my Senior Supervisor, Dr. R. Pomeroy, for his support and guidance and giving me the opportunity to be part of his research group.

My sincere gratitude is expressed to my interim Senior Supervisor, Dr. D. Leznoff, for everything that he has done for me. I am ever so grateful.

I would like to express my appreciation to the members of my Supervisory Committee, Dr. B. Gates, Dr. J. Clyburne and Dr. P. Wilson for their helpful suggestions and encouragement throughout my studies.

The skilled technical assistance of Dr. A. Lewis (NMR), Dr. M. Morton (NMR), Mrs. M. Tracy (NMR), Dr. D. McGillvary (MS), Mr. P. Ferreira (MS), Dr. G. Yap (X–ray crystallography), Dr. M. Jennings (X–ray crystallography) and Mr. M. Yang (CHN microanalysis) are gratefully acknowledged.

The past and present members of the Pomeroy research group are thanked for their friendship, assistance and the many helpful discussions.

Last but not least, thank you to everyone who encouraged and assist me during the making of this thesis, I could not have done this without you, with special thanks to Ms. E. Voisin, Ms. K. Chapple Cadieux and Dr. N. Merbouh.

"This is Os–some"

Dr. J. Pettigrew

TABLE OF CONTENTS

LIST OF FIGURES

LIST OF TABLES

LIST OF ABBREVIATIONS

Compound **1**	$Os_6(CO)_{18}$
Compound **2**	$Os_7(CO)_{21}$
Compound **3**	$Os_7(CO)_{20}(CNBu^t)$
Compound **4**	$Os_7(CO)_{20}(PMe_3)$
Compound **5**	$Os_7(CO)_{20}(PEt_3)$
Compound **6**	$Os_7(CO)_{20}[P(OMe)_3]$
Compound **7**	$Os_7(CO)_{20}[P(OCH_2)_3CMe]$
Compound **8**	$Os_7(CO)_{20}(PPh_3)$
Compound **9**	$Os_7(\mu\text{–}H)_2(CO)_{19}(PMe_3)$
Compound **10**	$Os_6(CO)_{17}[P(Bu^t)_3]$
Compound **11**	$Os_7(CO)_{20}[P(Bu^t)_3]$
Compound **12**	$Os_7(CO)_{19}(CNBu^t)_2$
Bu	Butyl
Me	Methyl
Et	Ethyl
Ph	Phenyl
η^n	Indicates the connectivity of the ligand to a metal atom. The superscript usually denotes the number of atoms that are bound. Subscript is omitted when all possible ligating atoms are bound to the metal atom.
μ_n	Indicates that the ligand bridges two or more transition metal atoms. The subscript usually denotes the number of metal atoms that are bridged. Subscript is omitted when n is equal to two.
(vw)	Very Weak (infrared peak)

(w)	Weak (infrared peak)
(m)	Medium (infrared peak)
(s)	Strong (infrared peak)
(vs)	Very Strong (infrared peak)
(sh)	Shoulder (infrared peak)
(br)	Broad (infrared peak)
s	Singlet (NMR resonance)
d	Doublet (NMR resonance)
t	Triplet (NMR resonance)
m	Multiplet (NMR resonance)
δ	Chemical Shift (NMR)
PSEPT	Polyhedral Skeletal Electron Pair Theory
SEP	Skeletal Electron Pair (PSEPT)
TEC	Total Electron Count (PSEPT)
C_6F_6	Hexafluorobenzene
Me_3NO	Trimethylamine *N*–oxide
THF	Tetrahydrofuran
P_2O_5	Phosphorus Pentoxide
T	Temperature
P	Pressure
COE	Cyclooctene
PSI	Pounds per Square Inch
CH_3CN	Acetonitrile
IR	Infrared
LSIMS	Liquid Secondary Ions Mass Spectrometry

NMR	Nuclear Magnetic Resonance
ν	Frequency
L	Generalized Ligand (a two electron donating ligand).
PR_3	Tertiary P–donor ligand
π–acceptor	Accepts electron density from a metal atom through empty π–orbitals.
σ–donor	Donates electron density to a metal atom through a filled σ–orbital.

1 INTRODUCTION

1.1 Transition Metal Carbonyl Clusters

Over the past 20 years the field of transition metal carbonyl cluster chemistry has grown such that it is now an important sub–discipline of inorganic chemistry.[1] There has been a large amount of curiosity in metal carbonyl clusters because of their proposed use as homogeneous and heterogeneous catalysts, but extremely few applications exist.[2] Some examples are $Rh_4(CO)_{12}$ (a hydroformylation catalyst) and $Os_3(\mu\text{–}H)_2(CO)_{10}$ (used in the hydrogenation of alkenes).

In addition to being used as catalysts directly, transition metal carbonyl clusters may also be used as models for the processes that are occurring on the surface of heterogeneous bulk metal catalysts.[3] Transition metal carbonyl clusters consist of a variety of structures that can imitate the surfaces of bulk metal catalysts. They also possess ligands (CO, H_2) that are involved in heterogeneous catalytic processes on these surfaces; very little is known about the chemistry of bulk metal catalysts at the molecular level. Heterogeneous bulk metal catalysts are used in the production of various chemicals, for example the production of methanol (CH_3OH) from methane (CH_4) occurs through the use of two heterogeneous bulk metal catalysts.[1] In this instance, methane is first reacted with steam on a nickel catalyst to produce carbon monoxide and hydrogen gas (eq. 1.1).

$$CH_{4\,(g)} + H_2O \xrightarrow[1100K]{\text{Ni catalyst}} CO_{(g)} + 3H_{2\,(g)} \qquad (1.1)$$

The products of this reaction are then reacted with a second (copper) catalyst to produce methanol (eq. 1.2).

$$CO + 2H_2 \xrightarrow[\substack{520\ K \\ 750\ PSI\ of\ pressure}]{\text{Cu catalyst}} CH_3OH \qquad (1.2)$$

Although the chemistry at the molecular level is not entirely understood in heterogeneous catalysis, ligands (CO, H_2) bonded to transition metal carbonyl clusters may allow for insight into the bonding modes of different compounds to the surface sites of heterogeneous catalysis.

Metal clusters, as defined by Shriver and Atkins, are "molecular complexes with metal–metal bonds that form triangular or large closed structures. This definition excludes linear M–M–M compounds."[4] Also excluded from this definition are cage compounds, in which the structures are held together by non–transition metal ligands.

With the exception of ruthenium, osmium forms more carbonyl cluster compounds than any other transition metal. Osmium carbonyl clusters are, however, more stable than the corresponding ruthenium compounds, especially for clusters that have six or more metal atoms.[5] With the recent report of the synthesis of $Os_{12}(CO)_{30}$[6] (eq. 1.3) there are now 14 stable binary carbonyls of osmium known whereas only four are known for ruthenium, of which two ($Ru_2(CO)_9$ and the polymer $[Ru(CO)_4]_n$) are poorly characterized.

$$Os_6(CO)_{16}(\mu_4\text{–}O)(\mu\text{–}OH)_2(\mu\text{–}CO)_2 \xrightarrow{200\ ^\circ C} Os_{12}(CO)_{30} \qquad (1.3)$$

For a systematic study of the chemistry of metal carbonyl clusters, the clusters of osmium are a good place to start. The chemistry of osmium clusters has been critical in advancing the field of organometallic chemistry.[7]

1.1.1 Higher Nuclearity Clusters

Higher nuclearity clusters are defined as having greater than three and less than 12 metal atoms. Higher nuclearity clusters have a bewildering array of structures that current theories cannot fully rationalize (discussed in section 1.1.2). In 1994, 32 different metal skeletons had been reported for M_6 (M = Ru and Os) clusters and 13 different metal skeletons for M_7 (M = Ru and Os) clusters. Furthermore, the methods of synthesis of these compounds are often non–specific. The most common method remains the high temperature pyrolysis[a] of a lower nuclearity cluster to produce a higher nuclearity cluster, usually as a component of a mixture and in low yield.[8] Some recent examples of clusters prepared by pyrolysis are $Os_{12}(CO)_{30}$ (eq. 1.3) [which is a part of a mixture of $Os_4O_4(CO)_{12}$, $Os_5(CO)_{16}$, $Os_6(CO)_{18}$ (**1**), $Os_7(CO)_{21}$ (**2**), and $Os_8(CO)_{23}$] and the Ru_4 cluster $Ru_4(CO)_9(\mu\text{–}CO)\{\mu_4\text{–}\eta^2\text{–}PCH_2CH_2P(C_6H_5)_2\}(\mu_4\text{–}\eta^2\text{–}C_6H_4)$[9] (eq. 1.4) (which is a part of a mixture of four compounds).

$$Ru_3(CO)_{10}(dppe) \xrightarrow{110\ ^\circ C} Ru_4(CO)_9(\mu\text{-}CO)\{\mu_4\text{-}\eta^2\text{-}PCH_2CH_2P(C_6H_5)_2\}(\mu^4\text{-}\eta^2\text{-}C_6H_4) \qquad (1.4)$$

dppe = $(C_6H_5)_2PCH_2CH_2P(C_6H_5)_2$

[a] The use of high temperatures (thermal energy) to break metal–metal and/or metal–ligand bonds and produce new metal–metal bonds.

The beginning of higher nuclearity osmium cluster chemistry can be traced to the report in 1975 by Eady, Johnson and Lewis of the pyrolysis of solid $Os_3(CO)_{12}$ at 210 – 250 °C in a sealed, evacuated Carius tube[b] to yield a host of products with nuclearities ranging from five to eight (eq. 1.5).[10, 11]

$$Os_3(CO)_{12} \xrightarrow{210-250\ ^\circ C} \underset{0-7\%}{Os_5(CO)_{16}} + \underset{0-5\%}{Os_5(\mu_5\text{–}C)(CO)_{15}} + \underset{60-80\%}{Os_6(CO)_{18}} + \underset{10-20\%}{Os_7(CO)_{21}} + \underset{2-5\%}{Os_8(CO)_{23}} + \underset{0-8\%}{Os_8(\mu_6\text{–}C)(CO)_{21}} \quad (1.5)$$

This reaction is unique amongst the metal carbonyls. For example, pyrolysis of $Ru_3(CO)_{12}$ at 150 °C gives the carbido cluster $Ru_6(\mu_6\text{–}C)(CO)_{17}$ (eq. 1.6) with no evidence for any other higher nuclearity binary carbonyl clusters (the only other cluster that was isolated was unreacted $Ru_3(CO)_{12}$).[10, 12]

$$Ru_3(CO)_{12} \xrightarrow{150\ ^\circ C} \underset{(5\%\ \text{yield})}{Ru_6(\mu_6\text{–}C)(CO)_{17}} \quad (1.6)$$

Pyrolysis is still one of the most common methods to synthesize osmium carbonyl clusters,[13, 14] remaining the only known route to $Os_8(CO)_{23}$[10, 11] (shown above in eq. 1.5), $Os_{12}(CO)_{30}$[6] (shown above in eq. 1.3) and the anion[11] $[Os_{20}(CO)_{40}]^{2-}$.

1.1.2 Systematic Synthesis

One of the goals of a cluster chemist is to develop routes to clusters by means of systematic synthesis. Development of systematic synthetic routes

[b] A thick walled glass vessel which is sealed with a Teflon valve.

allows for the desired size and composition of a cluster to be achieved. However, attempts to develop systematic synthetic routes are extremely difficult.

In 1987, the Pomeroy group reported the synthesis of $Os_4(CO)_{15}$ by the addition of $Os(CO)_5$ to $Os_3(CO)_{10}(C_8H_{12})_2$[15] and its conversion to $Os_4(CO)_{16}$[16] and $Os_4(CO)_{14}$[17] (eqs. 1.7 – 1.9).

$$Os_3(CO)_{10}(C_8H_{12})_2 + Os(CO)_5 \longrightarrow Os_4(CO)_{15} + 2C_8H_{12} \qquad (1.7)$$

$$Os_4(CO)_{15} + CO \xrightarrow{0\ ^\circ C} Os_4(CO)_{16} \qquad (1.8)$$

$$Os_4(CO)_{15} \xrightarrow{80\ ^\circ C} Os_4(CO)_{14} + CO \qquad (1.9)$$

In 1992, the preparation of the known $Os_5(CO)_{19}$ cluster by the addition of $Os(CO)_5$ to $Os_4(CO)_{14}$ was also described along with its careful decarbonylation to yield the previously unknown $Os_5(CO)_{18}$ (eq. 1.10).[18]

$$Os_5(CO)_{19} \xrightarrow{50\text{-}55\ ^\circ C} Os_5(CO)_{18} + CO \qquad (1.10)$$

Heating $Os_5(CO)_{18}$ at 70 °C gave $Os_5(CO)_{16}$ (a minor product from the pyrolysis of solid $Os_3(CO)_{12}$, eq. 1.5).[10] The $Os_5(CO)_{18}$ cluster has a raft arrangement of osmium atoms that is not predicted by Polyhedral Skeletal Electron Pair Theory (PSEPT), the most popular theory used to rationalize the structures of clusters of intermediate nuclearity (PSEPT, discussed in Section 1.1.3).[19] By replacing $Os(CO)_5$ with $Os(CO)_4(L)$ (L = PR_3, $CNBu^t$) in the cluster-building reactions $Os_4(CO)_n(L)$ (n = 13, 14, 15) and $Os_5(CO)_n(L)$ (n = 15, 17, 18) clusters were

prepared, specifically and in good yield [it is not clear why $Os_5(CO)_{16}(L)$ clusters cannot be made].[20]

The rational synthesis of clusters with different metal atoms is still more of a challenge than the synthesis of homonuclear clusters.[8, 19, 21, 22] Nevertheless, addition of $Re(CO)_5(H)$ to $Os_4(CO)_{14}$ gives $ReOs_4(\mu\text{–}H)(CO)_{19}$ in good yield (>95%).[23] Mild heating of the product causes decarbonylation to produce $ReOs_4(\mu\text{–}H)(CO)_{18}$ and then $ReOs_4(\mu\text{–}H)(CO)_{16}$.[23] Crystallography reveals that $ReOs_4(\mu\text{–}H)(CO)_{19}$ has a spiked-planar-butterfly and $ReOs_4(\mu\text{–}H)(CO)_{18}$ a spiked-tetrahedral arrangement of osmium atoms. These are different metal skeletons compared to those of $Os_5(CO)_{19}$ (bow tie) and $Os_5(CO)_{18}$ (planar raft; see Figure 1.1), even though they have identical electron counts. The reasons for the different structures are not clear. These differences are what make heteronuclear clusters of interest to cluster chemists.[24]

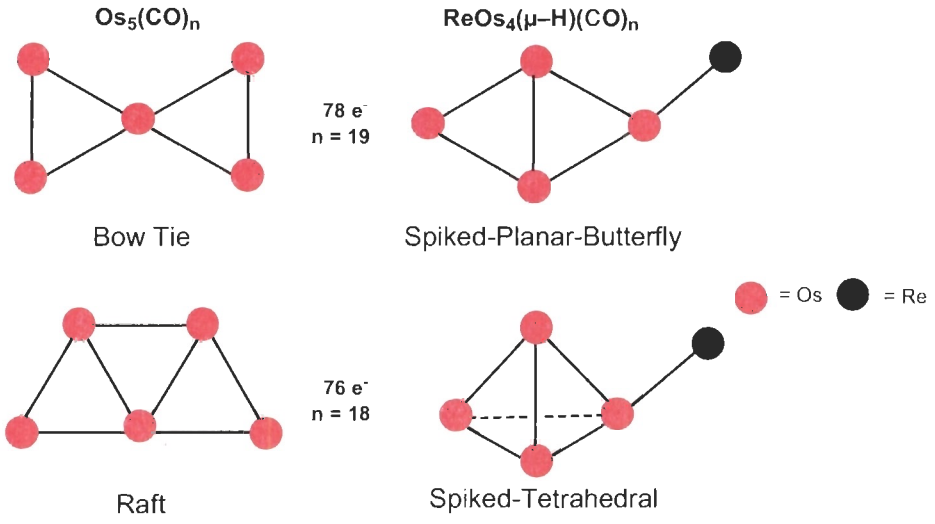

Figure 1.1 Difference in structures of M_5 heteronuclear and homonuclear clusters.

1.1.3 Polyhedral Skeletal Electron Pair Theory (PSEPT)

The hexa-osmium carbonyl cluster $Os_6(CO)_{18}$ (**1**) does not have an octahedral Os_6 metal skeleton as might be expected, but rather a bicapped tetrahedral or capped trigonal bipyramidal arrangement of metal atoms (Figure 1.2)[25], which is consistent with PSEPT.

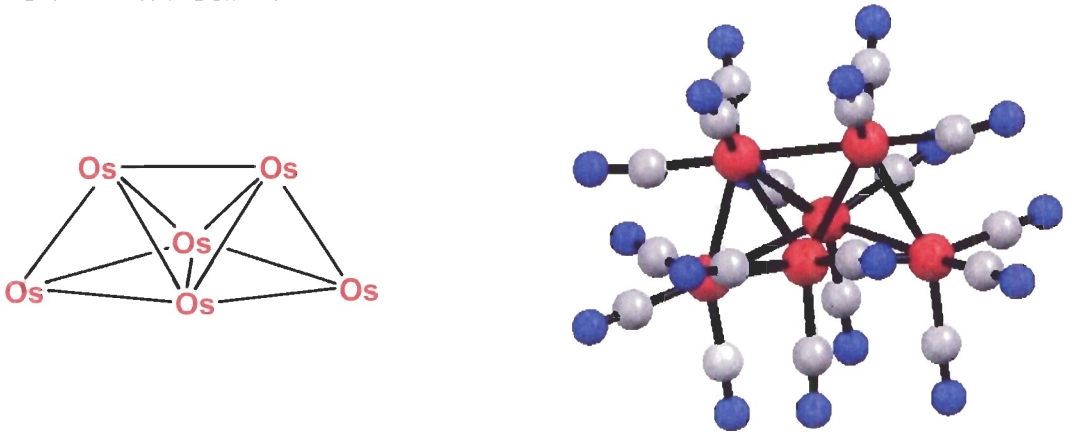

Figure 1.2 The Os_6 core (CO groups omitted) and the molecular structure of $Os_6(CO)_{18}$ (1).

PSEPT (also known as Wade's rules)[19] was initially developed to rationalize the structures of boron–containing clusters. Borane (boron–hydrogen) clusters form an extensive series of clusters that have deltahedron geometries (i.e. polyhedron structures that contain only triangular faces); examples are given in Figure 1.3.[19]

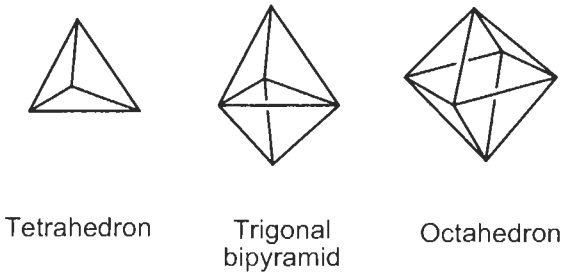

Figure 1.3 Examples of deltahedron geometries (containing four to six vertices).

The following method (i.e. application of Wade's rules) has been successful for rationalizing/predicting the structures of boron clusters.[26]

- Each B–H unit contributes two electrons to the bonding of the cluster
- Each additional H unit contributes one electron to the bonding of the cluster
- Ionic charge of the cluster must be included in the electron count

To determine the number of vertices occupied and therefore the structure, Table 1.1 is used (n = number of vertices occupied by boron and SEP = Skeletal Electron Pairs[c] The vertex removed is usually the vertex of highest connectivity.

Table 1.1 SEP, structure type and structure of boron clusters.

SEP	Structure Type	Structure
n + 1	*closo* (closed)	Polyhedron of n vertices 0 vertices unoccupied
n + 2	*Nido* (nest)	Polyhedron of n + 1 vertices 1 vertex unoccupied
n + 3	*arachno* (cobweb)	Polyhedron of n + 2 vertices 2 vertices unoccupied

[c] The number electrons that are available for skeletal bonding, these electrons are delocalized over the skeletal framework.

An example of how these rules predict the structure boron containing clusters:

$[B_5H_9]$

5 B–H units for a total of	(5x2)	10 electrons
4 H atoms for a total of	(4x1)	4 electrons
Charge		0 electrons
Total Electron Count (TEC)		14 electrons
Skeletal Electron Pairs (TEC/2)		7

n = 5 (vertices) and SEP = 7

(n+2) = 7, therefore the structure type is nido

Since the structure type is nido (having one vertex unoccupied) and n = 5 the structure is an octahedron with one vertex removed.

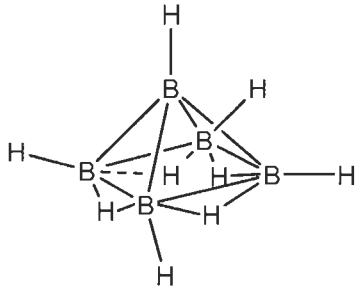

The relationship between boron clusters (closo, nido and arachno) is given in Figure 1.4.

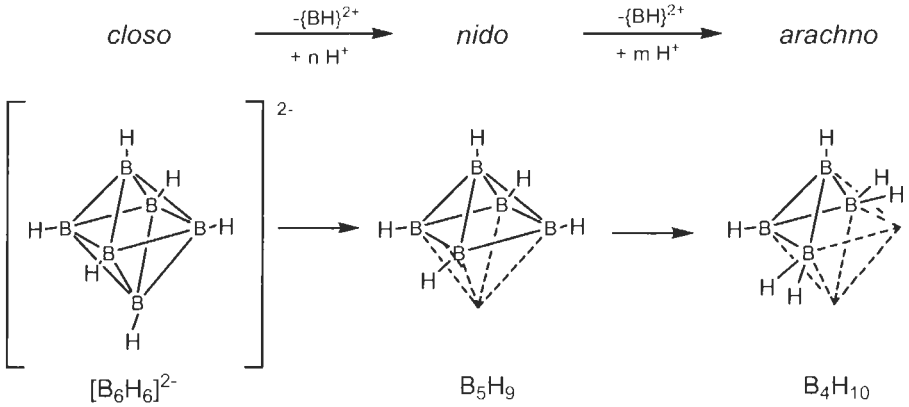

Figure 1.4 Relationship between closo, nido, and arachno boron clusters.

Through the use of the isolobal principle, Wade's rules were extended to rationalize the structures of carboranes and transition metal clusters. Two molecular orbital fragments that have similar symmetry, energy and contain the same number of electrons for cluster bonding are defined as being isolobal. For example B–H, $\{C–H\}^+$ and $M(CO)_3$ fragments (where M = Fe, Ru, Os only) are isolobal (Figure 1.5).[27]

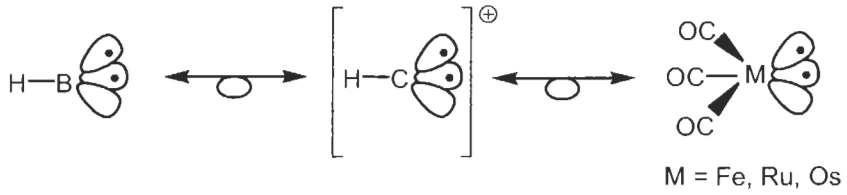

Figure 1.5 Isolobal relationship between B–H, $\{C–H\}^+$, and $M(CO)_3$.

By means of the isolobal relationship, Wade's rules can be extended from boron clusters to Group VIII transition metal (Fe, Ru and Os) clusters. A general formula (eq. 1.11) can be used to calculate the number of skeletal electron pairs (SEP) available for cluster bonding, for transition metal clusters, SEP + 1 electron pairs are required for bonding in a polyhedral of n vertices.[1] (TEC = total electron count, which is equal to the total number of metal valence electrons plus the number of electrons donated by the ligands, and m = the number of metal atoms.)

$$SEP + 1 = (½)[TEC - (12 \times m)] \qquad (1.11)$$

Each metal atom of the cluster has twelve electrons that are not used in cluster bonding. Six of these are used for bonding to the external ligands (i.e. carbonyl ligands) and six are not involved in bonding to the cage or the ligands (i.e. metal–centred d–electrons) for a total of twelve electrons.[28]

One difference between transition metal clusters and main group clusters is the ability of transition metal clusters to form condensed structures, where main group clusters form open structures. Condensed clusters are ones that share at least one face, where open clusters are those fused together by at least one atom or edge. For example, $Os_6(CO)_{18}$ (**1**) (Figure 1.2), appears to be a *closo* structure (trigonal bipyramid) with an additional vertex; this vertex is placed over a triangular face of the parent cluster. The additional vertex is referred to a "capping vertex". PSEPT accommodates these structures through the use of the "capping principle"[19], which states that the addition of one or more capping groups does not require additional bonding electrons. The addition of a capping group increases the total electron count by twelve.

To determine/predict the structure of transition metal clusters, additional rules are needed to those found in Table 1.1. These additional rules accommodate the ability of transition metal clusters to form condensed clusters that are capped (Table 1.2).[26]

Table 1.2 Additional rules for transition metal cluster that contain a capping group.

SEP + 1	Structure Type	Structure
n	*hypercloso*	polyhedron of n - 1 vertices 1 face capped
n – 1	*superhypercloso*	polyhedron of n - 2 vertices 2 faces capped

An example of how the structure of a transition metal cluster is predicted:

$Os_6(CO)_{18}$ (**1**)

TEC = 6 Os + 18 CO = (6x8) + (18x2) = 84

SEP + 1 = (1/2)[84 - 12(6)] = 6 pairs of electrons

Since SEP = 5 the parent cluster is trigonal bipyramid

SEP + 1 = 6 and n = 6, therefore the structure is mono-capped.

Since the parent cluster is a trigonal bipyramid and is capped the structure is a capped trigonal bipyramidal (also known as a bi-capped tetrahedron).

Note that for a trigonal bipyramid, the TEC is 72 and for $Os_6(CO)_{18}$ the TEC is 84. Therefore, 72 + 12 (one capping group) = 84.

The overview presented here is a simplified version; exceptions do exist. What has been found is that PSEPT works well for condensed transition metal clusters with $M(CO)_3$ (M = Fe, Ru, Os) units, but not for more open clusters containing $M(CO)_3(L)$ or $M(CO)_4(L)$ units.[19]

1.1.4 $Os_7(CO)_{21}$ (2) and $Os_7(CO)_{20}[P(OMe)_3]$ (6)

This thesis is concerned with the systematic synthesis of clusters of formula $Os_7(CO)_{20}(L)$ (L = 2–electron donor ligand); it is therefore appropriate to

describe here earlier work on this family of clusters. As shown in Equation 1.5, compound **2** is a minor product formed in the pyrolysis of $Os_3(CO)_{12}$. The yield of compound **2** is low (ranging from 0 – 20%) and is highly dependent on the temperature and dimensions of the Carius tube. Thus, $Os_7(CO)_{21}$ (**2**) is also formed by the action of CO on solid compound **1** (eq. 1.12–1.14).[29] It has been reasoned that under CO pressure compound **1** loses $Os(CO)_5$, forming $Os_5(CO)_{19}$, which under C O pressure forms $Os_2(CO)_9$ and $Os_3(CO)_{12}$. It is believed that compound **2** forms by the condensation of $Os_2(CO)_9$ and $Os_5(CO)_{19}$.

$$\underset{(\mathbf{1})}{Os_6(CO)_{18}} \xrightarrow{+6CO} Os(CO)_5 + Os_5(CO)_{19} \qquad (1.12)$$

$$Os_5(CO)_{19} \xrightarrow{+2CO} Os_3(CO)_{12} + Os_2(CO)_9 \qquad (1.13)$$

$$Os_2(CO)_9 + Os_5(CO)_{19} \xrightarrow{-7CO} \underset{(\mathbf{2})}{Os_7(CO)_{21}} \qquad (1.14)$$

The structure of compound **2** as determined by X–ray crystallography, reveals it to have a capped octahedral Os_7 metal skeleton consistent with PSEPT (Figure 1.6 and 1.7).[1, 30] The cluster has a total of 98 cluster valence electrons (56 electrons from the seven Os atoms and 42 from the 21 CO ligands). Of these, 84 electrons are required to satisfy the bonding requirements of the external ligands and the metal–centred d–electrons on the seven osmium atoms. Leaving 14 electrons or seven skeletal electron pairs (i.e. SEP + 1). The structure is therefore based on an octahedron (SEP = 6), since SEP + 1 and n are both equal to seven (Table 1.2), the structure is a mono-capped octahedron.

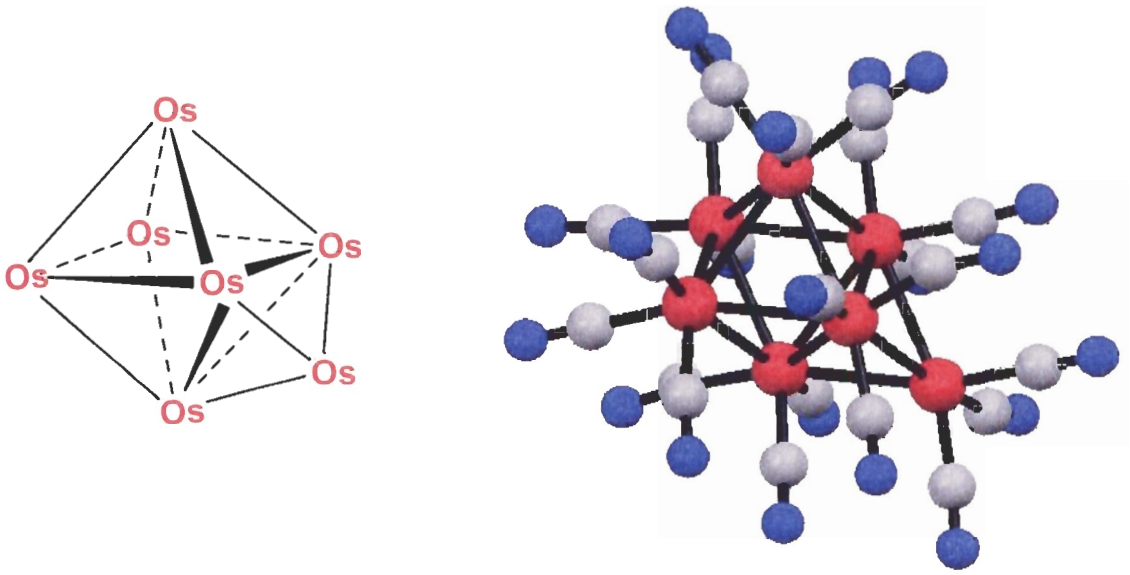

Figure 1.6 The Os_7 core (CO omitted) and the molecular structure of $Os_7(CO)_{21}$[30] (2).

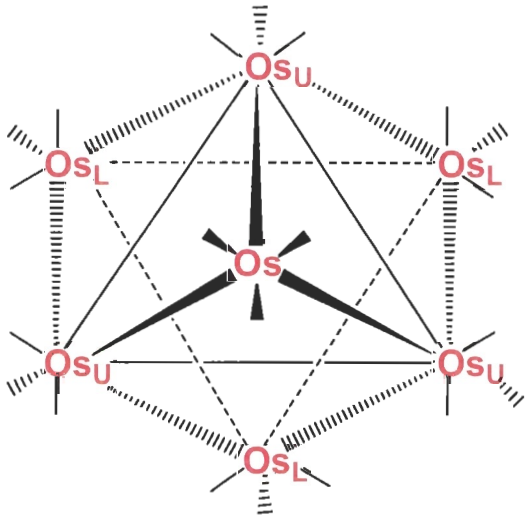

Figure 1.7 View of $Os_7(CO)_{21}$ (2) down the pseudo threefold axis.

The ^{13}C NMR spectrum of compound **2** in solution consists of three singlets in a 3:3:1 ratio from 90 to 0 °C. This is consistent with the view that compound **2** has the same structure in solution. The spectra are also consistent

with the view of rapid carbonyl exchange within the individual $Os(CO)_3$ units, and with no exchange between the other osmium atoms of the cluster. Only at -110 °C do the carbonyl groups associated with the two Os_3 planes show evidence slowed rotation on the NMR timescale. As will become evident in this thesis, a remarkable property of metal carbonyl clusters is the stereochemical nonrigidity (i.e. carbonyl exchange) they often exhibit.[30]

Prior to this work the only derivative of the type $Os_7(CO)_{20}(L)$ reported in the literature was $Os_7(CO)_{20}[P(OMe)_3]$ (**6**), prepared by the reaction of compound **2** with Me_3NO in the presence of MeCN, followed by the addition of $P(OMe)_3$ (eq. 1.15 and 1.16).[31] $Os_7(CO)_{21}$ (**2**) has idealized[d] C_{3v} symmetry and as a consequence of this symmetry, there is only one isomer for $Os_7(CO)_{20}(L)$ where L has replaced a carbonyl ligand of the capping $Os(CO)_3$ unit.

$$Os_7(CO)_{21} + MeCN \xrightarrow{Me_3NO} Os_7(CO)_{20}(MeCN) + CO_2 + NMe_3 \qquad (1.15)$$

$$Os_7(CO)_{20}(MeCN) + P(OMe)_3 \longrightarrow Os_7(CO)_{20}[P(OMe)_3] + MeCN \qquad (1.16)$$

Although $Os_7(CO)_{20}(MeCN)$ was not isolated, it is believed to be the intermediate that allows for the addition of $P(OMe)_3$. (Me_3NO serves as a means to chemically remove a CO ligand as CO_2.)[32] The structure of compound **6** is a capped octahedron as found in compound **2** with one of the carbonyl ligands of the capping $Os(CO)_3$ group replaced by the phosphite ligand (Figure 1.8)[31].

[d] The symmetry of the cluster is best represented by the symmetry group C_{3v}, small bond length and angle inequalities that exist in the structure that cause a deviation from this symmetry group are disregarded.

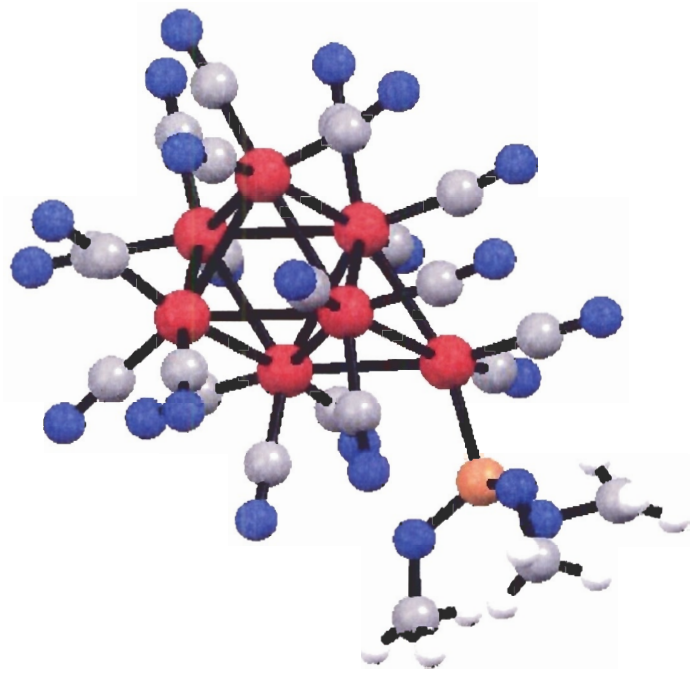

Figure 1.8 Molecular structure of $Os_7(CO)_{20}[P(OMe)_3]$ (6).[31]

1.2 Scope of this Thesis

Prior to the commencement of this project it was found by Hansen and Pomeroy that compound **1** could be conveniently and consistently prepared by heating $Os_3(CO)_{12}$ in the inert solvent C_6F_6 at 200 °C. The reaction takes place in an evacuated sealed Carius tube fitted with a Teflon valve. The progress of the reaction could be monitored by removing a small sample (< 1 mL) from the cooled reaction vessel and checking for the carbonyl stretches of $Os_3(CO)_{12}$ and compound **1** in the infrared spectrum of the sample (metal carbonyl compounds exhibit intense carbonyl stretches in the 1850–2150 cm^{-1} region of the infrared spectrum that are characteristic of a given compound). In this way, conversion of $Os_3(CO)_{12}$ to compound **1** could be brought about under relatively mild conditions

and gave the product in 40–60% yields (versus reported but irreproducible yields of 60–80%)[10, 11]. Only compound **1** is produced by this synthesis, as opposed to the mixture obtained in equation 1.5. Further improvements to the synthesis are described in this thesis.

Similar to $Os_3(CO)_{12}$, compound **1** does not undergo CO substitution with 2-electron donor ligands (L) under mild conditions unless a CO ligand is chemically removed by a reagent such as Me_3NO. Examples of reactions utilizing thee selective removal of CO are the formation of $Os_3(CO)_{11}(PPh_3)$[33, 34] (eq. 1.17) and $Os_6(CO)_{17}(PPh_3)$[35] (eq. 1.18).

$$Os_3(CO)_{12} + PPh_3 \xrightarrow[25\ ^\circ C]{Me_3NO} Os_3(CO)_{11}(PPh_3) + CO_2 + NMe_3 \qquad (1.17)$$

$$Os_6(CO)_{18} + PPh_3 \xrightarrow[-\ 78\ ^\circ C]{Me_3NO} Os_6(CO)_{17}(PPh_3) + CO_2 + NMe_3 \qquad (1.18)$$

Previous studies in the Pomeroy laboratory had shown that $Os(CO)_4(L)$ (L = $CNBu^t$, PR_3) complexes are able to act as 2-electron donor ligands in much the same way as PR_3 ligands. For example, $M(CO)_5(THF)$ (M = Cr, Mo, W) readily react with PR_3 to give $M(CO)_5(PR_3)$ complexes (eq. 1.19 and eq. 1.20).

$$M(CO)_6 + THF \xrightarrow{h\nu} M(CO)_5(THF) + CO \qquad (1.19)$$

$h\nu$ = irradiated with UV light

$$M(CO)_5(THF) + PR_3 \longrightarrow M(CO)_5(PR_3) + THF \qquad (1.20)$$

M = Cr, Mo, W

Likewise, treatment of $M(CO)_5(THF)$ with $Os(CO)_4(L)$ yields $(L)(OC)_4OsM(CO)_5$, isolated as air stable crystalline solids (eq. 1.21)[36]. (The iron and ruthenium analogues of the $(L)(OC)_4OsM(CO)_5$ complexes cannot be prepared.[36])

$$M(CO)_5(THF) + Os(CO)_4PR_3 \longrightarrow (R_3P)(CO)_4OsM(CO)_5 \qquad (1.21)$$

M = Cr, Mo, W

It was also known that $Os(CO)_4(PMe_3)$ will displace CH_3CN from $Os_3(CO)_{11}(CH_3CN)$ to yield $(Me_3P)(OC)_4OsOs_3(CO)_{11}$ (eq. 1.22),[37] which on mild heating produces $Os_4(CO)_{14}(PMe_3)$ and then $Os_4(CO)_{13}(PMe_3)$.

$$Os_3(CO)_{11}(CH_3CN) + Os(CO)_4(PMe_3) \xrightarrow{25\ ^\circ C} (Me3P)(OC)_4OsOs_3(CO)_{11} + CH_3CN \qquad (1.22)$$

Although most transition metal clusters contain metal–metal bonds that are non–dative covalent bonds, the metal–metal bonds found in the complexes describe in equations 1.21 and 1.22 are dative bonds (dative bonds are bonds in which one atom donates both electrons to the bond).

The object of the work described in this thesis was to show that this protocol could be extended to the systematic synthesis of $Os_7(CO)_{21-x}(L)$ clusters by the method shown in equations 1.21 and 1.22. Accordingly, the reaction of compound **1** with various $Os(CO)_4(L)$ compounds was targeted, the results of which form the bulk of this thesis.

2 Synthesis and Characterization of $Os_7(CO)_{20}(CNBu^t)$, $Os_7(CO)_{20}PR_3$ [R = PMe_3, PEt_3, $P(OMe)_3$, $P(OCH_2)_3CMe_3$, PPh_3] and $Os_7(\mu\text{-}H)_2(CO)_{20}(PMe_3)$[e]

2.1 Introduction

Structural studies of metal carbonyl clusters that contain the same number of metal atoms and are of the same electron count have been a significant aspect of cluster chemistry.[8, 19, 22] The replacement of carbonyl ligands by other two–electron donor ligands (such as phosphine (PR_3), phosphite [$P(OR)_3$] ligands and isocyanide (CNR) ligands) has been extensively used in metal carbonyl cluster chemistry.[39] PR_3 and CNR ligands are known to be stronger σ–donors and weaker π–acceptors, in comparison to CO.[40] With a wide variety of R–groups available, the steric and electronic properties of PR_3 and CNR ligands can be easily manipulated, thereby affecting the coordination of the PR_3 and CNR ligands to the metal cluster. It is known that slight changes in composition such as the number of carbonyl ligands, the presence of hydride(s) and non–carbonyl ligands will create changes in the properties (i.e. structure, bond lengths, carbonyl infrared stretching frequencies and reactivity) of the metal clusters.[7]

As discussed in Chapter 1, $Os_6(CO)_{18}$ (**1**) undergoes CO substitution by 2-electron donor ligands (L = PR_3 and CNR) under mild conditions when a carbonyl

[e] The $Os_7(CO)_{20}(CNBu^t)$ work in this chapter was reproduced with permission. Reference 38. Wilcox, C.T.; Jennings, M.C.; Pomeroy, R.K. *J. Cluster Sci.*, **2004**, *15*, 107. Copyright 2004 with kind permission of Springer Science and Business Media.

group is chemically removed by a reagent such as Me_3NO (eq. 1.18).[35, 41] In this thesis, similar methodology was used, but the ligand was replaced with $Os(CO)_4(L)$ (L = PR_3 and $CNBu^t$) to prepare heptanuclear osmium clusters. Their properties are described in this chapter. The $Os_7(CO)_{20}L$ clusters were systematically synthesized from compound **1** and $Os(CO)_4L$ and not directly from $Os_7(CO)_{21}$ (**2**) because there is no straightforward synthesis of compound **2** that is reliable. The only known synthesis of compound **2** is the solid state pyrolysis of $Os_3(CO)_{12}$ (eq. 1.5), but the reaction is sensitive to conditions (i.e. reaction vessel size, amount of water and air present in the reaction vessel size) and the yield varies from 0–20%. On the other hand, compound **1** can be reliably produced from $Os_3(CO)_{12}$ (discussed below, eq. 2.6) in yields of 65–70%.

There is only one report of an $Os_7(CO)_{20}(L)$ cluster in the literature. $Os_7(CO)_{20}[P(OMe)_3]$ (**6**) was prepared via the reaction of compound **2** with Me_3NO in the presence of MeCN, producing $Os_7(CO)_{20}(MeCN)$, this is then reacted this with $P(OMe)_3$ (eq. 1.15 and 1.16).[31] Only the structure of compound **6** was reported; no analytical or spectroscopic data was given. The structure of compound **6** is a capped octahedron with one of the carbonyl ligands of the capping $Os(CO)_3$ grouping replaced by the phosphite ligand (Figure 2.1).

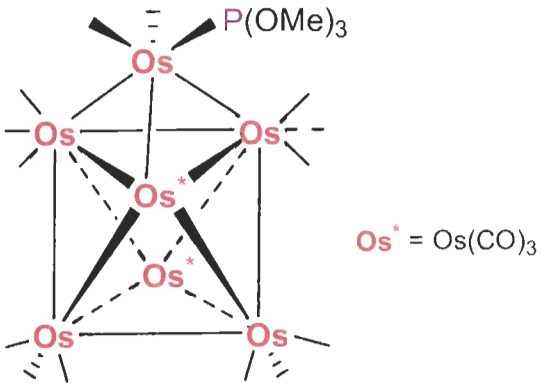

Figure 2.1 Structure of $Os_7(CO)_{20}[P(OMe)_3]$ (6).

Thus, in this chapter the synthesis and characterization of $Os_7(CO)_{20}(L)$ (L = $CNBu^t$, PMe_3, PEt_3. $P(OMe)_3$, $P(OCH_2)_3CMe$) and $Os_7(\mu\text{–}H)_2(CO)_{19}(PMe_3)$ (**9**) are described, along with the attempted preparations of $Os_7(CO)_{20}(L)$ [L = PPh_3 and $P(Bu^t)_3$].

2.2 Synthesis of Starting Materials

2.2.1 $Os_3(CO)_{12}$ and $Os(CO)_5$

All known preparations of $Os_6(CO)_{18}$ (**1**), including the synthesis presented in this thesis, use $Os_3(CO)_{12}$ as the starting compound. $Os_3(CO)_{12}$ can be readily synthesized by two different methods, which are summarized in equations 2.1 and 2.2.

$$4OsO_4 + 17CO \xrightarrow[\text{hexanes}]{P,T} Os_3(CO)_{12} + Os(CO)_5 + O_2 \qquad (2.1)$$

P = 1200 PSI of CO pressure, T = 180 °C
P = 2500 PSI of CO pressure, T = 300 °C

$$3OsO_4 + 12CO \xrightarrow[\text{methanol}]{P,T} Os_3(CO)_{12} + O_2 \qquad (2.2)$$

P = 1200 psi of CO pressure, T = 160 °C

The reactions presented in equation 2.1 are carried out in hexanes and also produce $Os(CO)_5$.[42, 43] Due to the volatility of $Os(CO)_5$, it can be easily separated from $Os_3(CO)_{12}$ by vacuum transfer. These methods can produce $Os(CO)_5$ in yields of up to 60%. On the other hand, when the reaction is carried in methanol, $Os_3(CO)_{12}$ is synthesized in 100% yield.[43]

2.2.2 $Os_6(CO)_{18}$ (1)

As mentioned in Chapter 1, $Os_6(CO)_{18}$ (**1**) was originally prepared from the pyrolysis of $Os_3(CO)_{12}$ in the solid state (eq. 1.5).[10, 11] As can be seen from equation 1.5, compound **1** is not the only product; also produced in the pyrolysis are $Os_5(CO)_{16}$, $Os_5C(CO)_{15}$, $Os_7(CO)_{21}$ (**2**), $Os_8(CO)_{23}$, $Os_8C(CO)_{21}$, $[Os_{10}C(CO)_{24}]^{2-}$ and $[Os_{11}C(CO)_{27}]^{2-}$. The solid state pyrolysis of $Os_3(CO)_{12}$ is extremely sensitive to reaction conditions (i.e. reaction vessel size, amount of water and air present in the reaction vessel size), with yields of the clusters varying with the conditions employed. Because of their similar solubility, the separation and purification of the neutral clusters is extremely tedious. Originally, fractional crystallization that took several weeks to complete was used to isolate each of the clusters in equation 1.5.[10, 11] The only other preparation of compound **1** found in the literature also begins with $Os_3(CO)_{12}$ and requires two reaction steps to give compound **1** (eq. 2.3 and 2.4), with an

overall yield of 57%.[44] Although this method proceeds in relatively good yield, it was found by this author to be quite problematic and difficult to reproduce.

$$2Os_3(CO)_{12} + 2Na \xrightarrow[162\ ^\circ C]{\text{diglyme}} [Os_6(CO)_{18}]^{2-} + 6CO + 2Na^+ \qquad (2.3)$$

$$[Os_6(CO)_{18}]^{2-} \xrightarrow{FeCl_3} Os_6(CO)_{18} \qquad (2.4)$$

It is preferred to carry out the pyrolysis of transition metal carbonyl clusters in solution, as this gives the advantages of better temperature control and increased diffusion of reagents.[45] Pyrolysis in solution can, however, yield different products than those from the solid state pyrolysis.[5] It is also a challenge to find a solvent in which to perform the pyrolysis.[46] At the high temperatures involved, aromatic hydrocarbon solvents have been shown to act as ligands and replace some of the carbonyl groups in the metal complex.[47] On the other hand, alcohols, ketones and aldehydes have been shown to act as a source of hydrogen atoms that add to the cluster to form transition metal hydride clusters.[47] In a similar manner, pyrolysis in chlorinated solvents has given chlorinated transition metal clusters.[48]

Hanson and Pomeroy discovered that performing the pyrolysis of $Os_3(CO)_{12}$ in hexafluorobenzene (C_6F_6) at a slightly lower temperature (200 °C) than used in the solid–state pyrolysis (eq. 1.5) produces $Os_6(CO)_{18}$ (**1**) as the only identifiable product (eq. 2.5).[f]

$$2Os_3(CO)_{12} \xrightarrow[C_6F_6]{200\ ^\circ C} Os_6(CO)_{18} + 6CO \qquad (2.5)$$

[f] Unpublished result from the Pomeroy Laboratory.

Hexafluorobenzene is a suitable solvent for the pyrolysis as it is completely inert towards $Os_3(CO)_{12}$ under the reaction conditions employed. It is believed that the electron withdrawing properties of fluorine prevent C_6F_6 from acting as a ligand towards $Os_3(CO)_{12}$. Furthermore, the C–F bonds are quite strong; the dissociation energy of a C–F bond is 485 kJ mol^{-1} compared to 413 kJ mol^{-1} for a C–H bond and 327 kJ mol^{-1} for a C–Cl bond.[40] As a result the C–F bonds do not react with $Os_3(CO)_{12}$ at the temperatures employed. It has also been shown that $Os_6(CO)_{18}$ (**1**) is stable in C_6F_6 at 210 °C.[48]

In the original Hanson/Pomeroy preparation, the pyrolysis of $Os_3(CO)_{12}$ (500 mg) in C_6F_6 (50 mL) was carried out in an evacuated Carius tube over a period of about 7 days at a temperature of 200 °C, produced the brown $Os_6(CO)_{18}$ (**1**) in yields varying from 40–60%. A black insoluble material was also formed in the reaction, the nature of which is unknown, but it is not pure osmium metal (the material is believed to be osmium carbide).[48] Although this method reliably produces compound **1** from $Os_3(CO)_{12}$ there was some opportunity for refinement. It was found during the course of this project that the addition of a small amount (~10 mg) of phosphorus pentoxide (P_2O_5) to the reaction solution, doubling the reaction vessel size (from ~1.5 L to ~3 L) and decreasing the reaction temperature from 200 °C to ~180 °C produced $Os_6(CO)_{18}$ in a yield of between 65–70% (eq. 2.6) (using the same quantity of $Os_3(CO)_{12}$ and volume of solvent as mentioned before).

$$2Os_3(CO)_{12} \xrightarrow[C_6F_6]{183\ ^\circ C/P_2O_5} Os_6(CO)_{18} + 6CO \qquad (2.6)$$

It is believed that P_2O_5 removes any traces of water that may have not been removed in the drying of the starting materials and solvent [when water is present in the Carius tube a second cluster is formed, $Os_4(O)_4(CO)_{12}$, rather than $Os_6(CO)_{18}$]. The only drawback to the preparation is an increase in the reaction time, from 7 to 14 days (by infrared monitoring, at 7 days only half of the starting material has been converted). $Os_6(CO)_{18}$ (**1**) is obtained by simple filtration of the solution to give samples that are pure by infrared spectroscopy.

Although the preparation presented in this thesis (eq. 2.6) has only a slight improvement in yield (compared to literature preparations), it is the convenience factor that is greatly increased. Filtration is the only purification method required for a pure sample of compound **1**. The preparation presented here is much more convenient than those found in the literature.[10, 11, 44] This preparation reliably produces $Os_6(CO)_{18}$ (**1**) and has conditions that are less forcing than the conditions found in literature preparations (eq. 1.5, 2.3, 2.4 and 2.5).

2.2.3 $Os(CO)_4(L)$ [L = $CNBu^t$, PMe_3, PEt_3, $P(OMe)_3$, $P(OCH_2)_3CMe$, PPh_3 and $P(Bu^t)_3$] derivatives

The compounds $Os(CO)_4(L)$ used in the synthesis of the $Os_7(CO)_{20}(L)$ clusters were all prepared from the reaction of $Os(CO)_5$ with the appropriate ligand L. The compounds were synthesized by three different methods, which are summarized in equations 2.7, 2.8 and 2.9.

$$Os(CO)_5 + L \xrightarrow{P,\ T} Os(CO)_4(L) + CO \qquad (2.7)$$

L = $CNBu^t$: T = 80°C, P = 600 PSI of CO;
L = $P(OMe)_3$: T = 105°C, P = 500 PSI of CO;
L = PPh_3: T = 110°C, P = 400 PSI of CO;
L = PMe_3: T = 120°C, P = 600 PSI of CO .

$$Os(CO)_5 + L \xrightarrow{h\nu} Os(CO)_4(L) + CO \qquad (2.8)$$

L = $P(Bu^t)_3$ and PPh_3
$h\nu$ = irradiated with UV light

$$Os(CO)_5 + L \xrightarrow{Me_3NO} Os(CO)_4(L) + CO \qquad (2.9)$$

L = PEt_3 and $P(OCH_2)_3CMe$

All of the $Os(CO)_4(L)$ compound have been previously reported in the literature and were prepared by the respective methods presented in equations 2.7[49-52] and 2.8[42]. The reactions presented in equations 2.7 and 2.8 were carried out under CO pressure to prevent the formation of Os_3 clusters [$Os(CO)_4(L)$ compounds readily form Os_3 clusters when heated in the absence of CO]. The $Os(CO)_4(L)$ [L = PEt_3 and $P(OCH_2)_3CMe$] compounds prepared by the method presented in equation 2.9 have been previously prepared in the literature by the conditions used for L = PMe_3 in equation 2.7.[50] The reaction indicated in equation 2.9, is believed to be the first preparation of an $Os(CO)_4(L)$ compound by the removal of a carbonyl ligand chemically from $Os(CO)_5$. The $Os(CO)_4(L)$ [L = PEt_3 and $P(OCH_2)_3CMe$] compounds prepared by the method presented in equation 2.9 were isolated in yields [L = PEt_3 (41%) and L = $P(OCH_2)_3CMe$ (57%)] similar to the yields for the methods presented in equations 2.7 and 2.8

(40–60%).[49-52] All of the $Os(CO)_4(L)$ compounds were isolated as pale yellow solids.

Compounds of the type $Os(CO)_4(L)$ have been previously shown to have a trigonal-bipyramidal structure with L in an axial site (insert in Figure 2.2).[50, 53, 54] These compounds have C_{3v} symmetry and are expected to have three carbonyl stretches in the infrared spectra. As can be seen in Figure 2.2 and Table 2.1 the $Os(CO)_4(L)$ compounds exhibit a distinctive pattern of three carbonyl stretches in the infrared spectrum, the exception being the $Os(CO)_4[P(OMe)_3]$ and $Os(CO)_4[P(OCH_2)_3CMe]$ complexes, which exhibit additional carbonyl stretches in the infrared spectrum. It is believed that the lack of three-fold symmetry of the $P(OMe)_3$ ligand causes the lowest energy band to be split. The one up, two down arrangement of the OMe groups causes the symmetry to be reduced from C_{3v} to C_s, therefore four carbonyl stretches are seen in the infrared spectra.[55] The additional peaks in $Os(CO)_4[P(OCH_2)_3CMe]$ complex are due to the presence of a second isomer in solution.[50] The second isomer is believed to be the trigonal bipyramidal form with the ligand attached in an equatorial site rather than an axial site. The equatorial form of $Os(CO)_4(L)$ is expected to have four carbonyl stretches in the infrared spectra (because of C_{2v} symmetry); only two are visible in the spectrum due to their weak signal intensities.

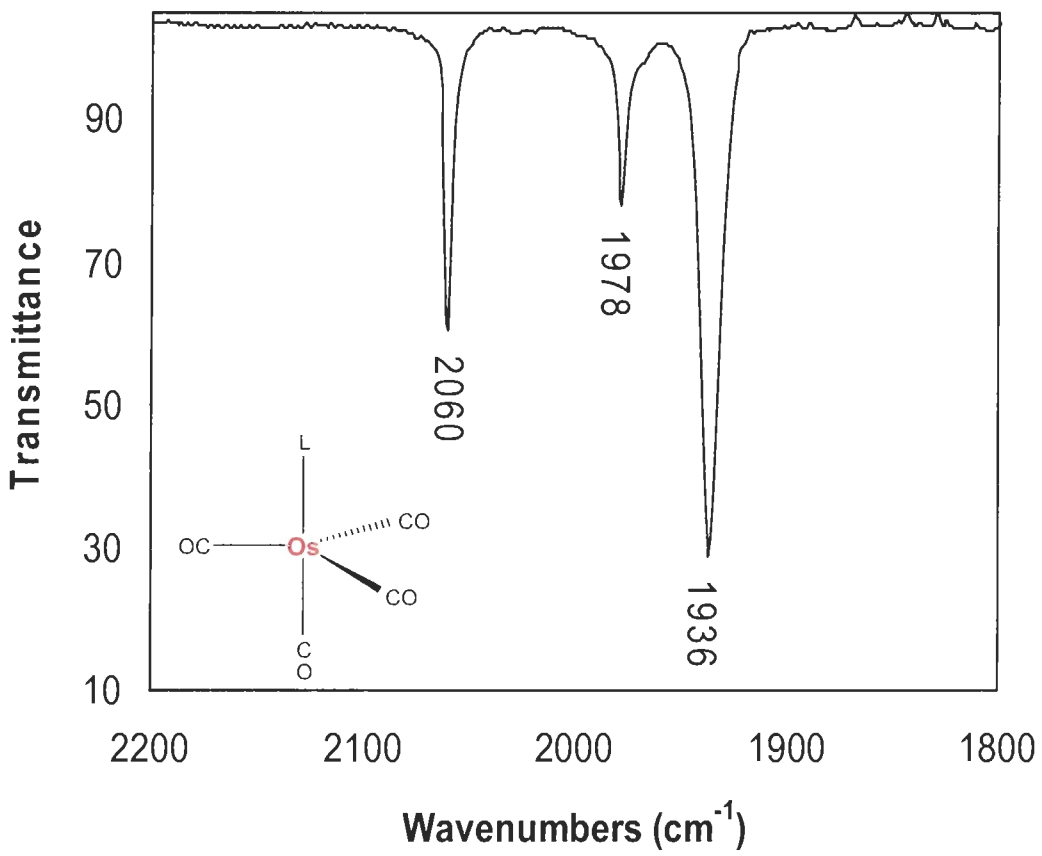

Figure 2.2 Typical pattern seen in the carbonyl stretching region of the infrared spectrum [$Os(CO)_4(PEt_3)$ solution in hexanes] and the structure of $Os(CO)_4(L)$ compounds.

Table 2.1 Infrared data for $Os(CO)_4(L)$ Compounds .

Compound	ν(CO),[g] cm^{-1}
$Os(CO)_5$	2035 (vs), 1993(vs)
$Os(CO)_4[P(Bu^t)_3]$	2058 (s), 1970 (m), 1926 (vs)
$Os(CO)_4(PEt_3)$	2060 (s), 1978 (m), 1936 (vs)
$Os(CO)_4(PMe_3)$	2062 (s), 1980 (m), 1939 (vs)
$Os(CO)_4(PPh_3)$	2061 (s), 1982 (m), 1945 (vs)
$Os(CO)_4[P(OMe)_3]$	2071 (s), 1995(m), 1961 (vs), 1948(vs)
$Os(CO)_4(CNBu^t)$[h]	2061 (s), 1996 (m), 1960 (vs)
$Os(CO)_4[P(OCH_2)_3CMe]$	2093 (vw)[i], 2076 (s), 2009 (w)[i], 2001 (m), 1968 (vs)

The carbonyl stretching frequencies have been previously assigned to their respective vibrational modes.[53] Based on the lowest energy A_1 carbonyl-stretching frequency (Figure 2.3) of the axial isomer[53] (these stretching frequency are highlighted in blue in Table 2.1), the donor/acceptor properties and order of the ligands was determined to be:

$$CO > P(OCH_2)_3CMe > CNBu^t \approx P(OMe)_3 > PPh_3 > PMe_3 > PEt_3 > P(t\text{–}Bu)_3$$

Strong π–acceptor
Weak σ–donor

Weak π–acceptor
Strong σ–donor

[g] All spectra recorded in hexanes.
[h] ν(CN) 2190 (m–w, broad) cm^{-1}.
[i] Due to the equatorial isomer of $Os(CO)_4(L)$.

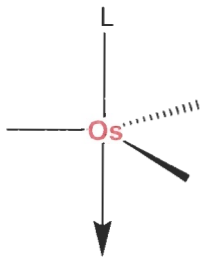

Figure 2.3 The A_1 carbonyl stretching frequency of the axial isomer of the $Os(CO)_4(L)$ compounds.[53]

The donor/acceptor properties of the ligands were based on the lowest energy A_1 carbonyl-stretching frequency[i] because this vibrational mode corresponds to the carbonyl ligand that is *trans* to the ligand. In theory, the donor/acceptor properties of the ligand should have the greatest influence on the carbonyl ligand that it is *trans* to.[53] For example, PMe_3 is a strong σ–donor and poor π–acceptor (when compared to CO), therefore it donates more electron density to the metal centre. With the increase in electron density, there is an increase in the π–back bonding to the carbonyl groups, especially the carbonyl ligand that is *trans* to the ligand. This increase in π–back bonding causes there to be more electron density in the anti–bonding orbitals of the carbonyl ligands, therefore the stretching frequencies shift to a lower wavenumbers. Based on the lowest energy A_1 carbonyl stretching frequency of the axial isomer (Table 2.1), it can be seen that $CNBu^t$ is as strong of π–acceptor ligand as $P(OMe)_3$.

[i] $Os(CO)_5$ does not have a corresponding A_1 carbonyl stretching frequency, nevertheless it is known that CO is a stronger π–acceptor and a weaker σ–donor in comparison to PR_3 and CNR ligands; this can be seen in the lowest carbonyl stretching frequency (i.e. the very strong peak in the infrared spectra).[40]

2.3 Synthesis of $Os_7(CO)_{20}(L)$ Clusters.

2.3.1 General overview of the synthesis of $Os_7(CO)_{20}(L)$ clusters.

The displacement of weakly coordinated substituents such as acetonitrile (CH_3CN) and cyclooctene (COE) by donor ligands has been extensively used in the synthesis of substituted osmium clusters.[15, 48, 56] $[Os_6(CO)_{18-n}(L)_n]$ (n = 1 or 2) clusters were originally prepared by the displacement of acetonitrile (CH_3CN) from $[Os_6(CO)_{18-n}(CH_3CN)_n]$ by donor ligands (eq. 2.10).[35, 57, 58]

$$Os_6(CO)_{18-n}(CH_3CN)_n + n\ PR_3 \longrightarrow Os_6(CO)_{18-n}(PR_3)_n + CH_3CN \qquad (2.10)$$

Using similar methodology, attempts to displace CH_3CN and COE bound to appropriate Os_6 clusters [i.e. $Os_6(CO)_{17}(CH_3CN)$ and $Os_6(CO)_{17}(COE)$] by $Os(CO)_4(L)$ were not successful (eq. 2.11).

$$Os_6(CO)_{17}(CH_3CN) + Os(CO)_4(L) \longrightarrow \text{No Reaction} \qquad (2.11)$$

Even upon heating to 50 °C, $Os(CO)_4(L)$ was not able to displace either CH_3CN or COE from the Os_6 cluster [the reaction could not be performed at higher temperatures due to the decomposition of $Os(CO)_4(L)$]. Although CH_3CN and COE are weakly coordinated to the Os_6 cluster, $Os(CO)_4(L)$ is not a strong enough nucleophile to displace them. Due to this result, chemical labilization of CO using trimethylamine *N*–oxide was attempted, successfully.

Thus, the targeted $Os_7(CO)_{20}(L)$ (L = $CNBu^t$ and PR_3) clusters were all prepared by the reaction of $Os_6(CO)_{18}$ (**1**) with trimethylamine *N*–oxide (Me_3NO)

in the presence of an excess of $Os(CO)_4(L)$ at -78 °C (eq. 2.12) [an excess of $Os(CO)_4(L)$ was used to increase the likelihood of a reaction between $Os_6(CO)_{17}(NMe_3)$ and $Os(CO)_4(L)$]. It was found that performing the reaction at -78 °C resulted in an increase in the yields (1-2%) of the $Os_7(CO)_{20}(L)$ cluster.

$$Os_6(CO)_{18} + Os(CO)_4(L) \xrightarrow[-78\ ^\circ C]{Me_3NO} Os_7(CO)_{20}(L) + CO_2 + NMe_3 + CO \quad (2.12)$$

L = $CNBu^t$, PMe_3, PEt_3, PPh_3, $P(OMe)_3$, $P(OCH_2)_3CMe$

After chromatography and recrystallization the $Os_7(CO)_{20}(L)$ clusters were isolated as red/orange crystals in yields of 8–29%. With the exception of the $Os_7(CO)_{20}(PEt_3)$ (**5**) derivative, the crystals are air stable. The major product in all cases appeared to be the brown salt $[Os_6(H)(CO)_{17}][N(CH_2)Me_2]$ (apparent by a strong band at 2016 cm^{-1} in the IR spectrum).[35] The salt is a known product of the reaction of $Os_6(CO)_{18}$ (**1**) with Me_3NO (eq 2.13 and 2.14).[58]

$$Os_6(CO)_{18} + 2Me_3NO \longrightarrow Os_6(CO)_{16}(NMe_3) + NMe_3 + 2CO_2 \quad (2.13)$$

$$Os_6(CO)_{16}(NMe_3) + CO \longrightarrow [N(CH_2)Me_2][Os_6(H)(CO)_{17}] \quad (2.14)$$

The salt is believed to form when the NMe_3 ligand undergoes C–H activation and β–elimination of a hydrogen atom onto the Os_6 cluster.

Attempts to circumvent this problem by the use of pyridine *N*–oxide, quinuclidine *N*–oxide, and iodosylbenzene in the synthesis of the $Os_7(CO)_{20}(L)$ derivatives were unsuccessful. Iodosylbenzene (PhIO) was found to react with $Os(CO)_4(L)$ and not compound **1** (eq. 2.15).

$$Os_6(CO)_{18} + Os(CO)_4(L) \xrightarrow[\text{room Temp.}]{PhIO} Os_6(CO)_{18} + 4CO + Os + L \qquad (2.15)$$

After the addition of iodosylbenzene, an infrared spectrum of the reaction solution revealed only the carbonyl peaks of $Os_6(CO)_{18}$ (**1**). It appears as though iodosylbenzene reacts with $Os(CO)_4(L)$, causing its decomposition to osmium metal, carbon monoxide and free ligand. Iodosylbenzene may not react with compound **1** because of the reaction conditions used; different conditions may be required for a reaction to occur between iodosylbenzene and compound **1**.

On the other hand, the reactions with pyridine *N*–oxide and quinuclidine *N*–oxide both gave $Os_6(CO)_{17}(L)$, not $Os_7(CO)_{20}(L)$ as the product (eq. 2.16 and 2.17). Both pyridine *N*–oxide and quinuclidine *N*–oxide react with $Os(CO)_4(L)$, causing its decomposition to osmium metal, carbon monoxide and free ligand, as observed with iodosylbenzene.

$$Os_6(CO)_{18} + Os(CO)_4(L) \xrightarrow[+40\ ^\circ C]{\text{Pyridine } N\text{-oxide}} Os_6(CO)_{17}(L) + 5CO + Os \qquad (2.16)$$

$$Os_6(CO)_{18} + Os(CO)_4(L) \xrightarrow[-78\ ^\circ C]{\text{Quinuclidine } N\text{-oxide}} Os_6(CO)_{17}(L) + 5CO + Os \qquad (2.17)$$

The conditions employed (eqs. 2.16 and 2.17) were appropriate for a reaction to occur between compound **1** and both pyridine *N*–oxide and quinuclidine *N*–oxide. With the decomposition of $Os(CO)_4(L)$, PR_3 and $CNBu^t$ would be free in solution. Since PR_3 and $CNBu^t$ are better ligands than $Os(CO)_4(L)$, $Os_6(CO)_{17}(L)$ would be the product instead of $Os_7(CO)_{20}(L)$.

Even the successful reactions with Me_3NO also result in the formation of trace amounts of $Os_6(CO)_{17}(L)$. There is no way to determine whether $Os_6(CO)_{17}(L)$ in this case forms from the decomposition of $Os(CO)_4(L)$ (discussed above) or the migration of the PR_3 or $CNBu^t$ from the $Os(CO)_4(L)$ ligand to Os_6.

For L = PPh_3, unexpectedly, the major product in the preparation of $Os_7(CO)_{20}(PPh_3)$ (**8**) was the brown compound $Os_6(CO)_{17}(PPh_3)$ (eq. 2.18).

$$2Os_6(CO)_{18} + Os(CO)_4(PPh_3) \xrightarrow{Me_3NO} \underset{\text{Major product}}{Os_6(CO)_{17}(PPh_3)} + \underset{\text{Minor product}}{Os_7(CO)_{20}(PPh_3)}\ (\mathbf{8}) \qquad (2.18)$$

A possible explanation as to why compound **8** is formed in anomalously low yield is that there seems to be a limit to the cone angle of the PR_3 ligand that can be attached to the $Os(CO)_2(L)$ unit of the $Os_7(CO)_{20}(L)$ cluster. PPh_3 has a fairly large cone angle (145°), therefore the steric hindrance of the $Os(CO)_4(L)$ ligand may hamper the reaction.[59] When the $Os(CO)_4(PPh_3)$ attaches to the Os_6 cluster, instead of the $Os(CO)_4(PPh_3)$ ligand attaching to the Os_6 complex and the cluster rearranging to form compound **8**, the PPh_3 migrates from the $Os(CO)_4(PPh_3)$ ligand to the Os_6 complex producing $Os_6(CO)_{17}(PPh_3)$. The migration of P–donor ligands is rare in osmium cluster chemistry, but has been previously observed.[36, 48, 60] Thus, given that compound **8** is isolated in only a very low yield (8%), the cone angle limit for this reaction appears to be ~ 145°.

The concept that there is a limit to the size of the cone angle of the PR_3 group that can be attached to the $Os(CO)_4(L)$ ligand became more apparent with the attempt to isolate $Os_7(CO)_{20}[P(Bu^t)_3]$ (**10**). $P(Bu^t)_3$ is a stronger σ–donor and

a weaker π–acceptor in comparison to CO, therefore $Os(CO)_4[P(Bu^t)_3]$ should be a strong donor ligand and should react with the unsaturated Os_6 cluster. However, no Os_7 cluster was formed for $Os_7(CO)_{20}[P(Bu^t)_3]$ (**10**). Unlike the attempted preparation of compound **8**, where the major product was $Os_6(CO)_{17}(PPh_3)$, the only product in this reaction was the brown salt $[Os_6(H)(CO)_{17}][N(CH_2)Me_2]$ (eq. 2.19).

$$Os_6(CO)_{18} + Os(CO)_4[P(Bu^t)_3] \xrightarrow[-78\ ^\circ C]{Me_3NO} [N(CH_2)Me_2][Os_6(H)(CO)_{17}] \qquad (2.19)$$

Some explanation, as to why $Os_6(CO)_{17}[P(Bu^t)_3]$ was not isolated in equation 2.19, may come from the attempted preparation of $Os_6(CO)_{17}[P(Bu^t)_3]$ (**11**). cluster by the reaction of $Os_6(CO)_{18}$ (**1**) and $P(Bu^t)_3$ (eq 2.20) was also unsuccessful.

$$Os_6(CO)_{18} + P(Bu^t)_3 \xrightarrow[-78\ ^\circ C]{Me_3NO} [N(CH_2)Me_2][Os_6(H)(CO)_{17}] \qquad (2.20)$$

Since $P(Bu^t)_3$ is a strong σ–donor, the large steric hindrance of $P(Bu^t)_3$ appears to prevent these reactions. Specifically, $P(Bu^t)_3$ has an extremely large cone angle of 182°, which is larger than the apparent cone angle limit of ~145°, supporting the assumption there is a cone angle limit for the target reaction.[59]

Comparing the yields of the $Os_7(CO)_{20}(L)$ clusters, there is a correlation between the size of the ligand and the yield. The correlation is particularly noticeable for the $Os_7(CO)_{20}(PR_3)$ clusters: as the PR_3 cone angle increases, the yield decreases (Table 2.2).

Table 2.2 Comparison of the ligand size and yields (%) of the $Os_7(CO)_{20}(L)$ clusters.

Cluster	Cone Angle (°)[59]	Yield (%)
$Os_7(CO)_{20}(CNBu^t)$ (**3**)	—	29
$Os_7(CO)_{20}[P(OCH_2)_3CMe]$ (**7**)	101	25
$Os_7(CO)_{20}[P(OMe)_3]$ (**6**)	107	21
$Os_7(CO)_{20}(PMe_3)$ (**4**)	118	17
$Os_7(CO)_{20}(PEt_3)$ (**5**)	132	12
$Os_7(CO)_{20}(PPh_3)$ (**8**)	145	8
$Os_7(CO)_{20}[P(Bu^t)_3]$ (**14**)	182	0

The $Os(CO)_4(CNBu^t)$ ligand generates the highest yield of the clusters; the $Os(CO)_4(CNBu^t)$ ligand has the smallest amount of steric interactions (with the carbonyl groups of the neighbouring osmium atoms) because of the rod–like structure of $CNBu^t$.[61] It has been previously found that, when reacting with unhindered molecules, such as $Cr(CO)_5(THF)$, $Os(CO)_4(CNBu^t)$ is a superior ligand in comparison to $Os(CO)_4(PMe_3)$.[52] As for the PR_3 ligands, with an increased cone angle there is an increase in the steric interactions of the $Os(CO)_4(PR_3)$ ligand with the carbonyl groups of the neighbouring osmium atoms, which appears to inhibit the formation of the $Os_7(CO)_{20}(PR_3)$ cluster.

The steric effects of the ligand also holds true for reactions with the $Os(CO)_3(CNBu^t)_2$. As seen above, the highest yield of the $Os_7(CO)_{20}(L)$ clusters was obtained with one rodlike ligand $CNBu^t$ [i.e. $Os(CO)_4(CNBu^t)$], but using two

of these ligands [i.e. $Os(CO)_3(CNBu^t)_2$] failed to produce $Os_7(CO)_{19}(CNBu^t)_2$ (**12**). The only product of the reaction of compound **1** with Me_3NO in the presence of $Os(CO)_3(CNBu^t)_2$ was the brown salt $[Os_6(H)(CO)_{17}][N(CH_2)Me_2]$ (eq. 2.21).

$$Os_6(CO)_{18} + Os(CO)_3(CNBu^t)_2 \xrightarrow[-78\ ^\circ C]{Me_3NO} [N(CH_2)Me_2][Os_6(H)(CO)_{17}] \qquad (2.21)$$

$Os(CO)_3(CNBu^t)_2$ is a strong donor ligand when reacted with unhindered molecules[52], therefore the failure to produce $Os_7(CO)_{19}(CNBu^t)_2$ (**12**) can be attributed to the steric effects of $Os(CO)_3(CNBu^t)_2$.

As mentioned in Chapter 1, the only known synthesis of $Os_7(CO)_{21}$ (**2**) is the solid state pyrolysis of $Os_3(CO)_{12}$ (eq 1.5), the outcome of which is sensitive to reaction conditions.[10] It was anticipated that compound **2** could be isolated in a greater than 20% yield via the reaction in equation 2.12, where L = CO [i.e. $Os(CO)_5$]. Unfortunately, the major product of the reaction was the brown salt $[Os_6(H)(CO)_{17}][N(CH_2)Me_2]$; compound **2** was only isolated in trace amounts (eq. 2.22).

$$Os_6(CO)_{18} + Os(CO)_5 \xrightarrow[-78\ ^\circ C]{Me_3NO} \underset{\text{Major Product}}{[N(CH_2)Me_2][Os_6(H)(CO)_{17}]} + \underset{\text{Trace amounts}}{Os_7(CO)_{21}} \qquad (2.22)$$

Since the steric hindrance of $Os(CO)_5$ would be negligible, $Os(CO)_5$ must not be a strong enough donor ligand; undeniably, it is the most electron–deficient of the $Os(CO)_4(L)$ compounds studied here (ν_{CO} = 1993 cm^{-1}, based on the lowest carbonyl stretching frequency, as discussed earlier). Therefore, the correlation between yield and size of the ligand attached to $Os(CO)_4(L)$ does not

hold true for L = CO, as the electronic requirements eventually trump the steric profile.

An unexpected second compound was produced in the preparations of $Os_7(CO)_{20}(PR_3)$ [L = PMe_3, $P(OMe)_3$ and PEt_3]. Chromatography of the PMe_3 system, resulted in the isolation of an orange and a red compound. The orange compound was identified as the desired product $Os_7(CO)_{20}(PMe_3)$ (**4**), while the red compound was identified as $Os_7(\mu\text{-}H)_2(CO)_{19}(PMe_3)$ (**9**) (see structure discussion in Section 2.4.5). The exact mechanism for the formation of compound **9** is not known, but one theory may come from the formation of the salt $[Os_6(H)(CO)_{17}][N(CH_2)Me_2]$ (as described above). It may be that more than one Me_3NO reacts with $Os_6(CO)_{18}$ (**1**), thus allowing for the possibility that two NMe_3 ligands attach to the cluster and undergo C–H activation. With this double β–elimination, two hydrogen atoms would thereby be placed onto the cluster. Upon attack by a third equivalent of Me_3NO, the NMe_3 would be displaced by a $Os(CO)_4(PMe_3)$ ligand, forming compound **9**.

2.3.2 Spectroscopic properties of the $Os_7(CO)_{20}(L)$ clusters.

All of the $Os_7(CO)_{20}(L)$ clusters were studied by various spectroscopic techniques. Among the techniques used were Liquid Secondary Ion Mass Spectroscopy (LSIMS), CHN microanalysis, infrared, ^1H NMR, $^{31}P\{^1H\}$ NMR (where the ligand contained a phosphorus atom) and $^{13}C\{^1H\}$ NMR spectroscopy. The $Os_7(CO)_{20}(L)$ clusters gave parent ions peaks, using Liquid Secondary Ion Mass Spectroscopy (LSIMS) (Table 2.3). An example of an LSIMS spectrum [$Os_7(CO)_{20}(CNBu^t)$ (**3**)] is given in Figure 2.4.

Table 2.3 CHN microanalysis and mass spectral data for $Os_7(CO)_{20}(L)$ (L = $CNBu^t$ and PR_3) derivatives.

Cluster	C% (Calc.)	H% (Calc.)	M^+ (*m/z*)[k]
$Os_7(CO)_{20}(CNBu^t)$ (**3**)	15.42 (15.20) 0.76 (0.71)[l]	0.54 (0.46)	1974.7
$Os_7(CO)_{20}(PMe_3)$ (**4**)	13.93 (14.04)	0.57 (0.46)	1968.4
$Os_7(CO)_{20}(PEt_3)$ (**5**)	15.32 (15.54)	0.72 (0.75)	2010.6
$Os_7(CO)_{20}[P(OMe)_3]$ (**6**)	13.95 (13.70)	0.54 (0.45)	2016.9
$Os_7(CO)_{20}[P(OCH_2)_3CMe]$ (**7**)	14.90 (14.72)	0.68 (0.44)	2039.3
$Os_7(CO)_{20}(PPh_3)$[m] (**8**)	—	—	2154.5

The LSIMS spectrum for compound **3** reveals the parent ion peak at *m/z* 1974.7, which corresponds to the molecular formula $Os_7(CO)_{20}(CNBu^t)$ (**3**). The pattern seen in the mass spectra is a result of the seven naturally occurring isotopes of osmium (^{184}Os, ^{186}Os, ^{187}Os, ^{188}Os, ^{189}Os, ^{190}Os, ^{192}Os). The spectra all show successive loss of ~13 carbonyl groups (loss of approximately 28 mass units per carbonyl). As the mass becomes lower, there is a lower signal to noise ratio and therefore the continued loss of carbonyl groups is not observed.

[k] Parent ion peak (LSIMS)
[l] %N (Calc.)
[m] Insufficient amount of sample to complete analysis.

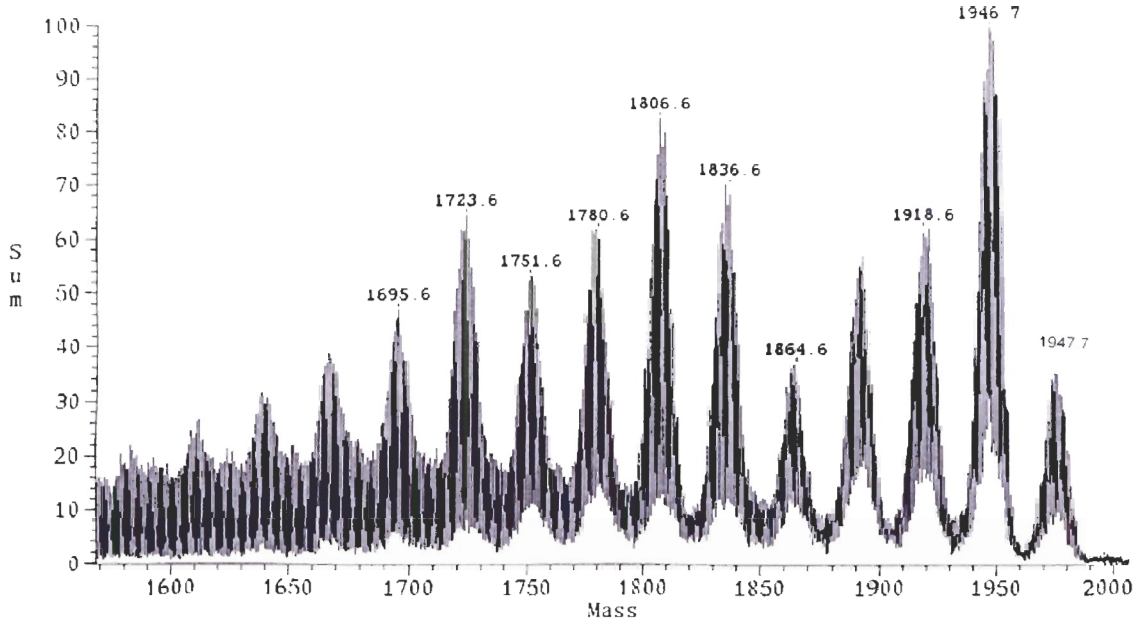

Figure 2.4 Liquid Secondary Ion Mass Spectrum of $Os_7(CO)_{20}(CNBu^t)$ (3).

Also shown in Table 2.3 are data from the CHN microanalysis of the $Os_7(CO)_{20}(L)$ clusters. All of the experimental values are within ± 0.3% of the calculated values. As discussed above, $Os_7(CO)_{20}(PPh_3)$ (**8**) was isolated in extremely low yields and therefore was only characterized by infrared and mass spectroscopy.

The $Os_7(CO)_{20}(L)$ clusters all have similar patterns in the infrared spectra (in CH_2Cl_2); the infrared spectrum for $Os_7(CO)_{20}(PMe_3)$ (**4**) is shown in Figure 2.5. The clusters all exhibit intense carbonyl stretches in the 1850–2150 cm^{-1} region of the infrared spectrum. No carbonyl stretches occur below 1850 cm^{-1}, indicating that there are no bridging carbonyls in the clusters (which is consistent with their solid–state structures, discussed in section 2.4.1–2.4.3).

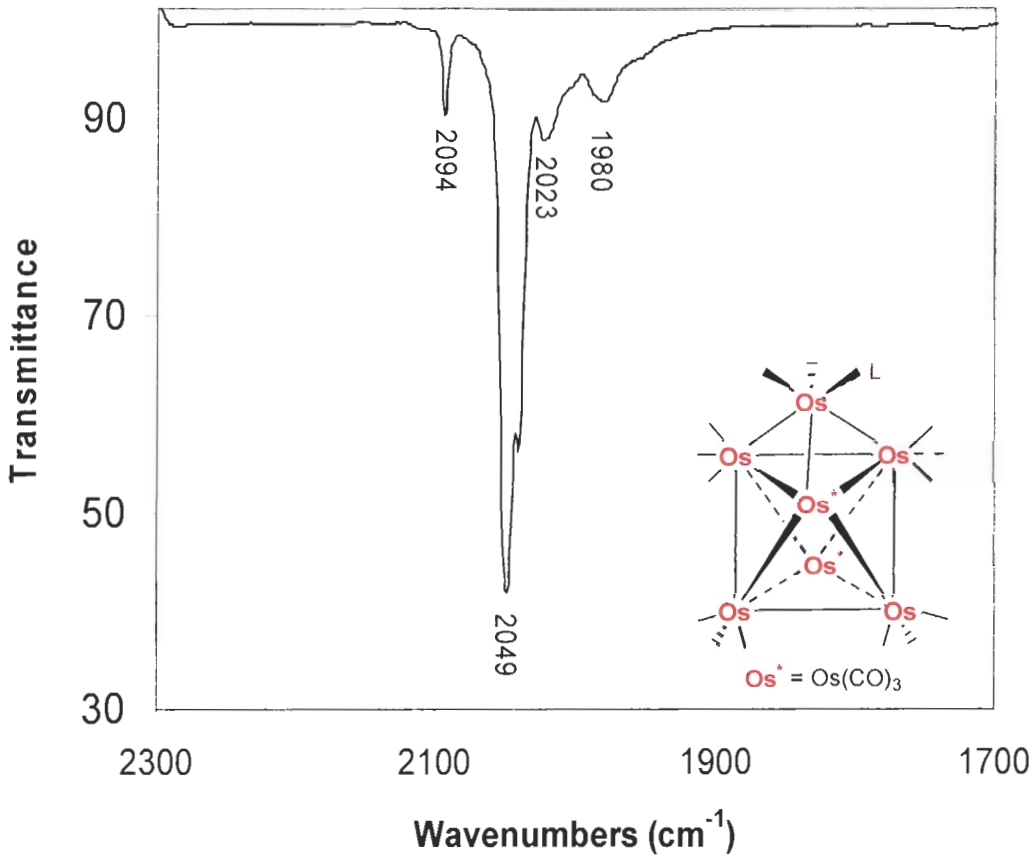

Figure 2.5 $Os_7(CO)_{20}(PMe_3)$ (4) in CH_2Cl_2; typical infrared pattern of the $Os_7(CO)_{20}(L)$ clusters and the structure of $Os_7(CO)_{20}(L)$ clusters.

The carbonyl stretching frequencies are tabulated in Table 2.4. The clusters are arranged in the order of decreasing π–acceptor and increasing σ–donor ability of the ligand (i.e. the order previously determined from the $Os(CO)_4(L)$ compounds, given below). Unfortunately the carbonyl stretching frequencies have not been assigned to their respective vibrational modes.

$$CO > P(OCH_2)_3CMe > CNBu^t \approx P(OMe)_3 > PPh_3 > PMe_3 > PEt_3 > P(Bu^t)_3$$

Strong π–acceptor
Weak σ–donor

Weak π–acceptor
Strong σ–donor

Table 2.4 Infrared data for $Os_7(CO)_{20}(L)$ (L = $CNBu^t$ and PR_3) derivatives.

Cluster	ν(CO),[n] cm^{-1}
$Os_7(CO)_{21}$ (**2**)	2111 (vw), 2075 (s), 2058 (vs), 2037 (m,br), 2000(w, br)
$Os_7(CO)_{20}[P(OCH_2)_3CMe]$ (**7**)	2101 (w, sh), 2097 (w), 2066 (m), 2051 (vs, br), 2029 (w, sh), 2008 (vw), 1990 (w, br), 1978 (vw, sh)
$Os_7(CO)_{20}(CNBu^t)$[o] (**3**)	2099 (w, sh), 2094 (m-w), 2067 (m-w), 2052 (vs), 2045 (s, sh), 2027 (m-w), 2007 (vw), 1988 (m-w, br)
$Os_7(CO)_{20}[P(OMe)_3]$ (**6**)	2095 (w), 2065 (w, sh), 2050 (vs), 2045 (s, sh), 2027 (w, sh), 2006 (vw), 1988 (w, br)
$Os_7(CO)_{20}(PPh_3)$ (**8**)	2093 (m), 2069 (m), 2050 (vs), 2043 (s, sh), 2026 (m), 2008 (vw), 1988 (w, br)
$Os_7(CO)_{20}(PMe_3)$ (**4**)	2094 (m-w), 2049 (vs), 2041 (s, sh), 2023 (m-w, br), 1980 (w, br)
$Os_7(CO)_{20}(PEt_3)$ (**5**)	2093 (m-w), 2048 (vs, br), 2040 (s, sh), 2023 (m-w, br), 1987 (w, sh) 1980 (w)

[n] All spectra recorded in CH_2Cl_2.
[o] ν(CN) 2190 (m–w, broad) cm^{-1}.

Similar to the $Os(CO)_4(L)$ compounds, the $Os_7(CO)_{20}(L)$ clusters exhibit a distinctive pattern in the infrared spectrum (Figure 2.5 and 2.6). As the donor/acceptor properties of the ligand are changed, the shifts observed in the carbonyl stretching frequencies remain consistent with the previously determined donor/acceptor properties of the ligand. For example, as the ligand becomes a stronger π–acceptor and a poorer σ–donor there will be less electron density on the metal cluster, causing a decrease in the π–back bonding to the carbonyl ligands. A decrease in the π–back bonding results in less electron density in the anti–bonding orbitals of the carbonyl ligands, shifting the carbonyl stretching frequencies to a higher wavenumbers. There are two carbonyl stretching frequencies that show the most variation as the ligands donor/acceptor properties are changed: (i) the very strong peak (at 2048 cm^{-1} in the PEt_3 derivative to 2051 cm^{-1} in the $P(OCH_2)_3CMe$ derivative, highlighted in blue in Table 2.4); and (ii) the strong shoulder (at 2040 cm^{-1} in the PEt_3 derivative to 2045 cm^{-1} in the $P(OMe)_3$ derivative to absent in the $P(OCH_2)_3CMe$ derivative, highlighted in red in Table 2.4). As the ligand becomes a stronger π–acceptor and a poorer σ–donor, the strong shoulder (at frequencies of ~2040–2045cm^{-1}) goes from being completely distinguishable in $Os_7(CO)_{20}(PMe_3)$ (**4**) (Figure 2.5) to being absent in $Os_7(CO)_{20}[P(OCH_2)_3CMe]$ (**7**) (Figure 2.6). A reason for this the merging of the two peaks may be that the donor/acceptor properties of the ligand has the greatest effect on the strong shoulder carbonyl stretching frequency (at frequencies of ~2040–2045cm^{-1}), consequently, shifting this peak

more than the very strong peak it shoulders. As a result, the two peaks merge into a single peak.

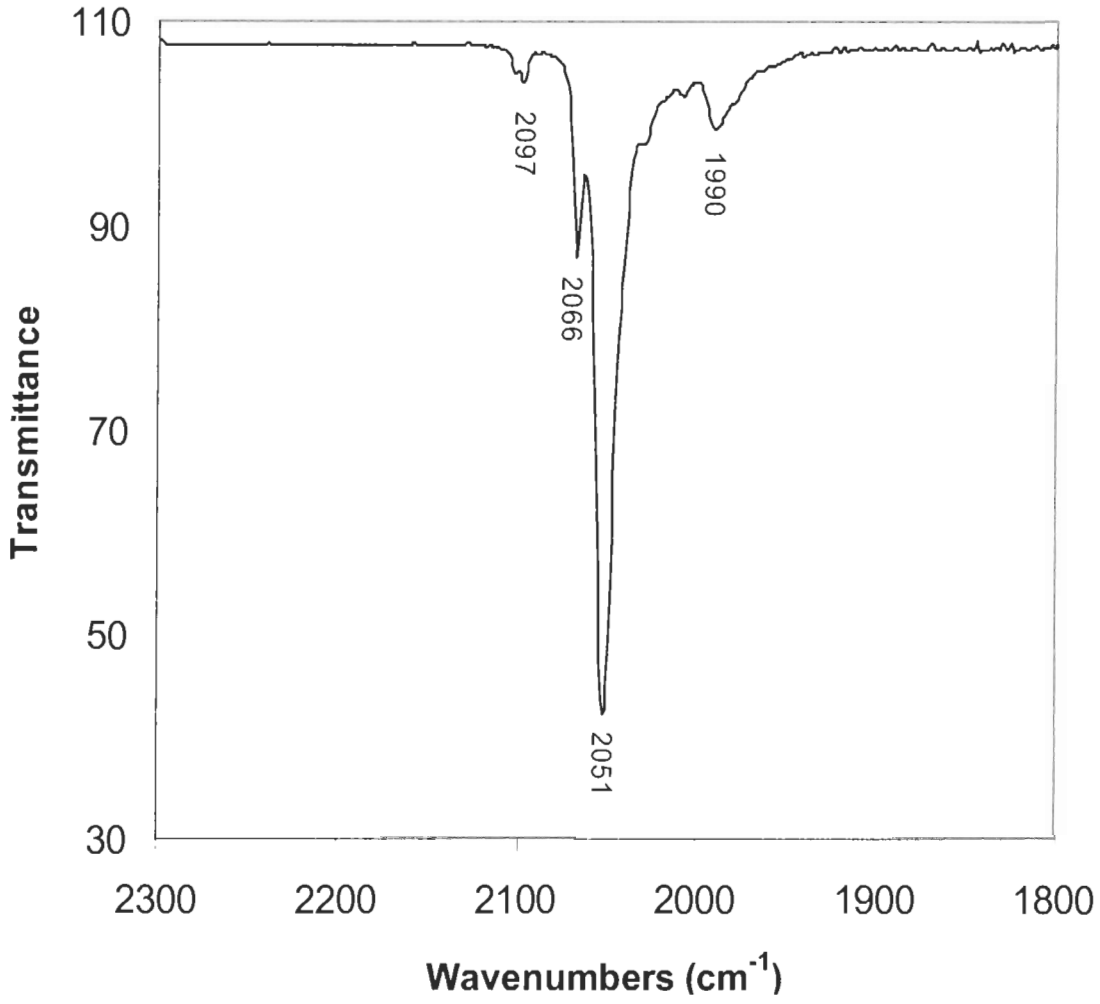

Figure 2.6 Infrared spectra of $Os_7(CO)_{20}[P(OCH_2)_3CMe]$ (7) in CH_2Cl_2.

The presence of additional peaks (at ~2100 and ~2065 cm^{-1}) in the infrared spectra of $Os_7(CO)_{20}(L)$ [L = $CNBu^t$, $P(OMe)_3$ and $P(OCH_2)_3CMe$] may indicate the existence of a second isomer in solution (Figure 2.6). In addition to the structurally characterized compound, there are two additional possible isomers of $Os_7(CO)_{20}(L)$, in which the ligand (L) is on the inner or base Os_3 triangles of the octahedral core rather than the capping group. Since there is no crystal structure of the second isomer, there is no way to tell whether the ligand is on the inner or base Os_3 triangle. The two additional possible isomers are shown in Figure 2.7.

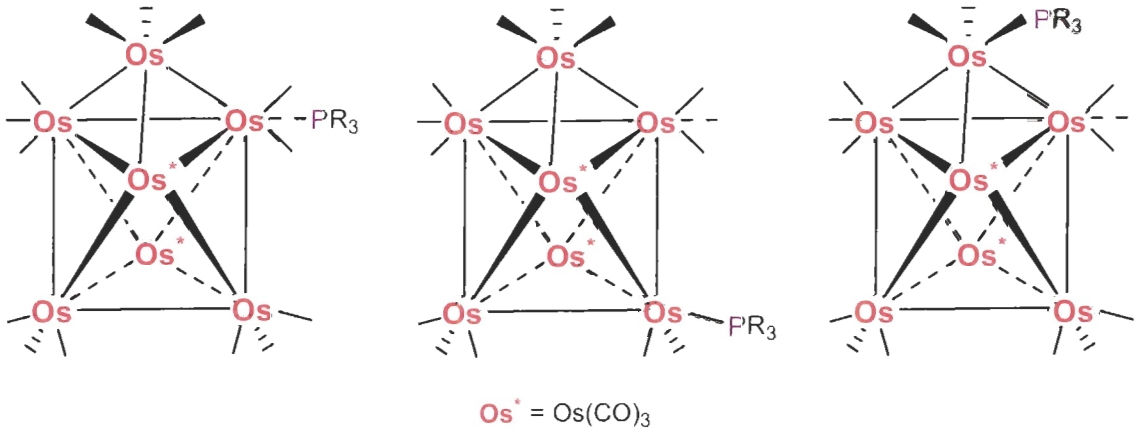

Figure 2.7 Three possible isomers of $Os_7(CO)_{20}(L)$ clusters.

The ^{1}H and $^{31}P\{^{1}H\}$ NMR spectral data for the $Os_7(CO)_{20}(L)$ clusters is given in Table 2.5.

Table 2.5 ^{1}H and $^{31}P\{^{1}H\}$ NMR data $Os_7(CO)_{20}(L)$ (L = $CNBu^t$ and PR_3) derivatives..

Cluster	^{1}H NMR,[p] ppm	$^{31}P\{^{1}H\}$ NMR,[q] ppm
$Os_7(CO)_{20}(CNBu^t)$ (**3**)	1.64[r] Weaker Peaks at 1.520 and 1.525	–
$Os_7(CO)_{20}(PMe_3)$ (**4**)	2.13 (d,10.7)[q]	-14.2
$Os_7(CO)_{20}(PEt_3)$ (**5**)	1.63 (m), 0.57 (dt, 17.3; 7.5)[s]	+20.0
$Os_7(CO)_{20}[P(OMe)_3]$ (**6**)	4.00 (d, 11.9)[q] Weaker peak at 3.84 (d, 11.3)	+94.9 +107.9
$Os_7(CO)_{20}[P(OCH_2)_3CMe]$ (**7**)	3.27 (d, 5.4), -0.54[s] Weaker Peaks at 3.19 (d, 5.1), -0.58	+94.1 +108.6

The ^{1}H NMR spectra of $Os_7(CO)_{20}(L)$ [L = $P(OMe)_3$ (**6**) and $P(OCH_2)_3CMe$ (**7**)] have additional resonances that are consistent with the view that a second isomer may be present in solution. On the other hand, the ^{1}H NMR spectrum for $Os_7(CO)_{20}(CNBu^t)$ (**3**) has two additional resonances, indicating the possibility that all three isomers exist in solution. The ratio of isomers for $Os_7(CO)_{20}(CNBu^t)$ (**3**) is approximately 1:1.5:5 (indicated by the ^{1}H NMR spectra). In general, the ^{1}H NMR spectra confirm the presence of a ligand in the $Os_7(CO)_{20}(L)$ clusters.

[p] J_{P-H} (Hz) are given in parentheses.
[q] Spectra recorded in CD_2Cl_2.
[r] Spectra recorded in $CDCl_3$.
[s] Spectra recorded in C_6D_6.

All of the $^{31}P\{^1H\}$ NMR spectra exhibit single resonances, which are consistent with only a single PR_3 ligand being attached to the clusters. The presence of an isomer in solution is evident for the $Os_7(CO)_{20}(L)$ [L = $P(OMe)_3$ (**6**), $P(OCH_2)_3CMe$ (**7**)] clusters, with an additional singlet in the $^{31}P\{^1H\}$ NMR spectra. The $^{31}P\{^1H\}$ NMR spectra of **6** shows that the ratio of isomers is approximately 1:10, while the $^{31}P\{^1H\}$ NMR spectrum of **7** (Figure 2.8) exhibits the ratio of isomers is approximately 2:1.

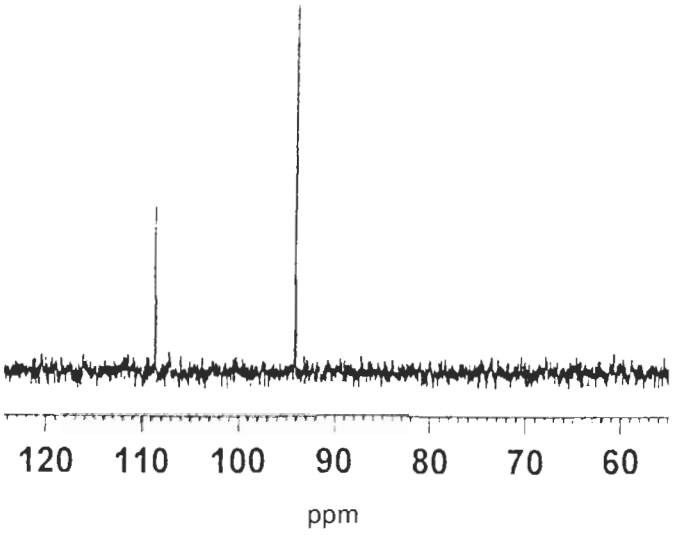

Figure 2.8 $^{31}P\{^1H\}$ NMR spectra of $Os_7(CO)_{20}[P(OCH_2)_3CMe]$ (7) (in CD_2Cl_2) showing the two resonances.

The room temperature $^{13}C\{^1H\}$ NMR spectral data for the $Os_7(CO)_{20}(L)$ clusters is given in Table 2.6. Figure 2.9 shows the ^{13}C NMR spectra of compound **5**. The $^{13}C\{^1H\}$ NMR spectral data was not pursued for compound **8** due to its extremely low yield.

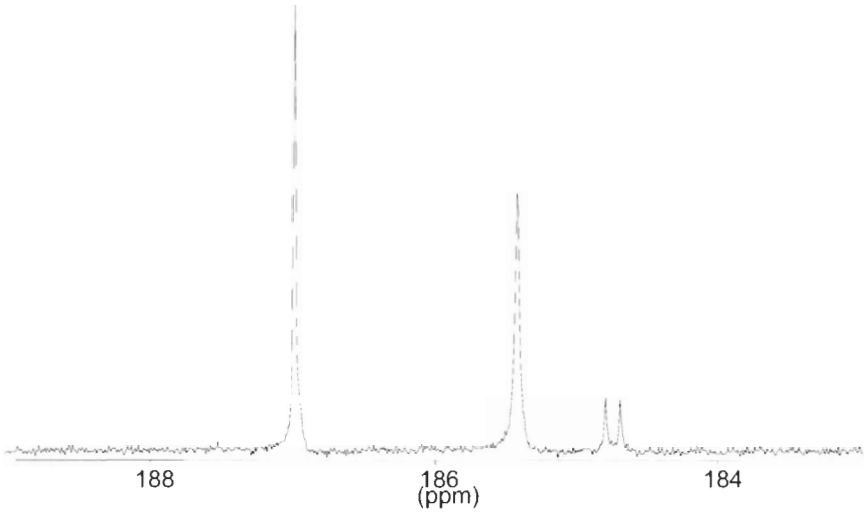

Figure 2.9 $^{13}C\{^1H\}$ **NMR spectrum of** $Os_7(CO)_{20}(PEt_3)$ **(5) in** CD_2Cl_2/CH_2Cl_2 **(1:4).**

Table 2.6 $^{13}C\{^1H\}$ **NMR data for** $Os_7(CO)_{20}(L)$ **(L =** $CNBu^t$ **and** PR_3**) derivatives.**

Cluster	$^{13}C\{^1H\}$ NMR[t] (ppm)
$Os_7(CO)_{20}(CNBu^t)$ (**3**)	187.1, 183.7, 181.4 Weaker peaks at 186.7, 184.1
$Os_7(CO)_{20}(PMe_3)$ (**4**)	187.7, 185.7, 184.2 (d, 10.7)
$Os_7(CO)_{20}(PEt_3)$ (**5**)	187.0, 185.4, 184.7 (d, 10.4)
$Os_7(CO)_{20}[P(OMe)_3]$ (**6**)	187.1, 184.7, 183.4 (d, 15.2) Weaker peaks at 187.7, 186.9, 182.4
$Os_7(CO)_{20}[P(OCH_2)_3CMe]$ (**7**)	187.5, 184.5, 182.4 (d, 20.0) Weaker peaks at 188.4 (d, 17.5 Hz), 187.2, 184.7, 183.5, 182.6, 182,2, 181.6

[t] Spectra recorded at 294 K in CD_2Cl_2/CH_2Cl_2 (1:4) solution, $J_{P\text{-}C}$ (Hz) in parentheses.

All of the room temperature $^{13}C\{^1H\}$ NMR spectra exhibit three major signals (in the carbonyl region) in an approximate ratio of 9:9:2 (assignment of the signals is made in Chapter 3). The $^{13}C\{^1H\}$ NMR spectra of $Os_7(CO)_{20}(L)$ [L = $CNBu^t$ or $P(OMe)_3$] have weaker resonances in the spectra, which is consistent with the view of a second isomer in solution. Given that the ratio of isomers is extremely low for compounds **3** and **6** (as previously mentioned), additional resonances due to a second isomer in solution maybe undetectable. It can be noted from the data in Table 2.6 that a larger $^{13}C–^{31}P$ coupling constant occurs when the PR_3 ligand is a phosphite (compounds **6** and **7**).

In the ^1H and $^{31}P\{^1H\}$ NMR spectra of compounds **7** the two sets of resonances are in ~2:1 ratio (from the $^{31}P\{^1H\}$ NMR spectra). Because of this, the $^{13}C\{^1H\}$ NMR spectra contains several additional intense peaks (Figure 2.10), making assignment of the peaks due to the structure observed in the solid state difficult. A tentative assignment was made using the approximate 9:9:2 ratio seen in the other $Os_7(CO)_{20}(L)$ clusters and the resonances of $Os_7(CO)_{20}[P(OMe)_3]$ (**6**).

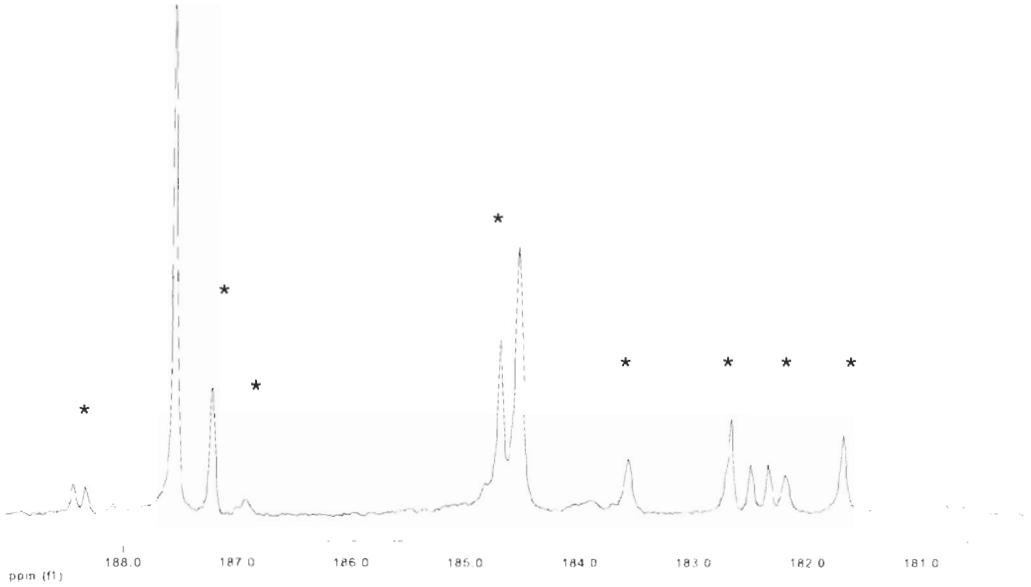

Figure 2.10 $^{13}C\{^{1}H\}$ **NMR spectra of** $Os_7(CO)_{20}[P(OCH_2)_3CMe]$ **(7) in** CH_2Cl_2**:**CD_2Cl_2 **(4:1). (Asterisk indicates the peaks believed to be due to a second isomer in solution.)**

2.4 Structural Studies

As mentioned in Chapter 1, the structures of $Os_7(CO)_{21}$ (**2**)[30] and $Os_7(CO)_{20}[P(OMe)_3]$ (**6**)[31] had been previously determined by X–ray crystallography and revealed a monocapped octahedral metal skeleton. In this study, three of the new compounds were characterized by X–ray crystallography and the structures of $Os_7(CO)_{20}(L)$ [L = $CNBu^t$, PMe_3 and $P(OCH_2)_3CMe$] were found to be analogous to compounds **2** and **6**. The $Os_7(CO)_{20}(L)$ clusters are all isoelectronic (each containing 98 valence electrons) and have the predicted PSEPT polyhedral form.[19] The monocapped octahedron metal skeletons are all similar, with the capping osmium group containing either the isocyanide or phosphorus ligand, along with two terminal carbonyl ligands. The six remaining osmium atoms, which make up the octahedral core, each have three terminal

carbonyl ligands (Figures 2.11 – 2.13). It is usually found that in condensed osmium clusters, Os–Os bond lengths are slightly shorter than 2.877 Å, the average bond length in $Os_3(CO)_{12}$.[62] This average is typically taken to represent an Os–Os single bond.

2.4.1 $Os_7(CO)_{20}(CNBu^t)$ (3)[u]

Compound **3** was crystallized by the slow evaporation of a CH_2Cl_2/hexanes solution and its molecular structure was confirmed by X–ray crystallography, at 25 °C. X–ray crystallography revealed two independent molecules in the unit cell. A view of the two molecules is given in Figure 2.11. The two molecules are chemically identical; selected bond lengths and bond angles are given in Table 2.7.

[u] Reproduced with permission. Reference 38. Wilcox, C.T.; Jennings, M.C.; Pomeroy, R.K. *J. Cluster Sci.*, **2004**, *15*, 107. Copyright 2004 with kind permission of Springer Science and Business Media

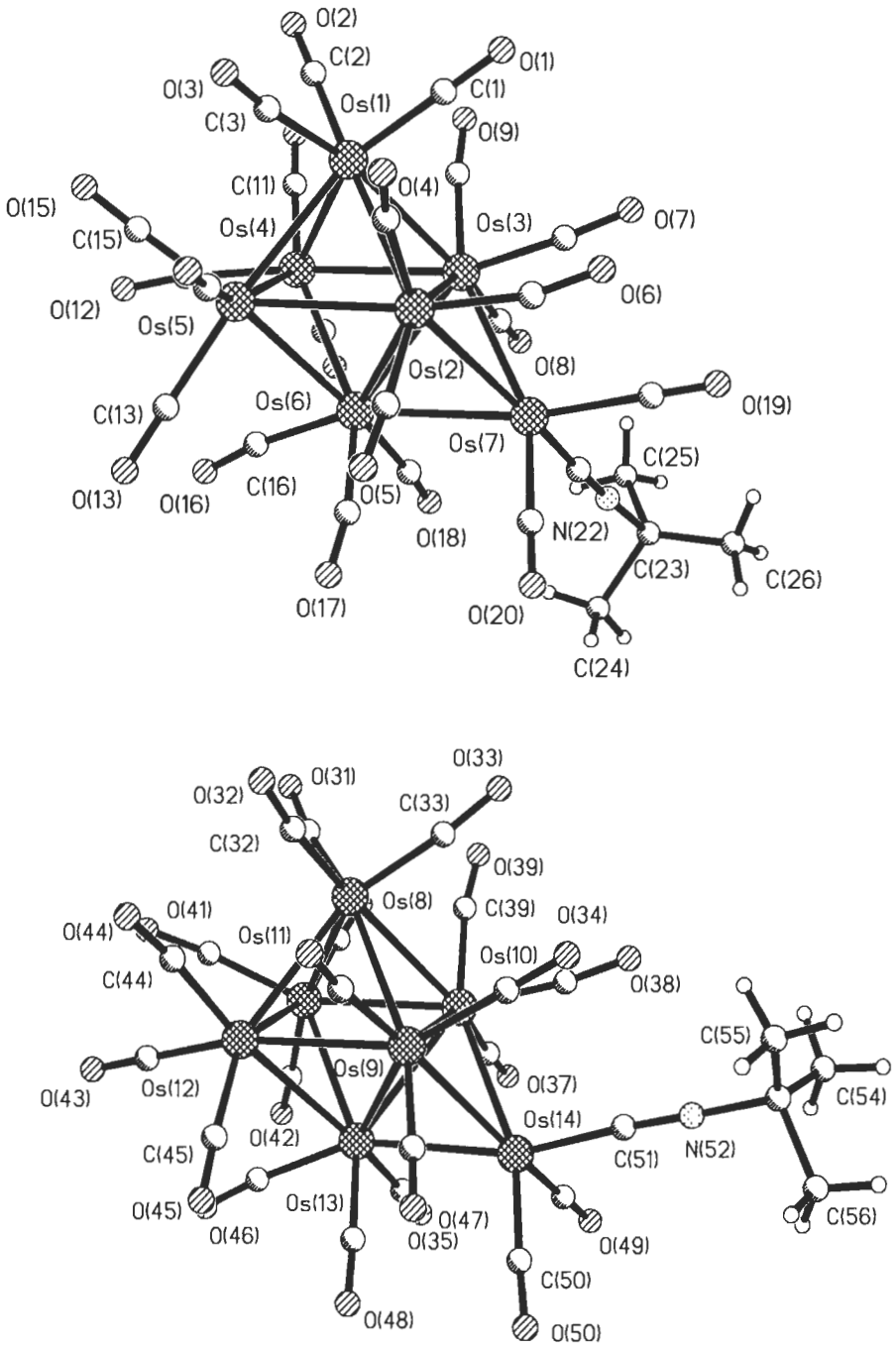

Figure 2.11 Molecular structure of the two independent molecules of $Os_7(CO)_{20}(CNBu^t)$ (3).[v]

[v] Structure determined by Dr. M.J. Jennings at the University of Western Ontario.

Table 2.7 Selected bond lengths (Å) and bond angles (°) for the two independent molecules of $Os_7(CO)_{20}(CNBu^t)$ (3).

Os(1)–Os(2)	2.868(1)	Os(8)–Os(9)	2.871(1)
Os(1)–Os(3)	2.851(1)	Os(8)–Os(10)	2.862(2)
Os(1)–Os(4)	2.922(1)	Os(8)–Os(11)	2.901(1)
Os(1)–Os(5)	2.860(2)	Os(8)–Os(12)	2.916(1)
Os(2)–Os(3)	2.833(1)	Os(9)–Os(10)	2.835(1)
Os(2)–Os(5)	2.876(1)	Os(9)–Os(12)	2.857(1)
Os(2)–Os(6)	2.858(1)	Os(9)–Os(13)	2.840(1)
Os(2)–Os(7)	2.841(1)	Os(9)–Os(14)	2.828(2)
Os(3)–Os(4)	2.849(1)	Os(10)–Os(11)	2.879(1)
Os(3)–Os(6)	2.847(1)	Os(10)–Os(13)	2.846(1)
Os(3)–Os(7)	2.823(1)	Os(10)–Os(14)	2.862(1)
Os(4)–Os(5)	2.917(1)	Os(11)–Os(12)	2.915(1)
Os(4)–Os(6)	2.849(1)	Os(11)–Os(13)	2.864(1)
Os(5)–Os(6)	2.869(1)	Os(12)–Os(13)	2.844(2)
Os(6)–Os(7)	2.874(1)	Os(13)–Os(14)	2.826(1)
Os(7)–C($CNBu^t$)	1.93(2)	Os(14)–C($CNBu^t$)	1.97(3)
Os–C(CO) (range)	1.81(3) –1.99(3)		
Os–Os–Os Bond angles (ranges)	58.66(3) – 61.68(3); 88.72(4) – 91.82(4); 119.12(4) – 121.15(4)		

The Os–Os–Os bond angles in compound **3** are close to the ideal values of 60°, 90° and 120° (Table 2.7). In each of the independent molecules, the Os–C bond lengths (to the $CNBu^t$ ligand) are 1.93(2) and 1.97(3) Å. These bond lengths are comparable to the Os–C bond lengths (to the $CNBu^t$ ligand) of $Os_6(CO)_{16}(CNBu^t)$ [1.87(3) and 1.98(2) Å][63], $Os_5(CO)_{18}(CNBu^t)$ [2.05(1) Å] and $Os_5(CO)_{16}(CNBu^t)$ [2.03(1) Å][63, 64].

2.4.2 $Os_7(CO)_{20}(PMe_3)$ (4)

Compound **4** was crystallized by the slow evaporation of a CH_2Cl_2/hexanes solution and its molecular structure was confirmed by X–ray crystallography, at -70 °C (Figure 2.12); selected bond lengths and angles are given in Table 2.8.

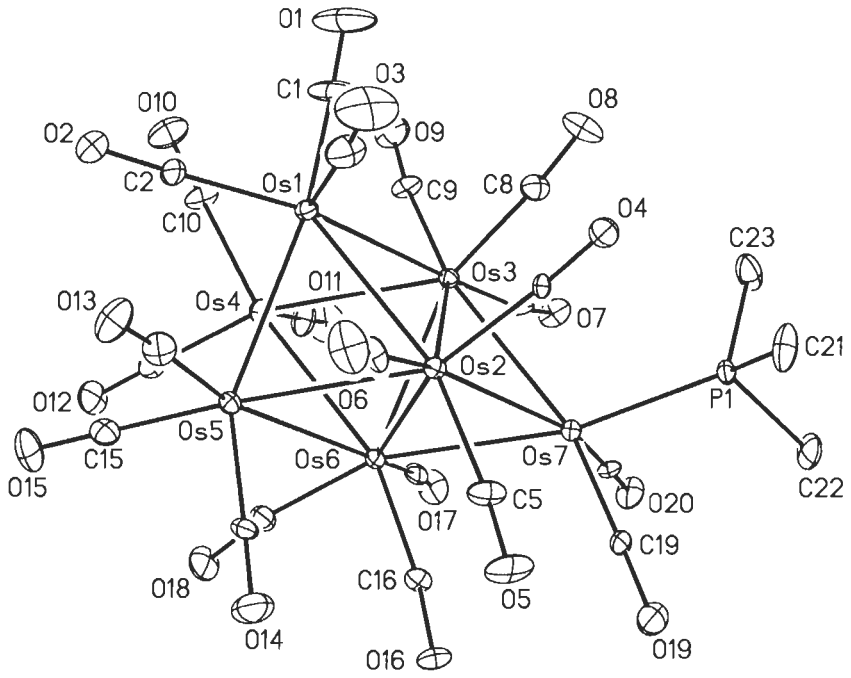

Figure 2.12 Molecular structure of $Os_7(CO)_{20}(PMe_3)$ (4).[w]

[w] Structure determined by Dr. G.P.A. Yap at the University of Ottawa.

Table 2.8 Selected bond lengths (Å) and bond angles (°) for $Os_7(CO)_{20}PMe_3$ (4).

Os(1)–Os(2)	2.8890(8)	Os(3)–Os(4)	2.8709(8)
Os(1)–Os(3)	2.8854(7)	Os(3)–Os(6)	2.8544(7)
Os(1)–Os(4)	2.8986(7)	Os(3)–Os(7)	2.8905(8)
Os(1)–Os(5)	2.8788(7)	Os(4)–Os(5)	2.9453(8)
Os(2)–Os(3)	2.8550(7)	Os(4)–Os(6)	2.8591(8)
Os(2)–Os(5)	2.8674(8)	Os(5)–Os(6)	2.8715(7)
Os(2)–Os(6)	2.8428(7)	Os(6)–Os(7)	2.8712(8)
Os(2)–Os(7)	2.8937(7)		
Os(7)–P(PMe_3)	2.349(3)		
Os–C(CO) (range)	1.85(1) – 1.94(1)		
Os–Os–Os Bond angles (ranges)	58.86(2) – 61.86(2); 89.07(2) – 91.34(2); 119.85 (2) – 121.07(2)		

The Os–Os–Os bond angles in compound **4** are close to the ideal values of 60°, 90° and 120° (Table 2.8). The Os–P bond length (to the PMe_3 ligand) was 2.349(3) Å. The bond length is comparable to the Os–P bond lengths (to the PMe_3 ligand) of $Os_5(CO)_{18}(PMe_3)$ [2.327(6) Å][65], $Os_5(CO)_{17}(PMe_3)$ [2.337(6) Å][65], and $Os_4(CO)_{15}(PMe_3)$ [2.354(6) Å].[20]

2.4.3 $Os_7(CO)_{20}[P(OCH_2)_3CMe]$ (7)

Compound **7** was crystallized from a concentrated toluene solution and its molecular structure was confirmed by X–ray crystallography, at -125 °C (Figure 2.13); selected bond lengths and angles are given in Table 2.9. The molecular structure of compound **7** was determined to be the toluene (C_7H_8) solvate [i.e. **7**·C_7H_8].

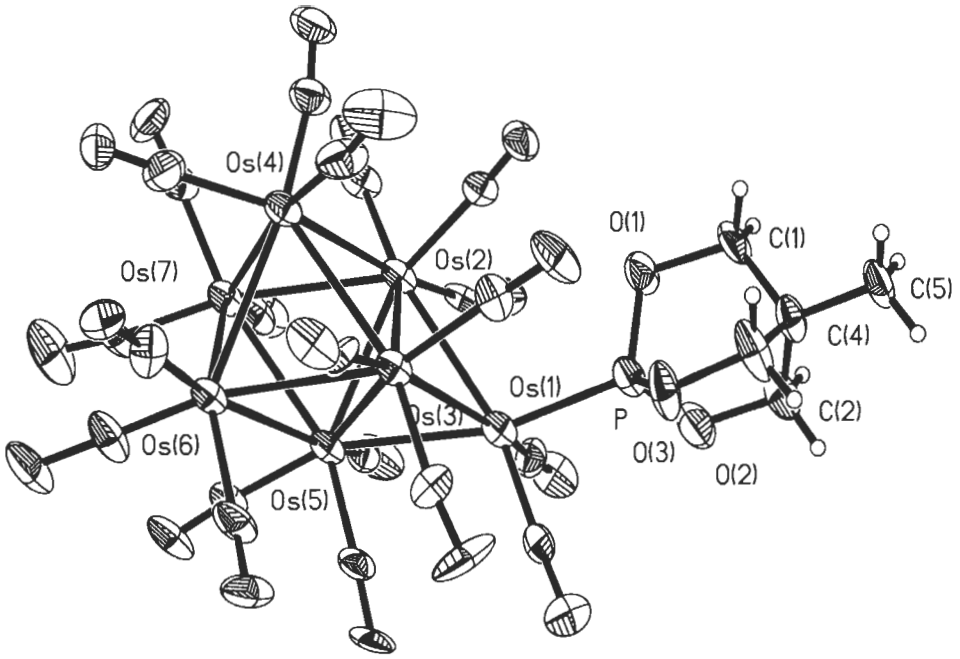

Figure 2.13 Molecular structure of $Os_7(CO)_{20}[P(OCH_2)_3CMe]$ $(7{\cdot}C_7H_8)$[x] [C_7H_8 is not shown].

Table 2.9 Selected bond lengths (Å) and bond angles (°) of $Os_7(CO)_{20}[P(OCH_2)_3CMe]$ $(7{\cdot}C_7H_8)$.

Os(1)–Os(2)	2.852(2)	Os(3)–Os(5)	2.845(2)
Os(1)–Os(3)	2.888(2)	Os(3)–Os(6)	2.859(2)
Os(1)–Os(5)	2.802(2)	Os(4)–Os(6)	2.911(2)
Os(2)–Os(3)	2.823(2)	Os(4)–Os(7)	2.868(2)
Os(2)–Os(4)	2.856(2)	Os(5)–Os(6)	2.838(2)
Os(2)–Os(5)	2.829(2)	Os(5)–Os(7)	2.841(2)
Os(2)–Os(7)	2.872(2)	Os(6)–Os(7)	2.920(2)
Os(3)–Os(4)	2.886(2)		
Os(1)–P ($P(OCH)_2CMe$)	2.259(8)		
Os–C(CO) (range)	1.71(3) – 2.01(3)		
Os–Os–Os Bond Angles (ranges)	58.50(4) – 61.89(4); 88.83(2) – 91.33(5); 118.14(5) – 122.21(5).		

[x] Structure determined by Dr. M.J. Jennings at the University of Western Ontario.

The Os–Os–Os bond angles in compound **7** are close to the ideal values of 60°, 90° and 120° (Table 2.9). The Os–P bond length [to the $P(OCH_2)_3CMe$ ligand] is 2.259(8) Å. The bond length is comparable to the Os–P bond lengths (to the $P(OCH_2)_3CMe$ ligand) of $Os_3(CO)_{11}[P(OCH_2)_3CMe]$ [2.252 (mean value) Å][34], $Os_4(CO)_{15}[P(OCH_2)_3CMe]$ [2.269(6) Å][66], and $[MeC(OCH_2)_3P](OC)_3(Me_3P)OsW(CO)_5$ [2.268(2) Å].[67]

2.4.4 Comparison of $Os_7(CO)_{20}(L)$ [L = $CNBu^t$, $P(OCH_2)_3CMe$, PMe_3] with $Os_7(CO)_{21}$ (2) and $Os_7(CO)_{20}[P(OMe)_3]$ (6)

The bond lengths of the $Os_7(CO)_{20}(L)$ [L = CO (**2**), $CNBu^t$ (**3**), PMe_3 (**4**), $P(OMe)_3$ (**6**) and $P(OCH_2)_3CMe$ (**7**)] clusters can be separated into four groups: lengths associated with the osmium/ligand bonds, the Os–Os bond lengths related to the tetrahedron that contains the capping osmium atom, the Os–Os bond lengths that connect the tetrahedron with the basal Os_3 triangle and the Os–Os bond lengths related to the basal Os_3 triangle. Comparison of the bond lengths found in the clusters will give some idea of how the steric and electronic properties of the $CNBu^t$ and PR_3 ligands affect the bonding.

The Os–C($CNBu^t$), Os–P(PR_3) and Os–C(CO) Bond Distances

The Os–C($CNBu^t$) and Os–P(PR_3) bond distances in the $Os_7(CO)_{20}(L)$ clusters are tabulated in Table 2.10 and Figure 2.14 indicates the bond of interest in the clusters.

Table 2.10 The Os–C and Os–P bond distances in the $Os_7(CO)_{20}(L)$ [L = $CNBu^t$, $P(OCH_2)_3CMe$, $P(OMe)_3$ and PMe_3] clusters.

Cluster	Os–C and Os–P distances (Å)	Cone Angle (°)[59]
$Os_7(CO)_{20}(CNBu^t)$ (**3**)	1.95(2)[y]	–
$Os_7(CO)_{20}[P(OCH_2)_3CMe]$ (**7**)	2.259(8)	101
$Os_7(CO)_{20}[P(OMe)_3]$ (**6**)[31]	2.27(1)	107
$Os_7(CO)_{20}(PMe_3)$ (**4**)	2.349(3)	118

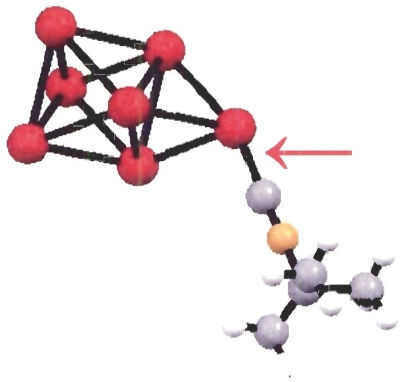

Figure 2.14 Structure of $Os_7(CO)_{20}(CNBu^t)$ (3) (with CO groups removed), arrow indicates the Os–L bond.

The Os–P bond lengths for the $Os_7(CO)_{20}(PR_3)$ clusters have been arranged in the Table 2.10 in order of increasing cone angle of the PR_3 ligand and the decreasing π–acceptor ability. The Os–P bond length changes with increased π–acceptor ability: as the PR_3 ligand increases in π–acceptor ability, the Os–P bond length decreases. It can also be seen in Table 2.10 that the Os–P bond length also changes with the size of the PR_3 ligand, as the cone

[y] Mean value.

angle increases the Os–P bond length also increases. Therefore the Os–P bond length appears to be affected by the electronic and steric properties of the PR_3 ligand. The changes in the Os–P bond lengths are in agreement with earlier observations in $M(CO)_5(PR_3)$ (M = Cr and W) compounds and Os–P bond lengths in $Os_3(CO)_{11}(PR_3)$ clusters where the M–P (M = Cr, W, and Os) bond lengths are influenced by the electronic and steric properties of the PR_3 ligand.[34, 68]

The shortest Os–L bond length of the $Os_7(CO)_{20}(L)$ clusters is observed in compound **3**, contrary to what is expected based on the donor/acceptor properties of the ligands. Both $CNBu^t$ and $P(OMe)_3$ have essentially the same π–acceptor ability (the donor/acceptor properties of the ligands were defined in Section 2.2.3) therefore the Os–P($P(OMe)_3$) and Os–C($CNBu^t$) bond lengths should be very similar. However, comparing the bond lengths (Table 2.10), the Os–C($CNBu^t$) bond length is considerably shorter than the Os–P($P(OMe)_3$) (a difference of 0.32 Å). This lengthening may be accounted for (in terms of) the rod–like[61] structure of $CNBu^t$, which would be sterically non–demanding[69] and therefore has the ability to form a stronger (i.e. shorter) Os–C($CNBu^t$) bond. Consequently, the Os–L bond length appears to be affected by both the electronic and steric properties of the ligand.

The Os–C(CO) bond distances in the $Os_7(CO)_{20}(L)$ clusters show a large range of values (as can be seen in Tables 2.7, 2.8 and 2.9). However, comparing the Os–C(CO) bond distances of the $Os_7(CO)_{20}(L)$ clusters, there is no obvious pattern in the bond distances.

The Os–Os Bond Lengths Related to the Tetrahedron (which contains the capping osmium atom).

The Os–Os bonds lengths that are *cis* and *trans* to the $CNBu^t$ and PR_3 ligands in the $Os_7(CO)_{20}(L)$ clusters are tabulated in Table 2.11 and Figure 2.15 (next page) indicates the bond of interest in the clusters.

Examining the Os–Os bonds that are *cis* and *trans* to the ligand, it is noticeable that the two bonds *cis* to the ligands are longer than the *trans* bond. The lengthening of the Os–Os bond that are *cis* to the ligand has been previously observed in $Os_3(CO)_{11}(PR_3)$ compounds.[33, 34] It was found that as the cone angle of the phosphorus ligand increased in the $Os_3(CO)_{11}(PR_3)$ compounds, there was an increase Os–Os bond length *cis* to the ligand. In addition to the steric influence of the phosphorus ligand, there was also a small electronic influence on the *cis* Os–Os bond. It is apparent from the data in Table 2.11 that these previously observed trends are also present in $Os_7(CO)_{20}(L)$ clusters. The shortest *cis* Os–Os bonds are observed in compound **3**. As mentioned before, the $CNBu^t$ has a rod–like[61] structure, that would be the most sterically non–demanding[69]. Comparing the *cis* Os–Os bonds in the $Os_7(CO)_{20}(PR_3)$ clusters, the bonds increase with an increasing PR_3 cone angle. The cone angles of $P(OCH_2)_3CMe$, $P(OMe)_3$, and PMe_3 are 101°, 107° and 118°, respectively.[59] Therefore, as the cone angle increases there is an increase in the steric interactions (between the PR_3 ligand and the carbonyl ligands on neighboring osmium atoms), causing a lengthening of the *cis*–Os–Os bond.

Table 2.11 The Os–Os bond lengths that are *cis* and *trans* to the $CNBu^t$ and PR_3 ligand in the $Os_7(CO)_{20}(L)$ clusters.

Cluster	*Cis*	*Cis*	*Trans*
$Os_7(CO)_{21}$ (**2**)[30]	2.806(6)	2.821(6)	2.830(6)
$Os_7(CO)_{20}(CNBu^t)$ (**3**)	2.842(1)	2.851(2)	2.831(1)
$Os_7(CO)_{20}[P(OCH_2)_3CMe]$ (**7**)	2.888(2)	2.852(2)	2.802(2)
$Os_7(CO)_{20}[P(OMe)_3]$ (**6**)[31]	2.892(2)	2.868(2)	2.837(2)
$Os_7(CO)_{20}(PMe_3)$ (**4**)	2.8905(8)	2.8937(7)	2.8712(8)

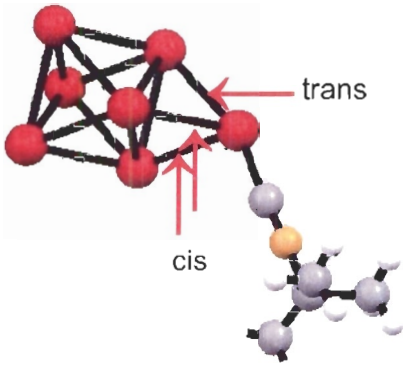

Figure 2.15 Structure of $Os_7(CO)_{20}(CNBu^t)$ (3) (with CO groups removed), arrows indicate the *cis* and *trans* Os–Os bonds.

As the donor/acceptor properties of the ligand are varied, there is a change in the length of the *trans* Os–Os bond. The longest *trans* Os–Os bond is seen in compound **4**, PMe_3 is a strong σ–donor and weak π–acceptor, while the shortest bond is seen in compound **7**, $P(OCH_2)_3CMe$ is a strong π–acceptor and a weak σ–donor. The variation in the *trans* Os–Os bond length has been

previously observed in mononuclear square planar and octahedral transition metal complexes[70], where the shortening has been accounted for in terms of the molecular orbitals; the two ligands that are *trans* to each other share and compete for the same σ–molecular orbital.[71] A strong σ–donor ligand will cause the σ–orbital to be concentrated towards the ligand, therefore, weakening and lengthening the bond that is *trans* to it. The completion for the same σ–molecular orbital could account for the lengthening of the *trans* Os–Os bond in the $Os_7(CO)_{20}(L)$ clusters. As the donor/acceptor properties of the ligand are changed to better π–acceptors and poorer σ–donors, the σ–orbital will be less concentrated towards the ligand, therefore, strengthening and shortening the *trans* Os–Os bond.

The Os–Os bond ranges that are related to the base of the tetrahedron in the $Os_7(CO)_{20}(L)$ clusters are tabulated in Table 2.12 and Figure 2.16 (next page) indicates the bond of interest in the clusters.

The bond lengths related to the base of the tetrahedron (i.e. the inner Os_3 triangle) are some of the shortest in the cluster. The length of these bonds is a good indication that the bonding within these Os_3 triangles is quite strong, but comparison of the ranges revealed no obvious pattern as the donor/acceptor properties of the ligands were varied.

Table 2.12 The Os–Os bond ranges related to the base of the tetrahedron in the $Os_7(CO)_{20}(L)$ clusters.

Cluster	Os–Os bond ranges (Å)
$Os_7(CO)_{21}$ (**2**)[30]	2.824(6) – 2.848(6)
$Os_7(CO)_{20}(CNBu^t)$ (**3**)	2.834(1) – 2.849(1)
$Os_7(CO)_{20}[P(OCH_2)_3CMe]$ (**7**)	2.823(2) – 2.845(2)
$Os_7(CO)_{20}[P(OMe)_3]$ (**6**)[31]	2.848(2) – 2.853(2)
$Os_7(CO)_{20}(PMe_3)$ (**4**)	2.8428(7) – 2.8550(7)

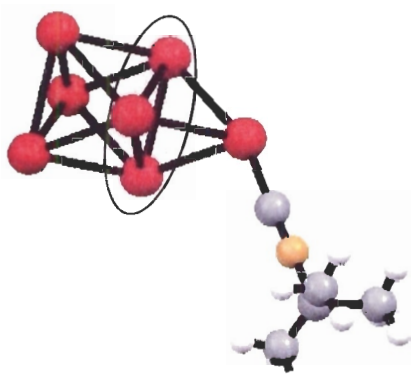

Figure 2.16 Structure of $Os_7(CO)_{20}(CNBu^t)$ (3) (with CO groups removed), coloured oval indicating the Os–Os bond of the base of the tetrahedron.

The Os–Os Bonds Lengths Related to the Connection between the Tetrahedron and Base Os_3 Triangle.

The Os–Os bond ranges for the six lengths that are related to the connect between the tetrahedron and the base Os_3 triangle are given in Table 2.13 and Figure 2.17 (next page) indicates the bond of interest in the clusters.

Table 2.13 The Os–Os bond ranges related to the connection between the tetrahedron and the base Os_3 triangle in the $Os_7(CO)_{20}(L)$ clusters.

Cluster	Os–Os bond ranges (Å)
$Os_7(CO)_{21}$ (**2**)[30]	2.839(6) – 2.876(6)
$Os_7(CO)_{20}(CNBu^t)$ (**3**)	2.844(1) – 2.879(1)
$Os_7(CO)_{20}[P(OCH_2)_3CMe]$ (**7**)	2.838(2) – 2.886(2)
$Os_7(CO)_{20}[P(OMe)_3]$ (**6**)[31]	2.844(2) – 2.887(2)
$Os_7(CO)_{20}(PMe_3)$ (**4**)	2.8591(8) – 2.8890(8)

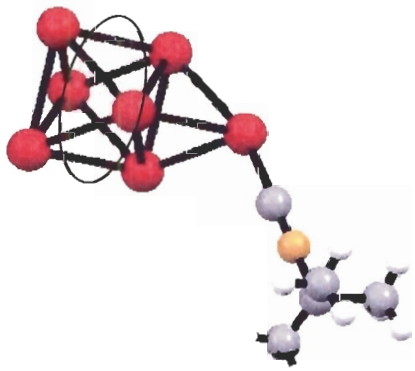

Figure 2.17 Structure of $Os_7(CO)_{20}(CNBu^t)$ (3) (with CO groups removed), coloured oval indicating the Os–Os bond connection between the tetrahedron and the base Os_3 triangle

A comparison of the bond ranges reveals that as the donor/acceptor properties of the PR_3 ligand are varied, the span of the ranges also varies. As the PR_3 ligand becomes a better π–acceptor, there is a larger difference between the shortest and longest Os–Os bond. Thus, the bond lengths that connect the

tetrahedron and the base Os_3 triangle appear to be affected by the electronic properties of the ligand.

The Os–Os Bond Lengths Related to the Base Os_3 Triangle.

The Os–Os bond distances related to the base Os_3 triangle of the $Os_7(CO)_{20}(L)$ clusters are tabulated in Table 2.14 and Figure 2.18 (next page) indicates the bond of interest in the clusters.

In all of the crystal structures (Figure 2.11–2.13), the bond lengths of the base Os_3 triangle are some of the longest lengths found in the clusters. The longer length of these bonds is a good indication that the bonds of the base Os_3 triangle are the weakest in the clusters. The crystal structures also reveal a twisting of the $Os(CO)_3$ units. The twisting means the carbonyl ligands on neighbouring osmium atoms are not in an eclipsed configuration, the Os–Os bonds may be weak enough to allow for the twisting of the $Os(CO)_3$ units, or the twisting may have caused the bonds of the base Os_3 triangle to become weak. There is no understanding to why the $Os(CO)_3$ groups of the base Os_3 triangle are twisted. A possible reason for the lengthening of the Os–Os bonds and twisting of the $Os(CO)_3$ units is it may be an attempt to relieve some of the steric interactions of the carbonyl ligands.

Table 2.14 Os–Os bond lengths related to the base triangle of the $Os_7(CO)_{20}(L)$ clusters. Bond numbering [i.e. Os(1)–Os(5)) correspond to the bonds of the $Os_7(CO)_{20}(PMe_3)$ (4) cluster.][z]

Cluster	Os(1)–Os(5)	Os(1)–Os(4)	Os(4)–Os(5)
$Os_7(CO)_{21}$ (**2**)[30]	2.892(6)	2.880(6)	2.935(6)
$Os_7(CO)_{20}(CNBu^t)$ (**3**)	2.888(2)	2.911(1)	2.916(1)
$Os_7(CO)_{20}[P(OCH_2)_3CMe]$ (**7**)	2.911(2)	2.868(2)	2.920(2)
$Os_7(CO)_{20}[P(OMe)_3]$ (**6**)[31]	2.892(2)	2.894(2)	2.928(2)
$Os_7(CO)_{20}(PMe_3)$ (**4**)	2.8788(7)	2.8986(7)	2.9453(8)

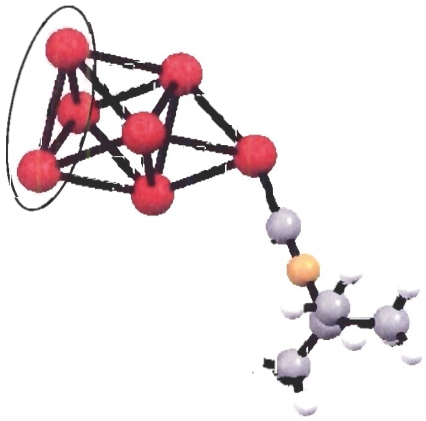

Figure 2.18 Structure of $Os_7(CO)_{20}(CNBu^t)$ (3) (with CO groups removed), coloured oval indicates the Os–Os bonds of the base Os_3 triangle.

These characteristics appear to be inherent to the $Os_7(CO)_{20}(L)$ (L = CO, $CNBu^t$ and PR_3) clusters, and therefore not likely due to packing forces in the crystal. A similar twisting and lengthening of the Os–Os bonds has been observed in the $Os_3(CO)_{11}[P(Bu^t)_3]$ cluster, where the $Os(CO)_4$ and $Os(CO)_3[P(Bu^t)_3]$ units are

[z] The same bonds were used in every cluster (i.e. the Os(1)–Os(5) bond in compound (**4**) corresponds to the Os(4)–Os(6) bond in compound (**7**) etc.

rotated so that the carbonyl ligands are not eclipsed (compared to the parent carbonyl cluster $Os_3(CO)_{12}$, in which the carbonyls are all eclipsed, Figure 2.19).[72]

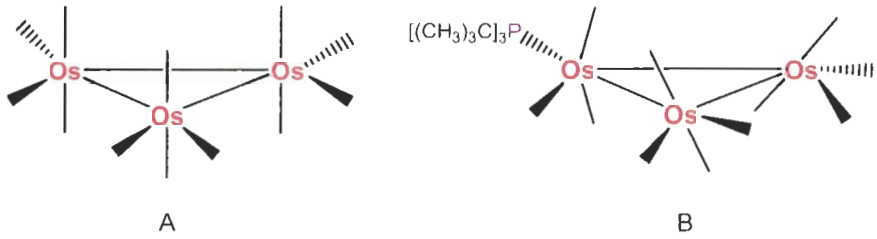

Figure 2.19 Structures of $Os_3(CO)_{12}$ (A) and $Os_3(CO)_{11}[P(Bu^t)_3]$ (B).

2.4.5 $Os_7(\mu\text{–}H)_2(CO)_{19}(PMe_3)$ (9)

As discussed above, a second compound was produced during the preparations of $Os_7(CO)_{20}(PR_3)$ [L = PMe_3, $P(OMe)_3$ and PEt_3]. Through chromatography of the PMe_3 system, an orange and a red compound were isolated. The orange compound was identified as the desired product **4**, while the red compound was identified as compound **9** (by infrared and mass spectrometry). Due to the very low yield of compound **9**, the complete characterization required that it be prepared independently in a targeted manner. This was achieved by reacting $Os_7(\mu\text{–}H)_2(CO)_{20}$ with Me_3NO in the presence of an excess of PMe_3 at -78 °C (eq 2.23). The product isolated from the reaction of $Os_6(CO)_{18}$ with $Os(CO)_4(L)$ (eq. 2.12) and the product isolated in equation 2.23 are the same product (based on infrared and mass spectroscopy).

$$Os_7(\mu\text{-}H)_2(CO)_{20} + PMe_3 \xrightarrow[-78\ ^\circ C]{Me_3NO} Os_7(\mu\text{-}H)_2(CO)_{19}(PMe_3) + CO \qquad (2.23)$$

Thus, compound **9** was characterized by C\H\N analysis, IR (Figure 2.15), mass (parent ion), ^1H and $^{31}P\{^1H\}$ NMR spectroscopy. Despite several crystallization attempts, X–ray quality crystals were not obtained. However, even in the absence of a crystal structure, information on the structure could be deduced from the spectral data [mainly the mass (parent ion) and ^1H NMR spectra].

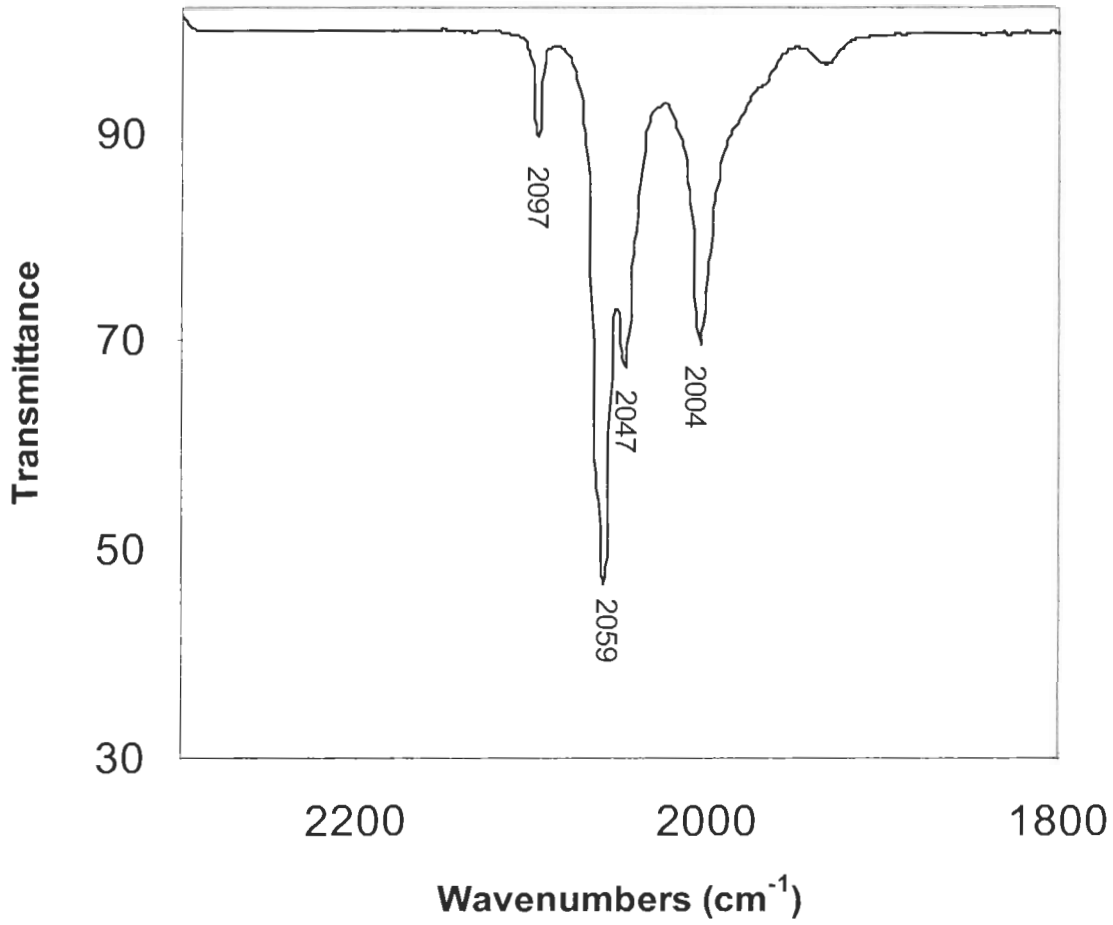

Figure 2.20 IR of the carbonyl region of $Os_7(\mu\text{–}H)_2(CO)_{19}(PMe_3)$ (9) in CH_2Cl_2.

The LSIMS mass spectrum revealed the parent ion peak at *m/z* 1941.8, which corresponds to the molecular formula $Os_7(\mu\text{–}H)_2(CO)_{19}PMe_3$ (**9**). The ^1H NMR spectrum has resonances at 2.02 ppm (doublet, $J_{P\text{-}H}$ = 2.1 Hz) and -13.90 ppm (singlet) and the resonances integrate in an approximately 9:2 ratio. Thus, the resonance at 2.02 ppm can be assigned to methyl groups of the PMe_3 ligand and the peak at -13.90 ppm to two bridging hydrides (hydrogen signals in the bridging region of the ^1H NMR spectra have resonances from -13 to -25 ppm.[2]) Since there is only one signal for the two bridging hydrides, it is assumed that both are in equivalent sites, although there is still a possibility that the hydrides are exchanging between equivalent sites. Due to instrumental difficulties, variable temperature ^1H NMR data of this compound was not obtained.

2.4.6 Mixed Metal Clusters

As mentioned in Chapter 1, the rational synthesis of clusters with different metal atoms is more challenging than the rational synthesis of homonuclear clusters presented in this thesis. Attempts to prepare a mixed metal cluster by replacing the $Os(CO)_4(L)$ compound with $HRe(CO)_5$, $Re(H)(CO)_4(PPh_3)$ and $(\eta^5\text{–}C_5Me_5)Ir(CO)_2$ (in eq. 2.12) were not successful. The only product in all of the reactions was the brown salt $[Os_6(H)(CO)_{17}][N(CH_2)Me_2]$ (eqs. 2.24, 2.25 and 2.26).

$$Os_6(CO)_{18} + HRe(CO)_4 \xrightarrow[-78\ ^\circ C]{Me_3NO} [N(CH_2)Me_2][Os_6(H)(CO)_{17}] + HRe(CO)_4 + CO_2 + NMe_3 \qquad (2.24)$$

$$Os_6(CO)_{18} + Re(H)(CO)_4(PPh_3) \xrightarrow[-78\ ^\circ C]{Me_3NO} [N(CH_2)Me_2][Os_6(H)(CO)_{17}] + Re(H)(CO)_4(PPh_3) + CO_2 + NMe_3 \quad (2.25)$$

$$Os_6(CO)_{18} + (\eta^5\text{-}C_5Me_5)Ir(CO)_2 \xrightarrow[-78\ ^\circ C]{Me_3NO} [N(CH_2)Me_2][Os_6(H)(CO)_{17}] + (\eta^5\text{-}C_5Me_5)Ir(CO)_2 + CO_2 + NMe_3 \quad (2.26)$$

It is apparent that $HRe(CO)_4$, $Re(CO)_4(PPh_3)$ and $(\eta^5\text{–}C_5Me_5)Ir(CO)_2$ are not sufficiently strong nucleophiles to displace the coordinated NMe_3 from the Os_6 cluster, therefore the NMe_3 β–eliminates a hydrogen atom onto the Os_6 cluster forming the brown salt $[Os_6(H)(CO)_{17}][N(CH_2)Me_2]$ (apparent by a strong band at 2016 cm^{-1} in the IR spectrum).

2.5 Conclusions and Future Work

Monosubstituted heptanuclear osmium clusters $[Os_7(CO)_{20}(L)]$ can be systematically synthesized in low to moderate yields by chemically removing a carbonyl ligand from $Os_6(CO)_{18}$ (**1**) and replacing it with $Os(CO)_4(L)$. Through the reactions discussed in this chapter, $Os_7(CO)_{20}(L)$ clusters can be consistently produced. On the other hand, there is no method that produces the parent carbonyl cluster $Os_7(CO)_{21}$ (**2**) reliably and consistently. The $Os_7(CO)_{20}(L)$ (L = CO, $CNBu^t$, PR_3) clusters all have the expected polyhedral metal skeleton; in the cases where L = $CNBu^t$ or PR_3 the ligand is found on the capping osmium group in the solid state. Because of the changes in electronic and steric properties of the ligand, changes are observed in the bond lengths and electronic properties. These changes are consistent with the known electronic and steric properties of the ligand.

Combining the results, two interesting characteristics emerged relating to the reaction of $Os_6(CO)_{18}$ (**1**) and $Os(CO)_4(L)$. First, an increase in the cone angle of the ligand results in a decrease in the yield of $Os_7(CO)_{20}(L)$ clusters (except for L = CO), indicating that there is a limit to the size of the ligand that can be attached to the capping osmium atom. The second characteristic is that certain ligands, for unknown reasons, produce a second cluster that contains two hydride ligands in place of a carbonyl.

Although a mixed metal cluster was not isolated, synthesis of a M_7 cluster (by replacing $Os(CO)_4(L)$ with a compound containing a different transition metal in equation 2.12) would be of interest because of the known differences in structures of heteronuclear clusters. Further work is needed to develop a convenient and reliable preparation of $Os_7(CO)_{21}$ (**2**), that consistently produces compound **2** in moderate to high yields. An improved preparation of compound **2** would allow for a possible systematic synthetic study and investigation of the properties (i.e. structure, bond lengths, carbonyl infrared stretching frequencies and reactivity) of $Os_8(CO)_{22}(L)$ (L = CO, PR_3, CNR) clusters. With a convenient and reliable preparation of compound **2**, $Os_7(CO)_{20}(PR_3)$ cluster could be synthesized by reacting compound **2** with Me_3NO in the presence of an excess of a PR_3 ligand. Then attempts to place a PR_3 ligand on the capping $Os(CO)_2(L)$ unit with a cone angle larger then 145° could be pursued, giving a better understanding to whether there is a cone angle limit for the targeted reaction or a limit to size of the PR_3 ligand that can be attached to the capping $Os(CO)_2(L)$ unit.

2.6 Experimental

Unless otherwise stated, all reagents were obtained from standard commercial sources and were used as received and manipulations of starting material and products were carried out under a nitrogen atmosphere with the use of standard Schlenk techniques. Hydrocarbon solvents were refluxed over potassium, distilled and stored over molecular sieves. Dichloromethane and hexafluorobenzene were refluxed over calcium hydride (CaH_2) and phosphorus pentoxide (P_2O_5) respectively, distilled and stored over molecular sieves. Trimethylamine *N*-oxide was sublimed in the presence of P_2O_5 before use.

A Parr autoclave (500 mL), equipped with a rocking heater, was used for reactions requiring pressures greater than 1200 psi and for reactions requiring less than 1200 psi of pressure; a Parr autoclave (200 mL) was used. NMR spectra were recorded on either a Bruker AMX 400 (operating at frequencies of 100.6 MHz, 162 MHz, and 400 MHz for ^{13}C, ^{31}P and ^{1}H NMR, respectively), Varian Inova 500 (operating at frequencies of 125.8 MHz and 500 MHz for ^{13}C and ^{1}H NMR, respectively) or a Bruker AVANCE II 600 MHz (operating at a frequency of 242.9 MHz for ^{31}P NMR). Chemical shifts for $^{31}P\{^{1}H\}$ NMR spectra referenced to external 85% phosphoric acid (0 ppm). Infrared spectra were recorded on a Bomen MB 100 spectrometer (recording 16 scans at a resolution of 2 cm^{-1}). Dr. D. McGillvary at the University of Victoria obtained mass spectra on Kratos Concept double focusing mass spectrometer with a LSIMS source (using Nitrobenzyl Alcohol as the matrix). M.K. Yang of the Microanalytical Laboratory at Simon Fraser University carried out C/H/N microanalysis.

An improved synthesis of $Os_6(CO)_{18}$ is given below. Alternate preparations of $Os(CO)_4(CNBu^t)$, $Os(CO)_4(PEt_3)$ and $Os(H)_2(CO)_4$ [which was used in the preparation of $Os_7(H_2)(CO)_{20}$] are given below. Quinuclidine *N*–oxide was prepared by a modification of the literature method (see below).[73] Samples used to obtain the $^{13}C\{^1H\}$ NMR spectra were enriched to ~25–30% with ^{13}CO. The ^{13}CO–enriched samples were prepared from ^{13}CO–enriched $Os_6(CO)_{18}$, which was sequentially prepared from ^{13}CO–enriched $Os_3(CO)_{12}$.[74] The following precursory compounds were prepared by literature methods: $Os_3(CO)_{12}$,[43] $Os(CO)_5$,[42] $Os(CO)_4(PMe_3)$,[50] $Os(CO)_4[P(OMe)_3]$,[74] $Os(CO)_4[P(Bu^t)_3]$,[49] $Os(CO)_4(PPh_3)$,[50, 51] $Os(CO)_4(CNBu^t)$,[49] $Os(CO)_3(CNBu^t)_2$,[49] $Os_7H_2(CO)_{20}$,[75] $P(OCH_2)_3CMe$,[76] $Os_6(CO)_{17}(MeCN)$,[77] $Re(H)(CO)_5$,[78] $Re(H)(CO)_4(PPh_3)$,[79] $(\eta^5\text{–}C_5Me_5)Ir(CO)_2$[80].

Improved Preparation of $Os_6(CO)_{18}$ (1) To a flame dried Carius tube (~2.5 L) was added dry $Os_3(CO)_{12}$ (500 mg, 0.551 mmol), dry C_6F_6 (50 mL) and P_2O_5 (~10 mg). The tube was cooled to -196 °C and degassed with three freeze-pump-thaw cycles; the tube was then sealed under vacuum. The reaction solution was heated to 183 °C for 14 days; the solution was degassed as described above and the tube sealed under vacuum once a day (everyday to remove CO). Over the 14 days, the solution colour changed from yellow to brown and a black insoluble solid was produced (this compound was not futher analyzed). The solvent was removed on the vacuum line and the residue washed with 50 mL of CH_2Cl_2. The solution was passed through a small column of silica gel–60, to remove the black insoluble solid. The collected solution was

evaporated to dryness on the vacuum line resulting in a pure sample of **1** (308 mg, 68% yield). The IR spectrum indicated that the sample was pure and therefore no further purification was carried out before use in other syntheses. IR (hexanes) ν(CO) 2106 (vw), 2075 (vs), 2063 (vs), 2039 (s), 2031 (m, sh), 2008 (m-w), 2003 (m-w), 1959 (w) cm^{-1}; IR (CH_2Cl_2, literature values[11]) ν(CO) 2108 (w), 2077 (vs), 2063 (vs), 2040 (vs), 2007 (m), 1955 (w) cm^{-1}; MS (LSIMS) *m/z* 1645.4 (M^+) (calculated for M^+ = 1645 (93.2%), 1646 (100%)).

Preparation of $Os_7(CO)_{21}$ (2) A Schlenk tube with (**1**) (75 mg, 0.030 mmol) and $Os(CO)_5$ (0.219 mol/L, 0.88 mmol) in 5 mL of hexanes dissolved in CH_2Cl_2 (5 mL) was cooled to -78 °C. To the cooled solution, Me_3NO (4 mg, 0.053 mmol) dissolved in 10 mL of CH_2Cl_2) was added dropwise over 30 minutes. The solution was left to stir for 30 minutes at -78 °C and then allowed to warm to room temperature. The solution was filtered through a small column of silica gel–60 (to remove the salt $[Os_6(H)(CO)_{17}][N(CH_2)Me_2]$) and evaporated to dryness on the vacuum line. The remaining solid was then subjected to chromatography on a silica gel–60 column (1.5 x 18 cm). Elution with CH_2Cl_2/hexanes (2:5) gave an orange band of compound **2** (only trace amount were isolated). The only other product of the reaction was the brown salt $[Os_6(H)(CO)_{17}][N(CH_2)Me_2]$ (detected by the presence of a strong band at 2016 cm^{-1} in the infrared spectrum of the reaction mixture) which was removed by filtering the reaction mixture through silica gel. IR (CH_2Cl_2) ν(CO) 2111 (vw), 2075 (s), 2058 (vs), 2037 (m, broad), 2000 (w,br) cm^{-1}; IR (CH_2Cl_2, literature

values[11]) ν(CO) 2112 (vw), 2076 (m), 2060 (vs), 2038 (w), 2002 (w) cm^{-1}; MS (LSIMS) *m/z* 1920.9 (M^+) [calculated for M^+ = 1920 (100%), 1921 (97.7%)].

Preparation of $Os_7(CO)_{20}(CNBu^t)$ (3) A Schlenk tube with compound **1** (20 mg, 0.012 mmol) and $Os(CO)_4(CNBu^t)$ (20 mg, 0.052 mmol) dissolved in CH_2Cl_2 (20 mL) was cooled to -78 °C. To the cooled solution, Me_3NO (2 mg, 0.027 mmol) dissolved in 5 mL of CH_2Cl_2) was added dropwise over 20 minutes. The solution was left to stir for 30 minutes at -78 °C and then allowed to warm to room temperature. The solution was filtered through a small column of silica gel–60 (to remove the salt $[Os_6(H)(CO)_{17}][N(CH_2)Me_2]$) and evaporated to dryness on the vacuum line. The remaining solid was then subjected to chromatography on a silica gel–60 column (1.5 x 18 cm). Elution with CH_2Cl_2/hexanes (1:9) gave an orange band of $Os_7(CO)_{20}(CNBu^t)$ (**3**) (7 mg, ~29% yield). The analytical sample of compound **3** was obtained as air stable red crystals by the slow evaporation of a CH_2Cl_2/hexanes solution. Besides the product mentioned above, the only other product of the reaction was the brown salt $[Os_6(H)(CO)_{17}][N(CH_2)Me_2]$ (detected by the presence of a strong band at 2016 cm^{-1} in the infrared spectrum of the reaction mixture) which was removed by filtering the reaction mixture through silica gel–60. IR (CH_2Cl_2) ν(CN) 2190 (m-w, br) cm^{-1}; ν(CO) 2099 (w, sh), 2094 (m-w), 2067 (m-w), 2052 (vs), 2045 (s, sh), 2027 (m-w), 2007 (vw), 1988 (m-w, br) cm^{-1}; ^1H NMR ($CDCl_3$) δ 1.64 with weak peaks at 1.520 and 1.525; $^{13}C\{^1H\}$ NMR (CH_2Cl_2/CD_2Cl_2, 4:1, rt) δ 187.1 (9C), 183.7 (9C), 181.4 (2C), 28.5 (CH_3); MS (LSIMS) *m/z* 1974.7 (M^+)

[calculated for M^+ = 1974 (93.8%), 1975 (100%)]. Anal. calc. for $C_{25}H_9O_{20}Os_7N$: C, 15.20, H, 0.46, N, 0.71. Found: C, 15.42, H, 0.54, N, 0.76.

Preparation of $Os_7(CO)_{20}(PMe_3)$ (4) A Schlenk tube with compound **1** (20 mg, 0.012 mmol) and $Os(CO)_4(PMe_3)$ (20 mg, 0.057 mmol) dissolved in CH_2Cl_2 (5 mL) was cooled to -78 °C. To the cooled solution, Me_3NO (2 mg, 0.027 mmol) dissolved in 5 mL of CH_2Cl_2) was added dropwise over 20 minutes. The solution was left to stir for 30 minutes at -78 °C and then allowed to warm to room temperature. The solution was filtered through a small column of silica gel–60 (to remove the salt $[Os_6(H)(CO)_{17}][N(CH_2)Me_2]$) and evaporated to dryness on the vacuum line. The remaining solid was then subjected to chromatography on a silica gel–60 column (1.5 x 20 cm). Elution with CH_2Cl_2/hexanes (2:3) gave an orange band of $Os_7(CO)_{20}(PMe_3)$ (**4**), $Os_7(\mu\text{-}H)_2(CO)_{20}(PMe_3)$ (**9**) and $Os_6(CO)_{17}(PMe_3)$. The orange solution was then subjected to chromatography on a second silica gel–60 column (1.5 x 20 cm). Elution with ethyl acetate/hexanes (1:9) gave three bands: the first was a brown band of $Os_6(CO)_{17}(PMe_3)$ (trace amounts), the second was an orange band of $Os_7(CO)_{20}(PMe_3)$ (**4**) (4 mg, ~17% yield) and the third was a red band of $Os_7(\mu\text{-}H)_2(CO)_{20}(PMe_3)$ (**9**) (trace amounts). The analytical sample of compound **4** was obtained as air stable red crystals by the slow evaporation of a CH_2Cl_2/hexanes solution. Besides the products mentioned above, the only other product of the reaction was the brown salt $[Os_6(H)(CO)_{17}][N(CH_2)Me_2]$ (detected by the presence of a strong band at 2016 cm^{-1} in the infrared spectrum of the reaction mixture) which was removed by filtering the reaction mixture through

silica gel. IR (CH_2Cl_2) ν(CO) 2094 (m-w), 2049 (vs), 2041 (s, sh), 2023 (m-w, br), 1980 (w, broad) cm^{-1}; ^1H NMR (CD_2Cl_2) δ 2.13 (d, $J(^1H–^{31}P)$ = 10.7 Hz); $^{31}P\{^1H\}$ NMR (CD_2Cl_2) δ -14.2; $^{13}C\{^1H\}$ NMR (CH_2Cl_2/CD_2Cl_2, 4:1, rt) δ 187.7 (9C), 185.7 (9C), 184.2 (2C, $J(^{13}C-^{31}P)$ = 10.7 Hz); MS (LSIMS) *m/z* 1968.4 (M^+) [calculated for M^+ = 1968 (100%), 1969 (97.8%)]. Anal. calc. for $C_{23}H_9O_{20}Os_7P$: C, 14.04, H, 0.46. Found: C, 13.93, H, 0.57.

Preparation of $Os_7(CO)_{20}(PEt_3)$ (5) A Schlenk tube with compound **1** (20 mg, 0.012 mmol) and $Os(CO)_4(PEt_3)$ (20 mg, 0.055 mmol) dissolved in CH_2Cl_2 (5 mL) was cooled to -78 °C. To the cooled solution, Me_3NO (2 mg, 0.027 mmol) dissolved in 5 mL of CH_2Cl_2 was added dropwise over 20 minutes. The solution was left to stir for 30 minutes at -78 °C and then allowed to warm to room temperature. The solution was filtered through a small column of silica gel–60 (to remove the salt $[Os_6(H)(CO)_{17}][N(CH_2)Me_2]$) and evaporated to dryness on the vacuum line. The remaining solid was then subjected to chromatography on a silica gel–60 column (1.5 x 20 cm). Elution with CH_2Cl_2/hexanes (3:7) gave an orange band of $Os_7(CO)_{20}(PEt_3)$ (**5**), $Os_7(\mu\text{-}H)_2(CO)_{20}(PEt_3)$ and $Os_6(CO)_{17}(PEt_3)$. The orange solution was then subjected to chromatography on a silica gel–60 gel column (1.5 x 20 cm). Elution with ethyl acetate/hexanes (1:7) gave three bands: the first was a brown band of $Os_6(CO)_{17}(PEt_3)$ (trace amounts), the second was an orange band of $Os_7(CO)_{20}(PEt_3)$ (**5**) (3 mg, ~12% yield), and the third was a red band of $Os_7(\mu\text{-}H)_2(CO)_{20}(PEt_3)$ (trace amounts). Air sensitive red/orange crystals were obtained by dissolving compound **5** in a minimal amount of CH_2Cl_2 with layer of hexanes on top and placing the solution

in the freezer (-29 °C). Besides the products mentioned above, the only other product of the reaction was the brown salt $[Os_6(H)(CO)_{17}][N(CH_2)Me_2]$ (detected by the presence of a strong band at 2016 cm^{-1} in the infrared spectrum of the reaction mixture) which was removed by filtering the reaction mixture through silica gel. IR (CH_2Cl_2) ν(CO) 2093 (m-w), 2048 (vs, br), 2040 (s, sh), 2023 (m-w, br), 1987 (w, sh) 1980 (w) cm^{-1}; ^1H NMR (C_6D_6) δ 1.63 (m, 2H) and 0.57 (dt, $J_1(^1H–^{31}P)$ = 7.5 Hz and J_2 = 17.3 Hz, 3H); $^{31}P\{^1H\}$ NMR (CD_2Cl_2) δ +20.0; $^{13}C\{^1H\}$ NMR (CH_2Cl_2/CD_2Cl_2, 4:1, rt) δ 187.0 (9C), 185.4 (9C), 184.7 (2C, $J(^{13}C-^{31}P)$= 10.4 Hz); MS (LSIMS) *m/z* 2010.6 (M^+) [calculated for M^+ = 2010 (100%), 2011 (98.0%)]. Anal. calc. for $C_{26}H_{15}O_{20}Os_7P$: C, 15.54, H, 0.75. Found: C, 15.32, H, 0.72.

Preparation of $Os_7(CO)_{20}[P(OMe)_3]$ (6) A Schlenk tube with compound **1** (20 mg, 0.012 mmol) and $Os(CO)_4[P(OMe)_3]$ (20 mg, 0.047 mmol) dissolved in CH_2Cl_2 (5 mL) was cooled to -78 °C. To the cooled solution, Me_3NO (2 mg, 0.027 mmol) dissolved in 5 mL of CH_2Cl_2 was added dropwise over 20 minutes. The solution was left to stir for 30 minutes at -78 °C and then allowed to warm to room temperature. The solution was filtered through a small column of silica gel (to remove the salt $[Os_6(H)(CO)_{17}][N(CH_2)Me_2]$) and evaporated to dryness on the vacuum line. The remaining solid was then subjected to chromatography on a silica gel–60 column (1.5 x 20 cm). Elution with CH_2Cl_2/hexanes (2:3) gave an orange band of $Os_7(CO)$ $[P(OMe)_3]$ (**6**), $Os_7(\mu\text{-}H)_2(CO)[P(OMe)_3]$ and $Os_6(CO)_{17}[P(OMe)_3]$. The orange solution was then subjected to chromatography on a second silica gel–60 column (1.5 x 20 cm). Elution with

ethyl acetate/hexanes (1:9) gave three bands: the first was a brown band of $Os_6(CO)_{17}[P(OMe)_3]$ (trace amounts), the second was an orange band of $Os_7(CO)_{20}[P(OMe)_3]$ (**6**) (5 mg, ~21% yield) and the third was a red band of $Os_7(\mu\text{-}H)_2(CO)[P(OMe)_3]$ (trace amounts). Air stable red/orange crystals were obtained by dissolving compound **6** in a minimal amount of CH_2Cl_2 with a layer of hexanes on top and placing the solution in the freezer (-29 °C). Besides the products mentioned above, the only other product of the reaction was the brown salt $[Os_6(H)(CO)_{17}][N(CH_2)Me_2]$ (detected by the presence of a strong band at 2016 cm^{-1} in the infrared spectrum of the reaction mixture) which was removed by filtering the reaction mixture through silica gel–60. IR (CH_2Cl_2) ν(CO) 2095 (w), 2065 (w, sh) 2050 (vs), 2045 (s, sh), 2027 (w, sh), 2006 (vw) 1988 (w, br) cm^{-1}; ^1H NMR (CD_2Cl_2) δ 4.00 (d, $J(^1H–^{31}P)$ = 11.9 Hz) with weak peaks at δ 3.84 (d, $J(^1H–^{31}P)$ = 11.3 Hz); $^{31}P\{^1H\}$ NMR (CD_2Cl_2) δ +94.9 with a weak peak at δ +107.9; $^{13}C\{^1H\}$ NMR (CH_2Cl_2/CD_2Cl_2, 4:1, rt) δ 187.1 (9C), 184.7 (9C), 183.4 (2C, $J(^{13}C\text{-}^{31}P)$ = 15.2 Hz); MS (LSIMS) *m/z* 2016.9 (M^+) [calculated for M^+ = 2016 (100%), 2017 (97.8%)]. Anal. calc. for $C_{23}H_9O_{23}Os_7P$: C, 13.70, H, 0.45. Found: C, 13.95, H, 0.54.

Preparation of $Os_7(CO)_{20}[P(OCH_2)_3CMe]$ (7) A Schlenk tube with compound **1** (20 mg, 0.012 mmol) and $Os(CO)_4[P(OCH_2)_3CMe]$ (20 mg, 0.044 mmol) dissolved in CH_2Cl_2 (5 mL) was cooled to -78 °C. To the cooled solution, Me_3NO (2 mg, 0.027 mmol) dissolved in 5 mL of CH_2Cl_2 was added dropwise over 20 minutes. The solution was left to stir for 30 minutes at -78 °C and then allowed to warm to room temperature. The solution was filtered through a small

column of silica gel–60 (to remove the salt $[Os_6(H)(CO)_{17}][N(CH_2)Me_2]$) and evaporated to dryness on the vacuum line. The remaining solid was then subjected to chromatography on a silica gel–60 column (1.5 x 20 cm). Elution with CH_2Cl_2/hexanes (9:31) gave an orange band of $Os_7(CO)_{20}[P(OCH_2)_3CMe]$ (**7**), and $Os_6(CO)_{17}[P(OCH_2)_3CMe]$. The orange solution was then subjected to chromatography on a second SilicAR (CC-7) column (1.5 x 20 cm). Elution with ethyl acetate/hexanes (1:9) gave two bands: the first was a brown band of $Os_6(CO)_{17}[P(OCH_2)_3CMe]$ (trace amounts) and the second band was an orange band of $Os_7(CO)_{20}[P(OCH_2)_3CMe]$ (**7**) (6 mg, ~25% yield). Air stable red crystals were obtained by dissolving compound **7** in a minimal amount of toluene and placing the solution in a refrigerator (0 °C). Besides the products mentioned above, the only other product of the reaction was the brown salt $[Os_6(H)(CO)_{17}][N(CH_2)Me_2]$ (detected by the presence of a strong band at 2016 cm^{-1} in the infrared spectrum of the reaction mixture) which was removed by filtering the reaction mixture through silica gel–60. IR (CH_2Cl_2) ν(CO) 2101 (w, sh), 2097 (w) 2066 (m), 2051 (s, br), 2029 (w, sh), 2008 (vw) 1990 (w, br) 1978 (vw, sh) cm^{-1}; ^1H NMR (C_6D_6) δ 3.27 (d, $J(^1H–^{31}P)$ = 5.4 Hz, 6H), and -0.54 (s, 3H) with a second set of weaker peaks at δ 3.19 (d, $J(^1H–^{31}P)$ = 5.1 Hz, 6H), and δ -0.58 (s, 3H); $^{31}P\{^1H\}$ NMR (CD_2Cl_2) δ +94.1 with a weaker peak at δ +108.6 ; $^{13}C\{^1H\}$ NMR (CH_2Cl_2/ CD_2Cl_2, 4:1, rt) δ 187.5 (9C), 184.5 (9C), 182.4 (2C, J_{C-P} = 20.0 Hz) with weaker peaks at δ 187.2, 184.7, 182.6; MS (LSIMS) *m/z* 2039.3 (M^+) [calculated for M^+ = 2039 (93.8%), 2040 (100%)]. Anal. calc. for $C_{25}H_9O_{23}Os_7P$: C, 14.72, H, 0.44. Found: C, 14.90, H, 0.68.

Preparation of $Os_7(CO)_{20}(PPh_3)$ (8) A Schlenk tube with (**1**) (20 mg, 0.012 mmol) and $Os(CO)_4(PPh_3)$ (20 mg, 0.052 mmol) dissolved in CH_2Cl_2 (5 mL) was cooled to -78 °C. To the cooled solution, Me_3NO (2 mg, 0.027 mmol) dissolved in 5 mL of CH_2Cl_2 was added dropwise over 20 minutes. The solution was left to stir for 30 minutes at -78 °C and then allowed to warm to room temperature. The solution was filtered through a small column of silica gel–60 (to remove the salt $[Os_6(H)(CO)_{17}][N(CH_2)Me_2]$) and evaporated to dryness on the vacuum line. The remaining solid was then subjected to chromatography on a silica gel–60 column (1.5 x 18 cm). Elution with CH_2Cl_2/hexanes (1:9) gave two bands: the first a brown band of $Os_6(CO)_{17}(PPh_3)$ (9 mg, 39% yield) and the second an orange band of $Os_7(CO)_{20}(PPh_3)$ (**8**) (~2 mg, ~8% yield). $Os_6(CO)_{17}(PPh_3)$ was identified by its infrared spectrum.[35] Besides the product mentioned above, the only other product of the reaction was the brown salt $[Os_6(H)(CO)_{17}][N(CH_2)Me_2]$ (detected by the presence of a strong band at 2016 cm^{-1} in the infrared spectrum of the reaction mixture) which was removed by filtering the reaction mixture through silica gel-60. IR (CH_2Cl_2) ν(CO) 2093 (m), 2069 (m), 2050 (vs), 2043 (s, sh), 2026 (m), 2008 (vw), 1988 (w, br) cm^{-1} ; MS (LSIMS) *m/z* 2154.5 (M^+) [calculated for M^+ = 2154 (100%), 2155 (99.1%)]. (Unfortunately, not enough material was isolated to fully characterize compound **8**.)

Preparation of $Os_7(\mu\text{-}H)_2(CO)_{19}(PMe_3)$ (9) A Schlenk tube with $Os_7(\mu\text{-}H)_2(CO)_{20}$ (20 mg, 0.011 mmol) and an excess of PMe_3 dissolved in CH_2Cl_2 (20 mL) was cooled to -78 °C. Me_3NO [2 mL of a solution of 8 mg (0.11

mmol) of Me_3NO dissolved in 20 mL of CH_2Cl_2] was added dropwise over 10 minutes. The solution was left to stir for 30 minutes at -78 °C and then allowed to warm to room temperature. The solution was filtered through a small column of silica gel-60 (to remove any excess Me_3NO) and evaporated to dryness on the vacuum line. The remaining solid was then subjected to chromatography on a silica gel–60 column (1.5 x 20 cm). Elution with CH_2Cl_2/hexanes (9/31) gave two red bands: the first $Os_7(\mu\text{-}H)_2(CO)_{20}$ and the second $Os_7(\mu\text{-}H)_2(CO)_{20}PMe_3$ (**9**) (11 mg, ~54% yield). Use of several crystallization methods to obtain single crystals were unsuccessful, such as: slow evaporation of CH_2Cl_2, CH_2Cl_2/hexanes, toluene or chlorobenzene solutions of **9**; cooling of saturated of CH_2Cl_2/hexanes, toluene or chlorobenzene solutions of **9** to -40 °C for several days. IR (CH_2Cl_2) ν(CO) 2097 (m), 2059 (vs, br), 2047 (s), 2004 (s, br), 1933 (vw, br) cm^{-1}; ^1H NMR (CD_2Cl_2) δ 2.02 (d, $J(^1H–^{31}P)$ = 8.4 Hz, 9H), -13.90 (s, 2H); $^{31}P\{^1H\}$ NMR (CH_2Cl_2) δ -36.2; MS (LSIMS) *m/z* 1941.8 (M^+) (calculated for M^+ = 1941 (93.8%), 1942 (100%)). Anal. calc. for $C_{22}H_{11}O_{19}Os_7P$: C, 13.61, H, 0.57. Found: C, 13.72, H, 0.52.

Preparation of $Os(CO)_4(PEt_3)$ To a Schlenk tube was added $Os(CO)_5$ (0.131 mol/L, 3.93 mmol) in 30 mL of hexanes and an excess of PEt_3. To the stirring solution, Me_3NO (295 mg, 3.93 mmol) dissolved in 30 mL of CH_2Cl_2 was added dropwise (via a dropping funnel) over several hours. The solution was filtered through a small column of silica gel–60, to remove excess Me_3NO, and evaporated to dryness on the vacuum line. Excess PEt_3 was also removed on the vacuum line. $Os(CO)_4(PEt_3)$ was purified by recrystallization from hexanes,

giving pale yellow crystals (677 mg, 41% yield). IR (hexanes) ν(CO) 2060 (s), 2078 (m), 1936 (vs) cm^{-1}. IR (hexanes, literature[81]) ν(CO) 2060 (s), 2078 (m), 1936 (vs) cm^{-1}.

Preparation of $Os(CO)_4[P(OCH_2)_3CMe]$ To a Schlenk tube was added $Os(CO)_5$ (0.122 mol/L, 2.44 mmol) in 20 mL of hexanes and an excess of $P(OCH_2)_3CMe$. To the stirring solution, Me_3NO (183 mg, 2.44 mmol) dissolved in 30 mL of CH_2Cl_2 was added dropwise (via a dropping funnel) over several hours. The solution was filtered through a small column of silica ge–60, to remove excess Me_3NO, and evaporated to dryness on the vacuum line. Excess $P(OCH_2)_3CMe$ was removed by sublimation on to a dry ice cooled probe, giving a pure sample of $Os(CO)_4[P(OCH_2)_3CMe]$ (**12**) (626 mg, 57% yield). IR (hexanes) ν(CO) 2093 (vw), 2076 (s), 2001 (m), 1967 (vs) cm^{-1}. IR (hexanes, literature[50]) ν(CO) 2092 (vw), 2076 (s), 2009 (w), 2001 (m), 1967 (vs) cm^{-1}.

Preparation of $Os(H)_2(CO)_4$ $Os_3(CO)_{12}$ (1.018 g, 1.123 mmol) and hexanes (130 mL) was added into a 500 mL autoclave. The autoclave was sealed and flushed three times with CO (~ 500 psi). The autoclave was then pressurized with 750 psi of H_2 and 2250 psi of CO (for a total pressure of 3000 psi). The vessel was heated to 300 °C for 24 hours. The vessel was returned to room temperature, the gases were vented and the contents transferred to a 250 mL round bottom flask. In order to assure that compound **13** was pure, the volatile compound was condensed *in vacuo* into another 250 mL round bottom flask kept at -196 °C. An IR spectrum of the solution showed that the sample was pure. The absence of $Os_3(CO)_{12}$ in the autoclave, round bottom flask and IR

spectrum indicated that **13** had formed in a quantitative yield. IR (hexanes) ν(CO) 2141 (w), 2067 (m), 2055 (s), 2049 (vs), 2017 (w) cm^{-1}. IR (hexanes, literature[82]) ν(CO) 2141 (w), 2067 (m), 2055 (s), 2048 (vs), 2016 (w) cm^{-1}.

Preparation of Quinuclidine *N*–oxide In a 100 mL round bottom flask, quinuclidine hydrochloride (103 mg, 0.70 mmol) was dissolved in 10 mL of chloroform. The solution was cooled to 0 °C and to the cooled solution; sodium bicarbonate (65 mg, 0.77 mmol) was added. To the stirring solution *m*-chloroperoxybenzoic acid [124 mg, 0.72 mmol (based 70% purity)] dissolved in 10 mL of chloroform was added dropwise over 30 minutes. The solution was left to stir for 3 hours, during which the solution was allowed to warm to room temperature. The solution was then passed through a small column of basic alumina (6.9 g, 20 times the combined starting material). The column was washed with chloroform, to remove any unreacted quinuclidine. Quinuclidine *N*–oxide was eluted from the column by washing the column with a mixture of chloroform/methanol (3:1). The collected solution was evaporated to dryness on the vacuum line, to give a grey paste. The product was dried by heating to 50 °C under vacuum overnight (74 mg, 86% yield). IR (NaCl) 942 cm^{-1}, ms (EI) *m/z* 127 (M^+).[73, 83]

Attempted preparation of $Os_7(CO)_{20}(PMe_3)$ (4) with Iodosylbenzene To a Schlenk tube was added compound **1** (20 mg, 0.012 mmol), $Os(CO)_4(PMe_3)$ (10 mg, 0.026 mmol), $(C_6H_5)IO$ (6 mg, 0.028 mmol) and CH_2Cl_2 (20 mL). The solution was left to stir. After 1 hour the infrared spectrum showed only compound **1** in solution (i.e. no peaks attributed to $Os(CO)_4(PMe_3)$; no new

peaks were observed. The solution was filtered through a small column of silica gel-60 and evaporated to dryness on the vacuum line; all of the 20 mg of compound **1** were recovered.

Attempted preparation of $Os_7(CO)_{20}(PMe_3)$ (4) with Pyridine *N*–oxide A Schlenk tube with compound **1** (20 mg, 0.012 mmol) and $Os(CO)_4(PMe_3)$ (20 mg, 0.057 mmol) dissolved in CH_2Cl_2 (20 mL) was warmed to 40 °C. To the warmed solution, pyridine *N*–oxide (2 mg, 0.021 mmol) dissolved in 5 mL of CH_2Cl_2 was added dropwise over 10 minutes. The solution was left to stir for 30 minutes at 40 °C and then cooled to room temperature. The solution was filtered through a small column of silica gel-60 (to remove any unreacted pyridine *N*–oxide) and evaporated to dryness on the vacuum line. The remaining solid was then subjected to chromatography on a silica gel–60 column (1.5 x 18 cm). Elution with ethyl CH_2Cl_2/hexanes (2:3) gave only a brown band of $Os_6(CO)_{17}(PMe_3)$ (which was identified on the basis of its infrared ν(CO) 2091 (w), 2056 (s), 2033 (vs), 2025 (vs), 1998 (w), 1974 (vw) cm^{-1}).[35]

Attempted preparation of $Os_7(CO)_{20}(PMe_3)$ (4) with Quinuclidine *N*–oxide A Schlenk tube with compound **1** (20 mg, 0.012 mmol) and $Os(CO)_4(PMe_3)$ (20 mg, 0.057 mmol) dissolved in CH_2Cl_2 (20 mL) was cooled to -78 °C. To the cooled solution, quinuclidine *N*–oxide (3 mg, 0.024 mmol) dissolved in 5 mL of CH_2Cl_2 was added dropwise over 10 minutes. The solution was left to stir for 30 minutes at -78 °C and then allowed to warm to room temperature. The solution was filtered through a small column of silica gel–60 (to remove any unreacted quinuclidine *N*–oxide) and evaporated to dryness on the

vacuum line. The remaining solid was then subjected to chromatography on a silica gel-60 column (1.5 x 18 cm). Elution with CH_2Cl_2/hexanes (2:3) gave only a brown band of $Os_6(CO)_{17}(PMe_3)$ (which was identified on the basis of its infrared spectrum, see attempted preparation above).[35]

Attempted preparation of $Os_6(CO)_{17}[P(Bu^t)_3]$ (11) A Schlenk tube with compound **1** (20 mg, 0.012 mmol) and an excess of $P(Bu^t)_3$ were dissolved in CH_2Cl_2 (5 mL) and cooled to -78 °C. To the cooled solution, Me_3NO (~1 mg, 0.013 mmol) dissolved in 5 mL of CH_2Cl_2 was added drop wise over 20 minutes. The solution was left to stir for 30 minutes at -78 °C and then allowed to warm to room temperature. An infrared spectrum of the reaction mixture revealed only a strong peak at 2016 cm^{-1}, indicating the only product was the brown salt $[Os_6(H)(CO)_{17}][N(CH_2)Me_2]$.

Attempted preparation of $Os_7(CO)_{20}[P(Bu^t)_3]$ (10) A Schlenk tube with compound **1** (20 mg, 0.012 mmol) and $Os(CO)_4[P(Bu^t)_3]$ (20 mg, 0.040 mmol) were dissolved in CH_2Cl_2 (5 mL) and cooled to -78 °C. To the cooled solution, Me_3NO (2 mg, 0.027 mmol) dissolved in 5 mL of CH_2Cl_2 was added drop wise over 20 minutes. The solution was left to stir for 30 minutes at -78 °C and then allowed to warm to room temperature. An infrared spectrum of the reaction mixture revealed only a strong peak at 2016 cm^{-1}, indicating the only product was the brown salt $[Os_6(H)(CO)_{17}][N(CH_2)Me_2]$.

Attempted preparation of $Os_7(CO)_{19}(CNBu^t)_2$ (12) A Schlenk tube with compound **1** (20 mg, 0.012 mmol) and $Os(CO)_3(CNBu^t)_2$ (20 mg, 0.045 mmol) were dissolved in CH_2Cl_2 (5 mL) and cooled to -78 °C. To the cooled solution,

Me_3NO (2 mg, 0.027 mmol) dissolved in 5 mL of CH_2Cl_2 was added drop wise over 20 minutes. The solution was left to stir for 30 minutes at -78 °C and then allowed to warm to room temperature. An infrared spectrum of the reaction mixture revealed only a strong peak at 2016 cm^{-1}, indicating the only product was the brown salt $[Os_6(H)(CO)_{17}][N(CH_2)Me_2]$.

Attempted preparation of a mixed metal cluster with $Re(H)(CO)_5$ A Schlenk tube with compound **1** (20 mg, 0.012 mmol) and an excess of $Re(H)(CO)_5$ in 5 mL of hexanes were dissolved in CH_2Cl_2 (5 mL) and cooled to -78 °C. To the cooled solution, Me_3NO (2 mg, 0.027 mmol) dissolved in 5 mL of CH_2Cl_2 was added drop wise over 20 minutes. The solution was left to stir for 30 minutes at -78 °C and then allowed to warm to room temperature. An infrared spectrum of the reaction mixture revealed only a strong peak at 2016 cm^{-1}, indicating the only product was the brown salt $[Os_6(H)(CO)_{17}][N(CH_2)Me_2]$.

Attempted preparation of a mixed metal cluster with $Re(H)(CO)_4(PPh_3)$ A Schlenk tube with compound **1** (20 mg, 0.012 mmol) and $Re(H)(CO)_4(PPh_3)$ (20 mg, 0.036 mmol) were dissolved in CH_2Cl_2 (5 mL) and cooled to -78 °C. To the cooled solution, Me_3NO (2 mg, 0.027 mmol) dissolved in 5 mL of CH_2Cl_2 was added drop wise over 20 minutes. The solution was left to stir for 30 minutes at -78 °C and then allowed to warm to room temperature. An infrared spectrum of the reaction mixture revealed only a strong peak at 2016 cm^{-1}, indicating the only product was the brown salt $[Os_6(H)(CO)_{17}][N(CH_2)Me_2]$.

Attempted preparation of a mixed metal cluster with $(\eta^5\text{–}C_5Me_5)Ir(CO)_2$ A Schlenk tube with compound **1** (20 mg, 0.012 mmol) and $(\eta^5\text{–}C_5Me_5)Ir(CO)_2$ (20 mg, 0.052 mmol) were dissolved in CH_2Cl_2 (5 mL) and cooled to -78 °C. To the cooled solution, Me_3NO (2 mg, 0.027 mmol) dissolved in 5 mL of CH_2Cl_2 was added drop wise over 20 minutes. The solution was left to stir for 30 minutes at -78 °C and then allowed to warm to room temperature. An infrared spectrum of the reaction mixture revealed only a strong peak at 2016 cm^{-1}, indicating the only product was the brown salt $[Os_6(H)(CO)_{17}][N(CH_2)Me_2]$.

3 Variable Temperature $^{13}C\{^1H\}$ NMR studies of $Os_7(CO)_{20}(L)$ [L = $CNBu^t$, PMe_3, $P(OMe)_3$, PEt_3 and $P(OCH_2)CMe_3$] Clusters[aa]

3.1 Introduction

Metal carbonyl clusters often exhibit the fascinating property of stereochemical nonrigidity.[14, 74, 84, 85] It has been suggested that migration of ligands on metal clusters could give insight into the migration of molecules on the surface of bulk metal catalysts.[85, 86] For example, it has been recently shown that nanoparticles of gold deposited on a range of support materials have the ability to catalyze the conversion of carbon monoxide to carbon dioxide.[87] Although the exact pathway for the migration of carbon monoxide on the surface is not known, some suggestion may come from the migration of carbonyl ligands on metal clusters. Often the migration of carbonyl ligands occurs on the NMR timescale (~10^2 to 10^5 s^{-1}). Therefore, the variable temperature $^{13}C\{^1H\}$ NMR studies of metal carbonyl clusters provides a means of investigating these fluxional processes.

The carbonyl clusters of group 8 (iron, ruthenium and osmium) and their derivatives show a wide range of nonrigidity (also referred to as fluxionality). Both $Fe_3(\mu\text{–}CO)_2(CO)_{10}$[88, 89] and $Ru_3(CO)_{12}$[89] exhibit only one ^{13}C NMR resonance, which persists even at extremely low temperatures. This indicates

[aa] The $Os_7(CO)_{20}(CNBu^t)$ work in this chapter was reproduced with permission. Reference 38. Wilcox, C.T.; Jennings, M.C.; Pomeroy, R.K. *J. Cluster Sci.*, **2004**, *15*, 107. Copyright 2004 with kind permission of Springer Science and Business Media.

that the carbonyl groups are exchanging faster than the NMR timescale. On the other hand, $Os_3(CO)_{12}$ exhibits two ^{13}C NMR resonances, which have been assigned to the axial and equatorial carbonyl groups.[89] Only upon heating to temperatures above 70 °C the two signals coalesce into a single resonance.[89] The activation barrier for axial/equatorial carbonyl exchange in $Os_3(CO)_{12}$ has thus been estimated to be 16.7 kcal mol^{-1}.[89] There has been a great deal of debate concerning plausible mechanisms for carbonyl exchange in the $M_3(CO)_{12}$ clusters.[1, 88, 90] For example, five mechanisms for carbonyl exchange in $Fe_3(\mu\text{–}CO)_2(CO)_{10}$ have been proposed so far.[88, 90, 91]

Although many transition metal binary carbonyl clusters and their derivatives have been extensively investigated, there has been very little examination of the fluxional processes in Os_7 clusters. The only study of the fluxional processes present in the literature is of the parent carbonyl cluster $Os_7(CO)_{21}$ (**2**)[30] (discussed in Chapter 1). Therefore, in this chapter the variable temperature $^{13}C\{^1H\}$ NMR studies of the nonrigidity in $Os_7(CO)_{20}(L)$ [L = $CNBu^t$, PMe_3, PEt_3, $P(OCH_2)_3CMe$ and $P(OMe)_3$] clusters are discussed.

3.2 Variable temperature $^{13}C\{^1H\}$ NMR studies of $Os_7(CO)_{20}(L)$ [L = $CNBu^t$, PMe_3, PEt_3, $P(OCH_2)_3CMe$ and $P(OMe)_3$] clusters

As mentioned in Section 2.3.2, all of the room temperature $^{13}C\{^1H\}$ NMR spectra of the ^{13}CO–enriched samples are consistent with the observed solid–state structures. The spectra all exhibit three major signals (in the carbonyl region) in an approximate ratio of 9:9:2. The room temperature spectra are

consistent with the rapid rotation of two types of $Os(CO)_3$ groups and the rotation of the $Os(CO)_2(L)$ unit (Figure 3.1) in solution.

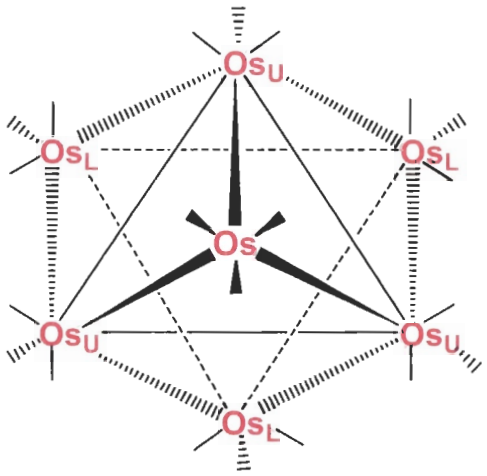

Figure 3.1 View of $Os_7(CO)_{20}(L)$ down the pseudo threefold axis. (U denotes the upper Os_3 triangle and L denotes the lower Os_3 triangle.)

Thus, carbonyl groups exchange rapidly on the individual osmium atoms, but do not exchange between the other osmium atoms of the cluster; if exchange were in fact occurring between the osmium atoms, a singlet would be observed. Even upon heating to 90 °C in toluene–d_8, the $^{13}C\{^1H\}$ NMR spectra of compounds **3** (Figure 3.2, page 94) and **6** (Figure 3.4, page 96) remained unchanged from the room temperature spectrum (additional peaks were observed in the spectrum of compound **3**, likely due to its decomposition). These high temperature spectra remain consistent with the view that the carbonyl groups are rapidly exchanging on individual $Os(CO)_3$ units and are not exchanging between the osmium atoms of the cluster. (Heating of compound **4** to 90 °C resulted in complete decomposition.) Rapid exchange of the carbonyl ligands on individual $Os(CO)_3$

units has been previously observed in $Os_6(CO)_{17}L$ (L = CO and PPh_3)[35, 92] and compound **2**[30].

It is proposed that the three major signals, of approximate 9:9:2 ratio, exhibited in the room temperature $^{13}C\{^1H\}$ NMR spectrum can be assigned on the basis of intensity of the three resonances and the temperatures at which the NMR resonances collapse at low temperatures. The peak of intensity two is assigned to the two carbonyls of the capping $Os(CO)_2(L)$ unit. When L = $CNBu^t$ this resonance is a singlet (Figure 3.2) and is a doublet when L = PMe_3, PEt_3, $P(OCH_2)_3CMe$ and $P(OMe)_3$, due to $^{13}C–^{31}P$ coupling (Figures 3.3–3.6). At lower temperatures in all of the $^{13}C\{^1H\}$ NMR spectra, one of the more intense signals (the resonance at lower frequency, δ 183.7–185.7 ppm, see Figures 3.2–3.6) collapses into the baseline, indicating that the rotation about one type of the $Os(CO)_3$ groups has slowed, but not stopped. The most probable explanation is that the rotation about the $Os(CO)_3$ groups of the inner Os_3 triangle (as indicated in Figure 2.16) have slowed because these carbonyls would have the greatest amount of steric interactions with the carbonyls ligands on neighbouring osmium atoms. For this reason the resonance at lower frequency (δ 183.7 – 185.7 ppm) is assigned to the $Os(CO)_3$ groups of the inner triangle. The resonance at higher frequency ($\delta \approx$ 187 ppm) is therefore assigned to the $Os(CO)_3$ units of the base Os_3 triangle (as indicated in Figure 2.18).

Further confirmation for the assignment of the resonances made above may come from Table 2.6 (page 48). In Table 2.6 it is noticeable that as the electronic and steric properties of the ligand are varied, the resonances at higher

frequency change only slightly (ranging from 187.0 to 187.7 ppm), while the resonances at lower frequency vary more significantly (ranging from 183.7 to 185.7 ppm). The $Os(CO)_3$ groups of the base Os_3 triangle are far enough away from the capping $Os(CO)_2(L)$ unit that a variation in electronic and steric properties of the ligand should have little effect on them, whereas the $Os(CO)_3$ groups of the inner Os_3 triangle are much closer to the capping $Os(CO)_2(L)$ unit and therefore should be more affected by the change in electronic and steric properties of the ligand. It has been previously shown that donor/acceptor properties of PR_3 ligands could be measured by the C–13 shifts of the *cis*–carbonyl groups in $M(CO)_5(PR_3)$ (M = Cr and Mo), $Ni(CO)_3(PR_3)$ and $(\eta^6\text{–}C_6H_6)Cr(CO)_2(PR_3)$ compounds.[93]

3.2.1 Variable Temperature $^{13}C\{^1H\}$ NMR Data for the $Os_7(CO)_{20}(L)$ [L = $CNBu^t$, PMe_3, PEt_3, $P(OCH_2)_3CMe$ and $P(OMe)_3$] clusters.

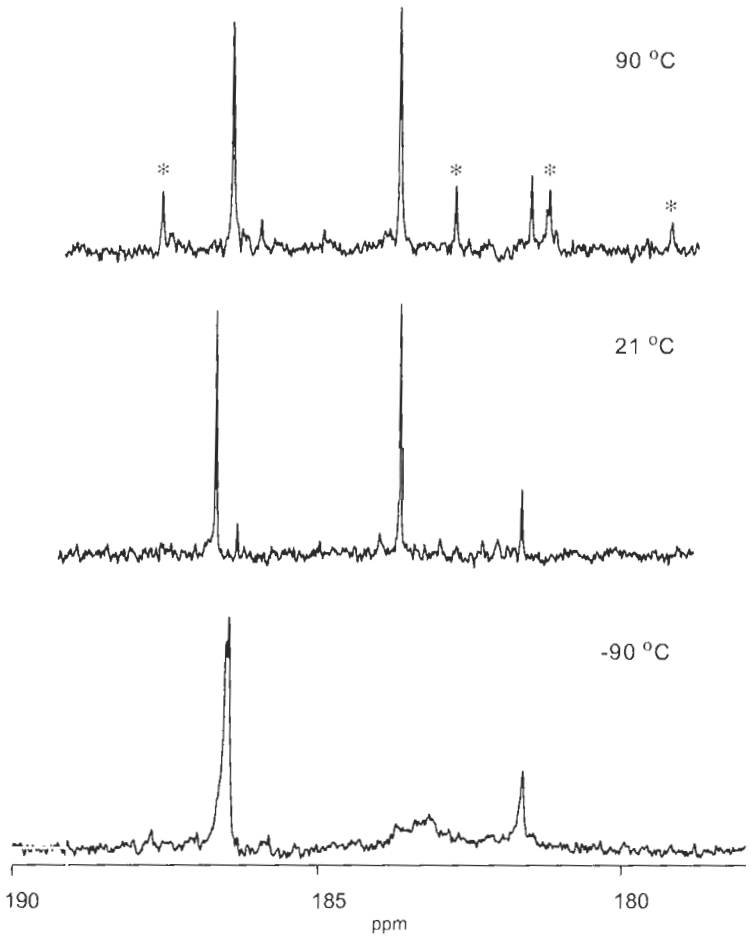

Figure 3.2 Variable temperature $^{13}C\{^1H\}$ NMR spectra of ^{13}CO–enriched $Os_7(CO)_{20}(CNBu^t)$ (3) [spectra recorded in C_7D_8 (+90 °C) and CD_2Cl_2:CH_2Cl_2 (1:4) (21 °C and -90°C)]. Peaks marked with an asterisk are due to decomposition products.

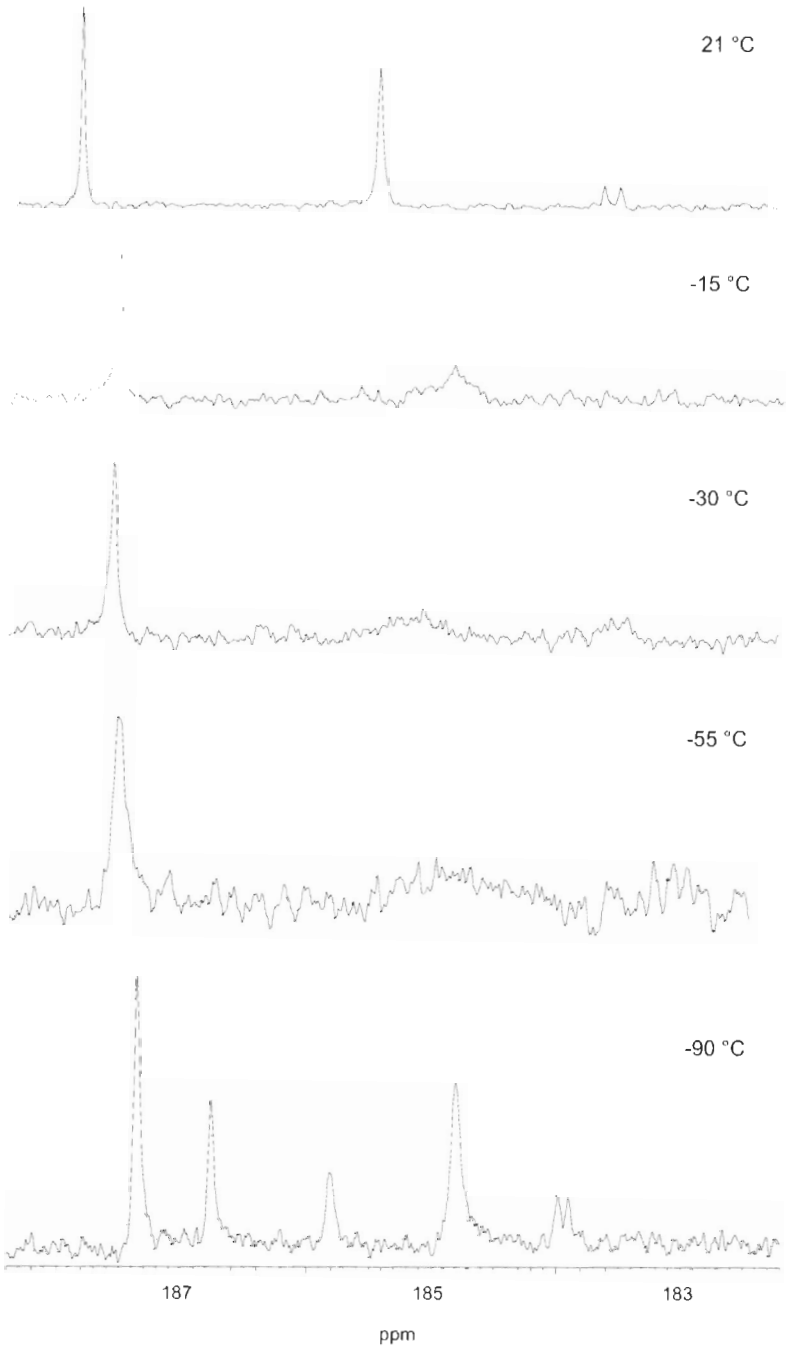

Figure 3.3 Variable temperature $^{13}C\{^1H\}$ NMR spectra of ^{13}CO–enriched $Os_7(CO)_{20}(PMe_3)$ (4) [spectra recorded in CD_2Cl_2:CH_2Cl_2 (1:4) (21 °C through -90°C)].

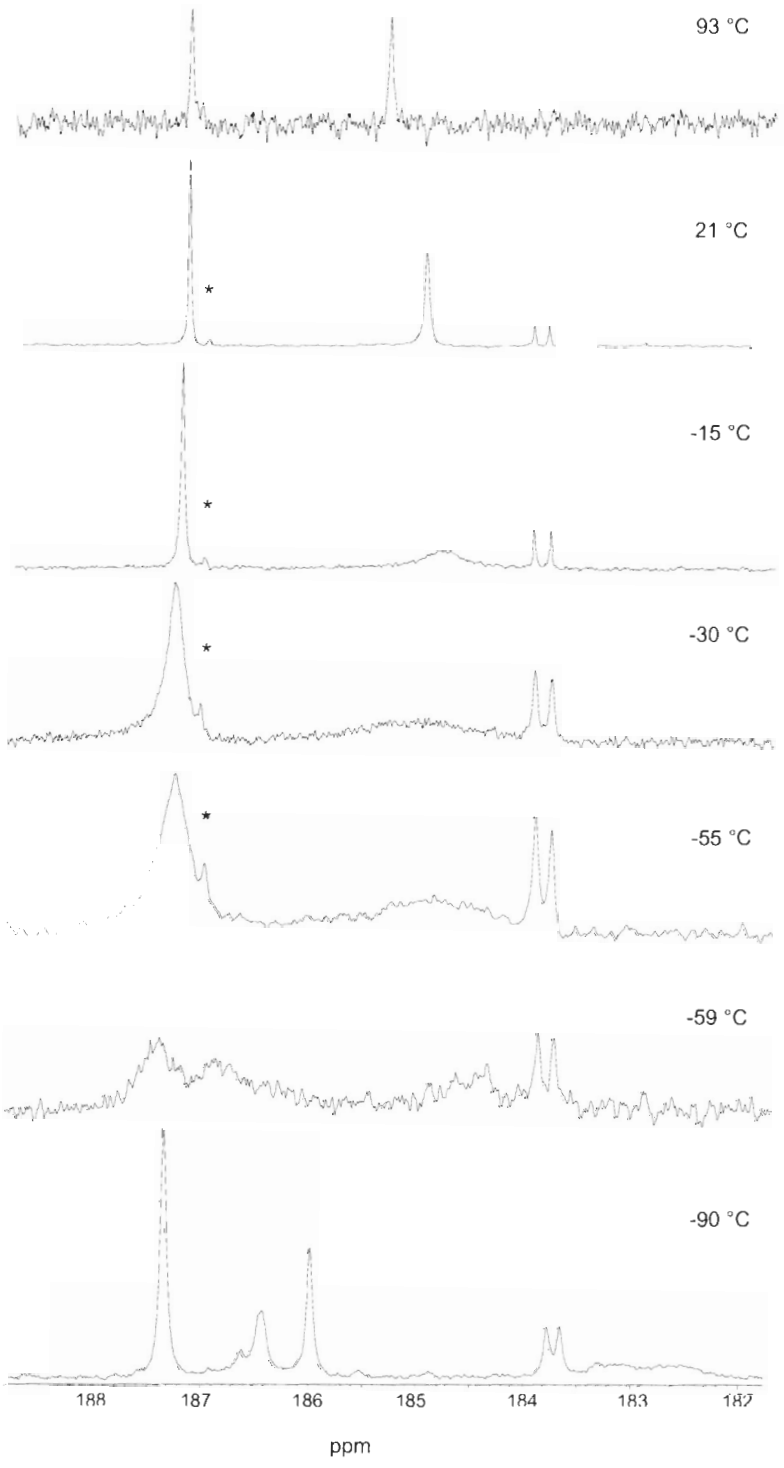

Figure 3.4 Variable temperature $^{13}C\{^{1}H\}$ NMR spectra of ^{13}CO–enriched $Os_7(CO)_{20}[P(OMe)_3]$ (6) [spectra recorded in C_7D_8 (+93 °C) and CD_2Cl_2:CH_2Cl_2 (1:4) (21 °C through -90°C)]. Peaks marked with an asterisk are due to an additional isomer.

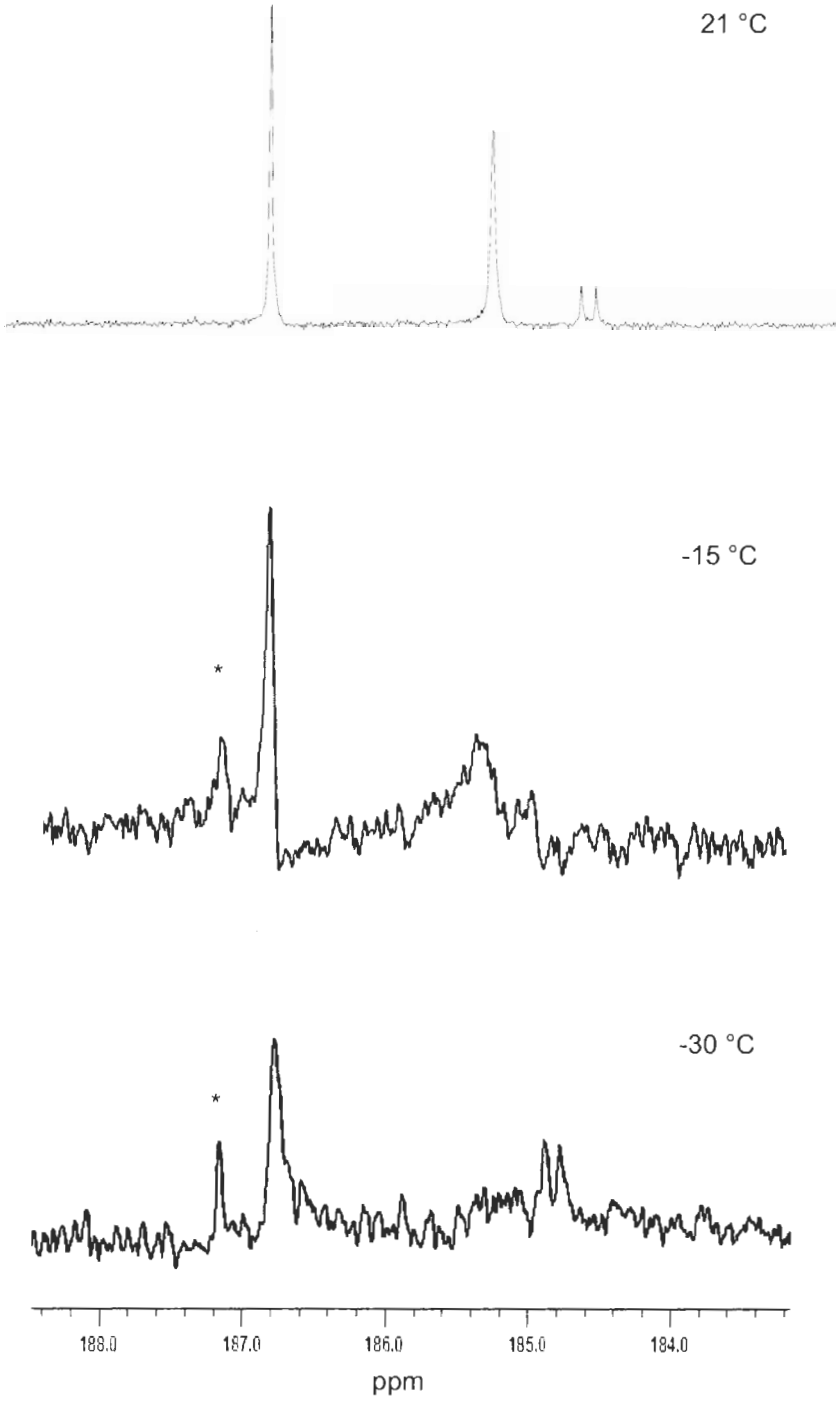

Figure 3.5 Variable temperature $^{13}C\{^1H\}$ NMR spectra of ^{13}CO–enriched $Os_7(CO)_{20}(PEt_3)$ (5) [spectra recorded in CD_2Cl_2:CH_2Cl_2 (1:4) (21 °C and -30°C)]. Peaks marked with an asterisk are due to decomposition products.

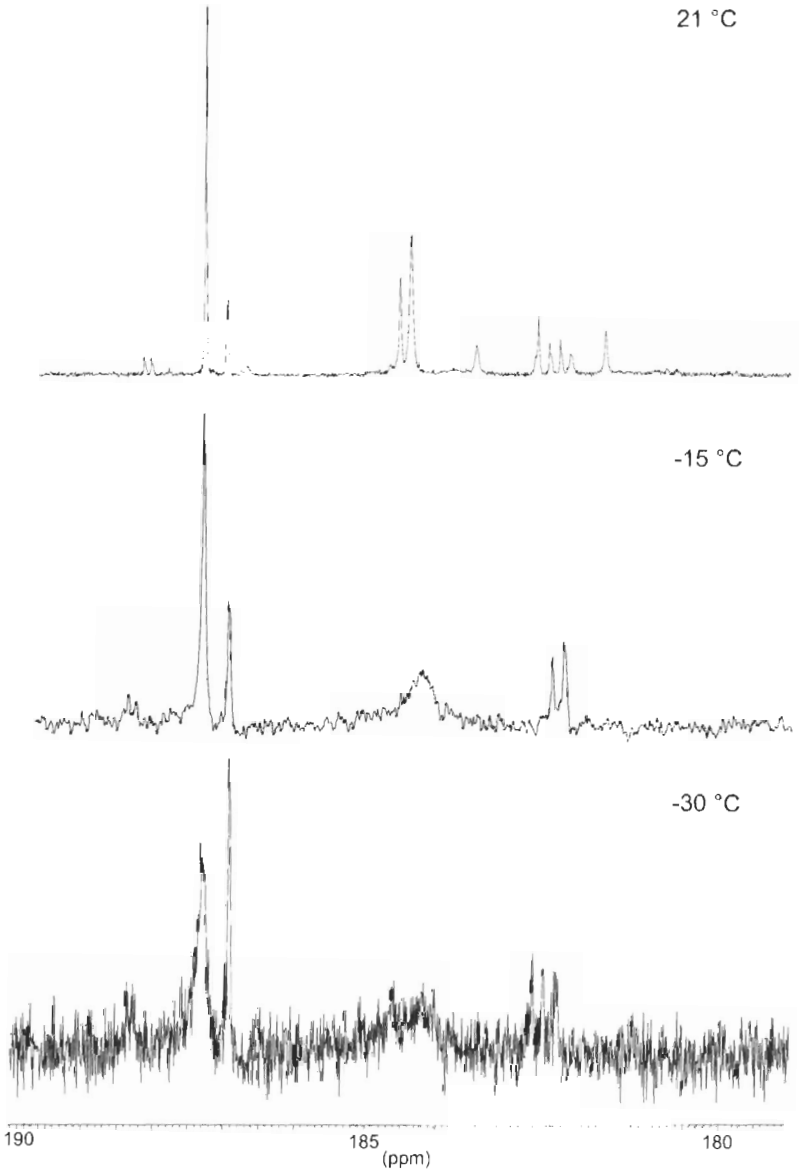

Figure 3.6 Variable temperature $^{13}C\{^1H\}$ NMR spectra of ^{13}CO–enriched $Os_7(CO)_{20}[P(OCH_2)_3CMe]$ (7) [spectra recorded in CD_2Cl_2:CH_2Cl_2 (1:4) (21 °C and -30°C)]. Peaks marked with an asterisk are due to an additional isomer.

Turning to the actual data, the variable temperature $^{13}C\{^1H\}$ NMR spectra of the $Os_7(CO)_{20}(L)$ clusters (Figures 3.2–3.6) are all quite similar, suggesting the mode of collapse of the carbonyl signals is likely the same for all five clusters. In

all of the variable temperature spectra, the two intense resonances (assigned to the $Os(CO)_3$ groups) collapse into the baseline at different temperatures. From this observation, the mechanism for the collapse of the carbonyl signals, at low temperature, in the $Os_7(CO)_{20}(L)$ clusters can be unambiguously determined from a choice of three possible models.

One possibility is that the $Os(CO)_3$ groups and the $Os(CO)_2(L)$ unit all become rigid on the NMR timescale. Fixing the groups to maximize the symmetry of the frozen clusters, the $^{13}C\{^1H\}$ NMR spectrum of the rigid molecule would have eleven different ^{13}CO signals (the mirror plane and equivalent carbonyls are shown in Figure 3.7 along with the proposed $^{13}C\{^1H\}$ NMR spectrum in Figure 3.8). In looking at the variable temperature $^{13}C\{^1H\}$ NMR data, this is clearly inconsistent and thus the carbonyl groups are not all becoming rigid.

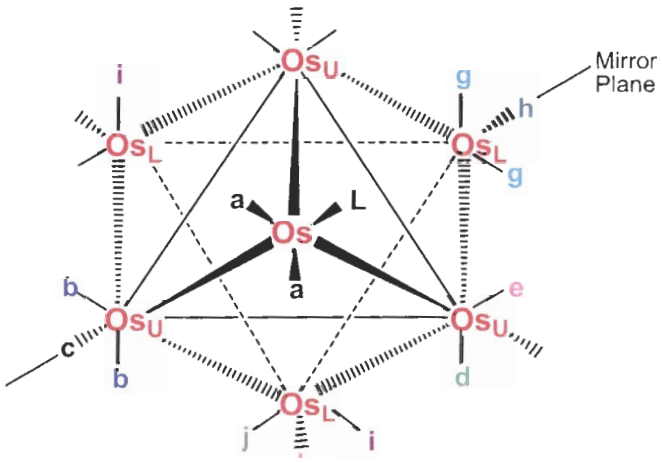

Figure 3.7 **View of $Os_7(CO)_{20}(L)$ down the pseudo threefold axis, showing the mirror plane and the carbonyls that are equivalent if all of the carbonyls are rigid.**

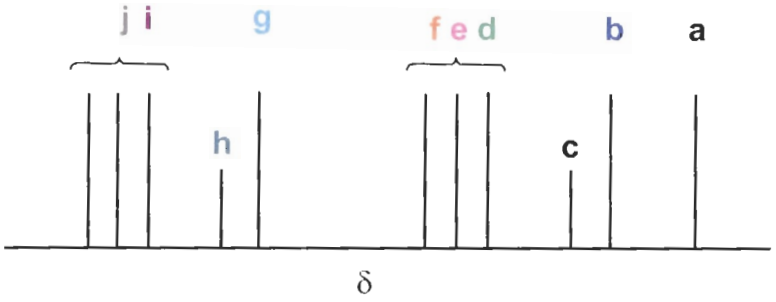

Figure 3.8 Proposed $^{13}C\{^1H\}$ NMR if the carbonyl ligands are rigid on the NMR timescale. In the clusters where PR_3 is the ligand, the carbonyl signal labelled "a" would be a doublet (due to $^{13}C–^{31}P$ coupling)

The other two models for the collapse of the carbonyl signals would have the same equivalent carbonyl groups and proposed $^{13}C\{^1H\}$ NMR spectra, but differ in the temperatures of the collapse of the more intense signals. The first possibility is that the rotation of the $Os(CO)_2(L)$ unit has slowed on the NMR timescale, while the $Os(CO)_3$ groups of the inner and base Os_3 triangles continue to rotate rapidly about their individual osmium atoms. Slowed exchange about the $Os(CO)_2(L)$ group would result in the two intense resonances at higher frequencies to each broaden into a 2:1 resonance pattern at the same temperature (the proposed mode of collapse of the $^{13}C\{^1H\}$ NMR spectra is shown in Figure 3.9 and the equivalent carbonyls are shown in Figure 3.10). Since the two carbonyls associated with the $Os(CO)_2(L)$ unit are chemically equivalent, this signal would remain a sharp singlet (or doublet, when L = PR_3) regardless of whether rotation has slowed. Again, an examination of the variable temperature $^{13}C\{^1H\}$ NMR data (Figures 3.2–3.6) indicated that the simultaneous broadening of the two intense peaks is not occurring, thus excluding a slowing of the $Os(CO)_2(L)$ unit.

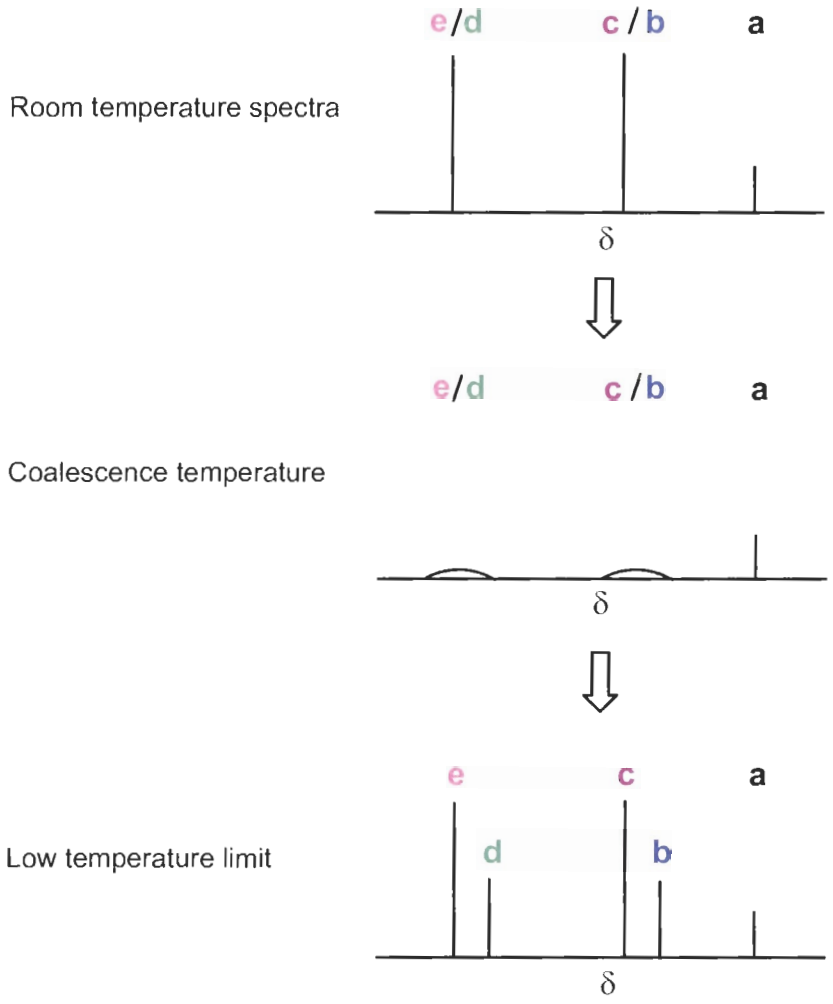

Figure 3.9 Proposed $^{13}C\{^1H\}$ NMR if the $Os(CO)_2(L)$ unit has slowed on the NMR timescale. In the clusters where PR_3 is the ligand, the carbonyl signal labelled "a" would be a doublet (due to $^{13}C–^{31}P$ coupling)

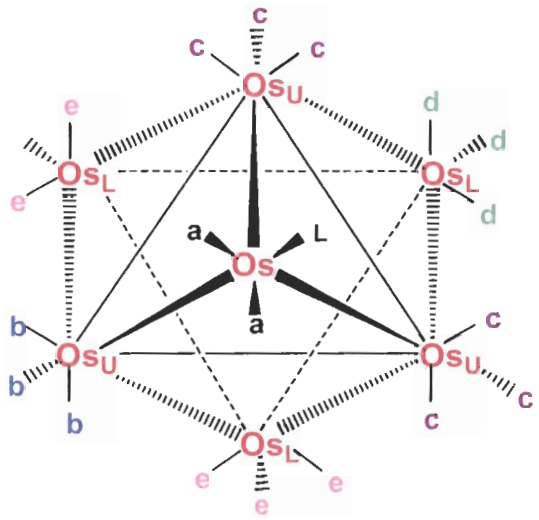

Figure 3.10 View of $Os_7(CO)_{20}(L)$ down the pseudo threefold axis, showing the carbonyls that are equivalent in the low temperature limit spectra of Figure 3.9 and 3.11.

The third possibility is that the rotation about the $Os(CO)_3$ groups of the inner and base Os_3 triangles have begun to slow on the NMR timescale, while the $Os(CO)_2(L)$ unit continues to exchange rapidly. The slowed rotation of the $Os(CO)_3$ groups of the inner and base Os_3 triangle would not likely occur at the same temperature. As a result, the more intense signals would each broaden into a 2:1 pattern at different temperatures (the equivalent carbonyls for the low temperature limit spectra are shown in Figure 3.10, the proposed mode of collapse of the $^{13}C\{^1H\}$ NMR spectra is shown in Figure 3.11 and the slowed rotation of the $Os(CO)_3$ groups of one of the Os_3 triangles is shown in Figure 3.12).

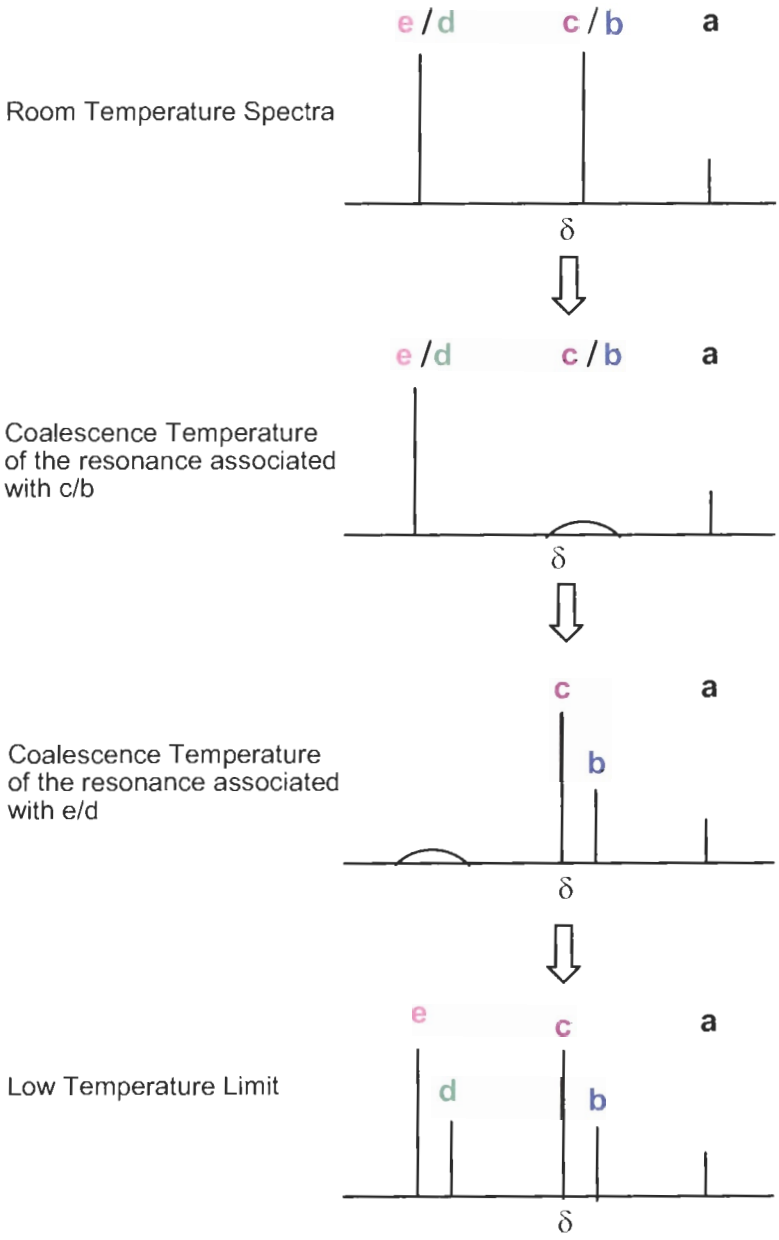

Figure 3.11 Proposed $^{13}C\{^{1}H\}$ NMR if the $Os(CO)_3$ groups of the inner and base Os_3 triangles have slowed on the NMR timescale. In the clusters where PR_3 is the ligand, the carbonyl signal labeled "a" would be a doublet (due to $^{13}C–^{31}P$ coupling).

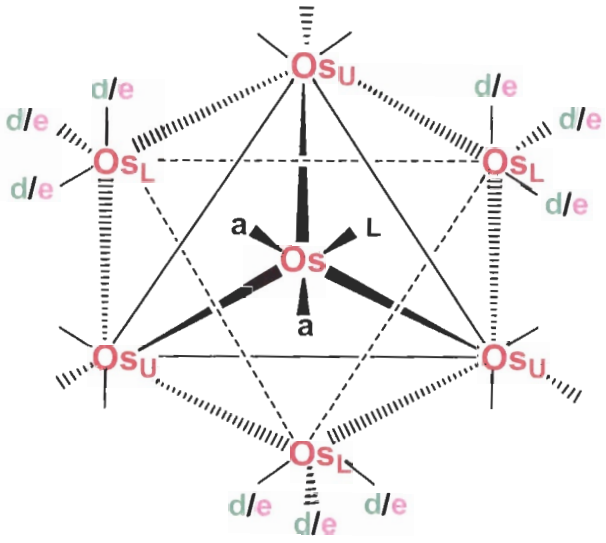

Figure 3.12 Equivalent carbonyls for the room temperature spectra and slowed rotation of the $Os(CO)_3$ groups of one of the Os_3 triangles (Figure 3.11)

Therefore, a collapse of the two intense signals at the same time indicates that the $Os(CO)_2(L)$ unit has slowed, whereas a collapse at different times indicates that the $Os(CO)_3$ groups have slowed on the NMR timescale. Since the signals collapse at different temperatures, the final fluxionality model is most consistent with the observed data.

3.2.2 Analysis of the Variable Temperature $^{13}C\{^1H\}$ NMR Spectra

The variable temperature $^{13}C\{^1H\}$ NMR spectra for $Os_7(CO)_{20}(PEt_3)$ (**5**) and $Os_7(CO)_{20}[P(OCH_2)_3CMe]$ (**7**) were measured, but were complicated due to additional peaks being present in the spectra. Compound **7** consists of two isomers in solution in an approximate ratio of 2:1 (from the ^{31}P NMR), and as can be seen in Figure 3.6, the room temperature spectrum contains additional peaks to those expected based on the structure found in the solid–state. The presence

of two independent molecules with similar fluxional processes makes a detailed analysis difficult. As for compound **5**, its decomposition when exposed to air resulted in additional peaks being present in the variable temperature spectra; delays associated with the spectrometer resulted in its complete decomposition for measurements below -30 °C (as a result the spectra below -30 °C were inconsistent with the solid–state structure). In particular, below -30 °C the variable temperature spectra become extremely complicated, with several additional peaks appearing. Only five peaks are expected in the lowest temperature spectra (i.e. all of the $Os(CO)_3$ units have become rigid on the NMR timescale and the $Os(CO)_2(L)$ unit continues to rotate) for the structure found in the solid-state [as seen in $Os_7(CO)_{20}(PMe_3)$ (**4**) and $Os_7(CO)_{20}[P(OMe)_3]$ (**6**)]. Unfortunately, there are approximately 15 peaks in both the -60 °C and -90 °C spectra, making assignment of peaks very difficult (more data would be required assign the peaks).

Nevertheless, the data obtained to -30 °C for both compounds **5** and **7** (Figures 3.5 and Figure 3.6) is consistent with what is observed for compounds **4** and **6** (Figures 3.3 and 3.4). In all of the five sets of variable temperature spectra (Figures 3.2 – 3.6) the resonance assigned to the $Os(CO)_3$ groups of the inner Os_3 triangle collapses into the baseline by -30 °C, followed by the broadening and eventual collapse of the resonance assigned to the $Os(CO)_3$ groups of the base Os_3 triangle (between -60 °C and -80 °C).[bb] As discussed above, the collapse of the two intense resonances at different temperatures signifies that the

[bb] In the -30 °C spectra of compound **7**, the complete collapse of the resonance assigned to the $Os(CO)_3$ groups of the inner Os_3 triangle is not seen because several new peaks (from the second isomer) have begun to form in this region.

$Os(CO)_3$ groups of the inner and base Os_3 triangles, but not the $Os(CO)_2(L)$ unit, have slowed on the NMR timescale.

Comparison of the variable temperature $^{13}C\{^1H\}$ NMR spectra of the $Os_7(CO)_{20}(L)$ clusters reveals a relatively similar pattern at -90 °C for compounds **6** and **4** (Figures 3.3 and 3.4). In both clusters the two intense resonances each broaden into an approximate 2:1 resonance pattern (in compound **6,** the resonance at higher frequency has not completely formed a 2:1 pattern), indicating that at -90 °C the rotations of the $Os(CO)_3$ groups of the inner and base Os_3 triangles have slowed sufficiently to be resolved on the NMR timescale. As for compound **3**, at -90 °C one of the more intense resonances has completely collapsed into the baseline (Figure 3.2) indicating the slowed rotation of the inner Os_3 triangle. While the intense resonance at higher frequency ($\delta \approx 187$ ppm) appears to be collapsing into a 2:1 pattern, it is not clear whether the 2:1 pattern is authentic or not; it may be that the chemical shift difference for the two resonances of the $Os(CO)_3$ groups related to the base Os_3 triangle is too small for there to be a change in the shape of the resonance. Unfortunately NMR studies at temperatures below -90 °C were not able to be completed for compound **3**.

Comparison of the variable temperature $^{13}C\{^1H\}$ NMR spectra shows a relationship between the coalescence temperature of the carbonyl groups of the inner and base Os_3 triangles and the steric properties of the ligand. When L = CO [i.e. $Os_7(CO)_{21}$ (**2**)], the carbonyl groups associated with the two Os_3 planes only begin to show evidence of slowed rotation at -110 °C.[30] More

sterically demanding ligands causes a decrease in the coalescence temperatures, particularly for the carbonyl groups of the inner Os_3 triangle. Changing the ligand to $CNBu^t$, which is slightly more sterically demanding than CO, causes the coalescence temperature of the carbonyl groups associated with the inner Os_3 triangle to be approximately -90 °C, while the $Os(CO)_3$ groups of the base Os_3 triangle appears to be just showing signs of static behaviour at -90 °C (Figure 3.2). The effect of the ligands size on the coalescence temperature becomes quite evident when L = PMe_3, $P(OMe)_3$, PEt_3 and $P(OCH_2)_3CMe$. In all of the clusters the resonance associated with the carbonyl groups of the inner Os_3 triangle broaden into the baseline by -30 °C (Figure 3.2–3.6), while the resonance related to the carbonyl groups of the base Os_3 triangle (L = PMe_3 and $P(OMe)_3$) broaden into the baseline somewhere between -60 °C and -85°C (Figure 3.3 and 3.4). [In the -59 °C $^{13}C\{^1H\}$ NMR spectrum of compound **6**, the resonance associated with the carbonyl groups of the base Os_3 triangle has not completely broadened into the baseline (Figure 3.3).]

3.2.3 Kinetic parameters

Based on the chemical shift separations of the ^{13}C resonances assigned to the $Os(CO)_3$ groups of the inner (for example see Figure 2.16) and base (for example Os(1)–Os(4)–Os(5) see Figure 2.18) Os_3 triangles and the coalescence temperature, the first order rate constant and the activation energy ($\Delta G^{\ddagger}$) for carbonyl exchange can be calculated by equations 3.1, 3.2 and 3.3, (values are given in Table 3.1).[94]

$$k = (\Delta\delta)\left[\frac{\pi}{(2)^{1/2}}\right] \qquad (3.1)$$

$\Delta\delta$ = difference in resonance frequencies (s^{-1})

$$k_r = \frac{\kappa k T_c}{h} \exp\left[\frac{-\Delta G^{\ddagger}}{RT_c}\right] \qquad (3.2)$$

h = Plank's Constant (6.626×10^{-34} J·s)

T_c = Temperature at coalescence (K)

R = Gas Constant (8.314 J mol^{-1}·K)

κ = Transmission coefficient = 1

k = Boltzmann constant (1.380×10^{-23}) J/K

Rearrangment of eq. 3.2 gives

$$\Delta G^{\ddagger} = [(1.914 \times 10^{-2}\ \text{kJ mol}^{-1})(T_c)][10.319 + \log(T_c/k_r)] \qquad (3.3)$$

Table 3.1 First order rate constant (k) and the activation energy ($\Delta G^{\ddagger}$) for the $Os(CO)_3$ groups of the inner and base Os_3 triangles for $Os_7(CO)_{20}[P(OMe)_3]$ (6) and $Os_7(CO)_{20}(PMe_3)$ (4)

Cluster	Inner $Os(CO)_3$ groups		Base $Os(CO)_3$ groups	
	$k(s^{-1})$	$\Delta G^{\ddagger}$(kJ mol^{-1})	$k(s^{-1})$	$\Delta G^{\ddagger}$(kJ mol^{-1})
$Os_7(CO)_{20}[P(OMe)_3]$ (**6**)	124	49 ± 3	203	41 ± 2
$Os_7(CO)_{20}(PMe_3)$ (**4**)	280	47 ± 2	166	40 ± 4

In comparison, the activation energies ($\Delta G^{\ddagger}$) of the $Os(CO)_3$ groups of the inner Os_3 triangle are higher than those of the $Os(CO)_3$ groups of the base Os_3 triangle. The activation energies are consistent with the steric properties of the cluster. The carbonyl groups of the base Os_3 triangle would only have steric

interactions with the carbonyls groups of the inner Os_3 triangle; this would result in a lower activation barrier. On the other hand, the carbonyl groups of the inner Os_3 triangle would have steric interactions with the carbonyl ligands of the base Os_3 triangle and the carbonyl groups and PR_3 ligand of the capping $Os(CO)_2(PR_3)$ unit therefore, resulting in an increased activation barrier. Comparing the activation energies ($\Delta G^{\ddagger}$) of compounds **4** and **6**, the activation energies of compound **6** are higher than those of compound **4** (Table 3.1). The cone angles of PMe_3 and $P(OMe)_3$ are 118° and 107° respectively[59]; if the activation energies were only being affected by the sterics of the ligand, the PMe_3 derivative would have the higher activation energy. Consequently, it appears as though the activation energies are being affected by both the steric and electronic properties of the ligand.

Looking at the rate constants of compounds **4** and **6**, the rate constants are reversed for the two clusters (in compound **6** the base $Os(CO)_3$ groups have a larger rate constant than the inner $Os(CO)_3$ groups whereas in compound **4**, the inner $Os(CO)_3$ groups have a larger rate constant than the base $Os(CO)_3$ groups). As to why the rates are reversed, one possible explanation is that the electronic properties of the PR_3 ligand may be affecting the rate constants of the inner Os_3 triangle (PMe_3 is a better σ–donor while $P(OMe_3)$ is a better π–acceptor).

Unfortunately, studies at temperatures lower than -90 °C were not able to be completed for **3** and therefore, calculations of the kinetic parameters were not performed.

3.3 Conclusions and Future Work

The mechanism for the collapse of the carbonyl signals, at low temperatures, for the $Os_7(CO)_{20}(L)$ clusters was determined to be similar. In all of the clusters the rotation about the $Os(CO)_3$ groups of the inner Os_3 triangle slows first followed by the slowed rotation about the $Os(CO)_3$ groups of the base Os_3 triangle. The 2:1 intensity pattern seen in the low temperature limit spectra (-90 °C), indicates the capping $Os(CO)_2(L)$ unit continues to rotate rapidly on the NMR timescale.

The variable temperature $^{13}C\{^1H\}$ NMR spectra of the $Os_7(CO)_{20}(L)$ clusters demonstrate relationship between the coalescence temperature of the carbonyl groups of the inner and base Os_3 triangles and the steric properties of the ligand. It appears as though the rate constants of the $Os(CO)_3$ groups of the inner Os_3 triangle are affected significantly by the electronic properties of the ligand, while the activation energies ($\Delta G^{\ddagger}$) appear to be affected by both the steric and electronic properties of the ligand. Further variable temperature $^{13}C\{^1H\}$ NMR experiments are needed to obtain a better understanding of how the electronic and steric properties of the ligand influence the activation energies and rate constants of the $Os_7(CO)_{20}(L)$ clusters.

3.4 Experimental

The ^{13}CO–enriched $Os_7(CO)_{20}(L)$ samples were all prepared by the reaction of ^{13}CO–enriched $Os_6(CO)_{18}$ with trimethylamine *N*–oxide in the presence of an excess of unlabelled $Os(CO)_4(L)$ at -78 °C (eq 3.1). Samples used to obtain the $^{13}C\{^1H\}$ NMR spectra were enriched to ~25–30% with ^{13}CO.

The ^{13}CO–enriched $Os_6(CO)_{18}$ was sequentially prepared from ^{13}CO–enriched $Os_3(CO)_{12}$.[74]

$$Os_6(^{13}CO)_{18} + Os(CO)_4(L) \xrightarrow[-78\ ^\circ C]{Me_3NO} Os_7(^{13}CO)_{20}(L) \qquad (3.1)$$

It is apparent from the room temperature $^{13}C\{^1H\}$ NMR spectrum of the products that that the C–13 isotope has been evenly distributed over all of the carbonyl sites of the clusters (Figures 3.2–3.6). The distribution of the C–13 isotope may occur during the synthesis of the clusters or through exchange of the carbonyl ligands of the octahedron core with the capping $Os(CO)_2(L)$ group (this exchange is not observed on the NMR time scale, however exchange may be occurring more slowly).[74]

The variable temperature $^{13}C\{^1H\}$ NMR spectra of the $Os_7(CO)_{20}(CNBu^t)$ cluster and the room temperature[cc] spectra of the $Os_7(CO)_{20}(PR_3)$ (PR_3 = PMe_3 and $P(OMe)_3$) clusters were obtained on a Bruker AMX 400 (operating at a frequency of 100.6 MHz for ^{13}C NMR).[dd] For the $Os_7(CO)_{20}(PR_3)$ clusters, the $^{13}C\{^1H\}$ NMR spectra from -15 to -60 °C were obtained on a Bruker DRX 400 (operating at a frequency of 100.6 MHz for ^{13}C NMR), and the spectra at +90 °C and -90 °C were obtained a Bruker AVANCE 500 (operating at a frequency of 125.65 MHz for ^{13}C NMR).[ee] For $^{13}C\{^1H\}$ NMR spectra below room temperature, temperatures were calibrated externally with 100% methanol.

[cc] All room temperature spectra obtained by the author.
[dd] Variable temperature spectra obtained at Simon Fraser University by Mrs. Marcy Tracy.
[ee] Variable temperature spectra obtained at the University of Connecticut by Dr. Martha Morton.

4 IMPLICATIONS OF THE WORK CONTAINED IN THIS THESIS

Twenty years ago, the field of osmium carbonyl cluster chemistry was at its peak, with several research groups investigating the properties and structural diversity observed in lower nuclearity clusters (less than six metal atoms). Once the synthesis and characterization of lower nuclearity clusters was exhausted, many research groups moved on to other fields. As a result, the more challenging area of the synthesis and characterization of higher nuclearity osmium clusters (six or more metal atoms) were left relatively untouched. The work of this thesis contributes a reliable synthesis to several high nuclearity clusters: $Os_6(CO)_{18}$ and $Os_7(CO)_{20}(L)$ (L = $CNBu^t$, PMe_3, PEt_3, $P(OMe)_3$, and $P(OCH_2)_3CMe$).

There has been a great deal of discussion about the use of transition metal carbonyl clusters as models for the surface chemistry occurring on bulk metal catalysts. As was discussed in the introduction, clusters possess ligands (CO, H_2) that are known to be involved in heterogeneous catalytic processes on bulk metal surfaces. However, low nuclearity clusters are not good representations of the surfaces of bulk metal catalysts; for the reason that there are not enough metal atoms to give a good representation of a bulk metal catalyst surface. Higher nuclearity clusters are better suited to mimic these surfaces; with more metal atoms, a better representation of a bulk metal surface

is given. Also the metals are not all directly attached to the atom that contains the ligand. This can be seen in the $Os_7(CO)_{20}(L)$ [L = $CNBu^t$, PMe_3 and $P(OCH_2)_3CMe$] clusters (Figures 2.11–2.13), where the base Os_3 triangle has no direct connection to the capping osmium atom. Because of this, some understanding of how changes of a ligand attached to one of the metal atoms in the cluster affects the bonding of metal atoms remote to the substitution site within the cluster (i.e. the reactivity of the cluster). The obvious prerequisite to addressing these questions is the ability to systematically synthesize higher nuclear clusters (i.e. > 6 metal atoms) and the results in this thesis begin to fulfill this need.

With a systematic synthesis in hand, the $^{13}C\{^1H\}$ NMR studies of the $Os_7(CO)_{20}(L)$ [L = $CNBu^t$, PMe_3, $P(OMe)_3$, PEt_3 and $P(OCH_2)_3CMe$] clusters gave some idea of the effects of the ligand on the reactivity of the cluster. When L = CO, the carbonyl groups of the two Os_3 planes only begin to show evidence of slowed rotation at -110 °C (on the NMR timescale) whereas upon changing the ligand to PMe_3, the carbonyl groups of the two Os_3 planes become stationary at -90 °C. Consequently, the ligand not only changes the fluxional behaviour of the $Os(CO)_3$ groups attached to the osmium atom that contains the phosphorus ligand but also impacts the fluxional behaviour of the remote $Os(CO)_3$ groups furthest from the osmium atom containing the phosphorus ligand. Relating this to bulk metal catalysts, for example, if the surface was contaminated purposely or accidentally with trace amounts of a phosphorus ligand, some inference could be made as to how the catalysis rate would be affected.

The next logical step would be the synthesis, characterization and study of the reactivity of $Os_7(H)_2(CO)_{19}(L)$ (L = $CNBu^t$ and PR_3) compounds. Clusters of this type could possibly be used as hydrogenation catalysts and thus as models for heterogeneous hydrogenous systems. A $^{13}C\{^1H\}$ NMR study of these clusters would also be of interest to see how the electronic and steric properties of different ligands affect the fluxional behaviour of the clusters.

APPENDIX

Crystallographic Data for $Os_7(CO)_{20}(CNBu^t)$ (3)

Empirical Formula	$C_{25}H_9NO_{20}Os_7$
Formula Weight (g mol^{-1})	1974.73
Crystal Description	Red Needle
Crystal System	Triclinic
Space Group	*P*-1
a (Å)	10.3357(2)
b (Å)	11.2787(2)
c (Å)	31.2552(7)
α (°)	95.2290(10)
β (°)	98.5790(10)
γ (°)	97.3030(10)
Volume ($Å^{-3}$), *Z*	3550.94(12), 4
D (calculated, Mg m^{-3})	3.694
Absorption Coefficient	25.026
Independent Reflections	12080
R_1, R_w ($I \geq 2.0\sigma(I)$)	0.0638, 0.1479

Fractional Atomic Coordinates for $Os_7(CO)_{20}(CNBu^t)$ (3)

Atom	X	Y	Z
Os1	0.37862(10)	0.09139(9)	0.30140(3)
Os2	0.31224(9)	0.29870(8)	0.34896(3)
Os3	0.57621(9)	0.29123(8)	0.33538(3)
Os4	0.58594(9)	0.07258(8)	0.37398(3)
Os5	0.31216(9)	0.07520(8)	0.38650(3)

Os6	0.51195(8)	0.27595(8)	0.42035(3)
Os7	0.51169(9)	0.49703(8)	0.38134(3)
Os8	0.2516(1)	-0.67277(9)	-0.19447(4)
Os9	0.20199(9)	-0.43939(8)	-0.16184(3)
Os10	0.32837(8)	-0.58511(8)	-0.10420(3)
Os11	0.11209(9)	-0.77806(8)	-0.13001(4)
Os12	-0.01675(9)	-0.62628(9)	-0.18873(4)
Os13	0.06519(9)	-0.54304(9)	-0.09891(3)
Os14	0.27596(9)	-0.35268(9)	-0.07260(3)
O1	0.318(2)	0.207(2)	0.2176(7)
C1	0.338(3)	0.165(2)	0.2487(9)
O2	0.484(2)	-0.1139(18)	0.2547(8)
C2	0.447(3)	-0.038(3)	0.2721(10)
O3	0.118(2)	-0.067(2)	0.2802(7)
C3	0.214(2)	-0.012(2)	0.2903(9)
O4	0.056(2)	0.204(2)	0.2869(8)
C4	0.149(3)	0.225(2)	0.3090(11)
O5	0.138(2)	0.378(2)	0.4144(8)
C5	0.202(3)	0.351(3)	0.3888(10)
O6	0.268(2)	0.494(2)	0.2899(10)
C6	0.291(2)	0.430(2)	0.3166(11)
O7	0.551(3)	0.458(2)	0.2668(9)
C7	0.552(3)	0.398(3)	0.2946(10)
O8	0.8667(18)	0.392(2)	0.3685(7)
C8	0.754(2)	0.359(2)	0.3578(9)
O9	0.693(2)	0.1511(19)	0.2658(8)
C9	0.645(3)	0.196(2)	0.2926(10)
O10	0.8552(17)	0.1594(18)	0.4284(7)
C10	0.750(3)	0.131(2)	0.4069(9)
O11	0.724(2)	-0.076(3)	0.3154(8)
C11	0.671(3)	-0.020(2)	0.3382(10)
O12	0.5662(18)	-0.1409(14)	0.4254(7)
C12	0.565(2)	-0.067(2)	0.4038(8)
O13	0.264(2)	0.0787(19)	0.4813(8)
C13	0.287(3)	0.075(3)	0.4465(12)
O14	0.016(2)	0.0614(19)	0.3647(8)
C14	0.129(3)	0.070(2)	0.3746(9)
O15	0.282(2)	-0.1993(16)	0.3690(8)
C15	0.296(2)	-0.102(3)	0.3762(11)
O16	0.592(2)	0.1166(17)	0.4922(7)
C16	0.555(2)	0.169(3)	0.4634(10)
O17	0.3656(17)	0.3888(19)	0.4869(7)
C17	0.421(3)	0.357(2)	0.4602(11)
O18	0.7785(16)	0.4143(16)	0.4642(6)
C18	0.679(2)	0.373(2)	0.4474(8)
O19	0.491(2)	0.6977(17)	0.3231(8)

C19	0.500(3)	0.628(3)	0.3432(9)
O20	0.3757(19)	0.6348(16)	0.4442(8)
C20	0.425(2)	0.583(2)	0.4213(9)
C21	0.683(2)	0.5881(18)	0.4043(8)
N1	0.788(2)	0.643(2)	0.4175(8)
C22	0.918(2)	0.722(2)	0.4327(10)
C23	0.939(6)	0.718(6)	0.484(2)
H1	0.86110	0.73640	0.49530
H2	1.01320	0.77650	0.49800
H3	0.95580	0.63940	0.49100
C24	1.026(5)	0.640(4)	0.4170(18)
H4	1.04280	0.58230	0.43720
H5	1.10730	0.69080	0.41590
H6	0.99200	0.59830	0.38860
C25	0.909(6)	0.839(5)	0.416(2)
H7	0.85570	0.88380	0.43190
H8	0.86970	0.82650	0.38550
H9	0.99610	0.88410	0.41860
C26	0.971(10)	0.671(9)	0.460(4)
H10	0.92730	0.67580	0.48500
H11	1.06190	0.70660	0.46820
H12	0.96740	0.58760	0.44910
C27	1.013(7)	0.705(7)	0.391(3)
H13	0.99580	0.76330	0.37070
H14	0.98980	0.62570	0.37560
H15	1.10530	0.71810	0.40290
C28	0.892(6)	0.845(5)	0.445(2)
H16	0.83800	0.84450	0.46720
H17	0.84680	0.87490	0.41960
H18	0.97420	0.89680	0.45510
O21	0.273(3)	-0.937(2)	-0.2084(10)
C29	0.255(4)	-0.833(3)	-0.2036(14)
O22	0.207(3)	-0.671(3)	-0.2926(11)
C30	0.217(3)	-0.675(3)	-0.2549(13)
C31	0.428(2)	-0.622(3)	-0.1960(8)
O23	0.541(2)	-0.603(2)	-0.1982(7)
O24	0.4723(19)	-0.313(2)	-0.1725(7)
C32	0.372(3)	-0.360(3)	-0.1682(10)
O25	0.078(2)	-0.2078(18)	-0.1572(8)
C33	0.125(4)	-0.297(3)	-0.1556(13)
O26	0.132(3)	-0.425(2)	-0.2598(8)
C34	0.150(3)	-0.442(3)	-0.2233(11)
O27	0.368(2)	-0.645(2)	-0.0103(6)
C35	0.348(3)	-0.624(2)	-0.045(1)
O28	0.6010(17)	-0.4279(17)	-0.0938(6)
C36	0.495(2)	-0.478(2)	-0.0976(9)

O29	0.5040(17)	-0.7767(15)	-0.1182(7)
C37	0.430(2)	-0.713(2)	-0.1154(8)
O30	0.297(2)	-0.949(2)	-0.1015(13)
C38	0.225(3)	-0.885(3)	-0.1130(12)
O31	-0.061(3)	-0.995(2)	-0.1884(8)
C39	0.011(3)	-0.909(3)	-0.1676(10)
O32	-0.019(3)	-0.848(2)	-0.0532(9)
C40	0.028(3)	-0.814(3)	-0.0812(12)
O33	-0.252(2)	-0.814(3)	-0.1911(9)
C41	-0.163(3)	-0.742(3)	-0.1908(11)
O34	-0.071(3)	-0.673(2)	-0.2876(7)
C42	-0.044(3)	-0.658(3)	-0.2520(12)
O35	-0.188(2)	-0.4268(18)	-0.1887(9)
C43	-0.126(3)	-0.498(3)	-0.1914(12)
O36	-0.211(2)	-0.674(3)	-0.0993(9)
C44	-0.110(3)	-0.633(3)	-0.1001(12)
O37	0.105(2)	-0.575(2)	-0.0029(7)
C45	0.094(2)	-0.556(3)	-0.0373(10)
O38	-0.0798(19)	-0.326(2)	-0.0915(10)
C46	-0.022(3)	-0.409(2)	-0.0935(11)
O39	0.350(2)	-0.369(2)	0.0253(8)
C47	0.321(3)	-0.360(2)	-0.0126(11)
C48	0.189(2)	-0.222(2)	-0.0607(10)
O40	0.141(2)	-0.138(2)	-0.0541(9)
C49	0.438(3)	-0.240(2)	-0.0720(9)
N2	0.532(2)	-0.166(2)	-0.0716(9)
C50	0.651(4)	-0.081(3)	-0.0696(14)
C51	0.760(3)	-0.126(4)	-0.0378(15)
H19	0.78510	-0.19760	-0.05150
H20	0.72710	-0.14360	-0.01170
H21	0.83610	-0.06490	-0.03080
C52	0.668(6)	-0.072(5)	-0.1118(19)
H22	0.59370	-0.04270	-0.12730
H23	0.67690	-0.14950	-0.12540
H24	0.74710	-0.01690	-0.11210
C53	0.622(3)	0.032(2)	-0.0446(13)
H25	0.55660	0.06700	-0.06230
H26	0.70200	0.08840	-0.03710
H27	0.59040	0.01170	-0.01850

Crystallographic Data for $Os_7(CO)_{20}(PMe_3)$ (4)

Empirical Formula	$C_{23}H_9O_{20}Os_7P$
Formula Weight (g mol^{-1})	1967.67
Crystal Description	Red Needle
Crystal System	Monoclinic
space group	C2/c
a (Å)	34.874(4)
b (Å)	12.2733(14)
c (Å)	16.1264(18)
α (°)	90
β (°)	103.652(2)
γ (°)	90
Volume ($Å^{-3}$), Z	6707.5(13), 8
D (calculated, Mg m^{-3})	3.897
Absorption Coefficient	26.541
Independent Reflections	24144
R1, Rw ($I \geq 2.0\sigma(I)$)	0.0445, 0.0900

Fractional Atomic Coordinates and Equivalent Isotropic Thermal Parameters (U_{eq} in $Å^2$) for $Os_7(CO)_{20}(PMe_3)$ (4)

Atom	X	Y	Z	U_{eq}
Os(1)	477(1)	2724(1)	480(1)	16(1)
Os(2)	1229(1)	3391(1)	1539(1)	16(1)
Os(3)	1073(1)	3680(1)	-266(1)	15(1)
Os(4)	885(1)	1410(1)	-535(1)	17(1)
Os(5)	1036(1)	1120(1)	1328(1)	17(1)
Os(6)	1621(1)	2062(1)	554(1)	15(1)
Os(7)	1830(1)	4323(1)	787(1)	17(1)
P(1)	1857(1)	6235(3)	821(2)	20(1)
C(1)	110(4)	3437(16)	-401(11)	46(5)
C(2)	100(4)	1604(12)	491(10)	32(4)

C(3)	268(5)	3567(15)	1258(11)	41(4)
C(4)	1077(4)	4864(10)	1649(8)	20(3)
C(5)	1704(4)	3441(12)	2443(9)	30(3)
C(6)	974(5)	3087(11)	2460(10)	30(3)
C(7)	1414(3)	4182(11)	-953(8)	22(3)
C(8)	843(4)	5080(12)	-160(9)	26(3)
C(9)	695(4)	3552(12)	-1323(8)	24(3)
C(10)	344(4)	1293(12)	-1158(8)	25(3)
C(11)	1095(5)	1582(12)	-1516(9)	32(3)
C(12)	931(4)	-132(12)	-665(8)	26(3)
C(13)	645(5)	953(13)	1974(9)	31(3)
C(14)	1452(4)	873(11)	2296(9)	24(3)
C(15)	960(4)	-384(12)	1080(9)	26(3)
C(16)	2096(4)	2056(11)	1444(8)	20(3)
C(17)	1888(4)	2190(11)	-354(10)	26(3)
C(18)	1675(4)	512(11)	524(9)	26(3)
C(19)	2266(4)	4390(11)	1697(9)	26(3)
C(20)	2180(4)	4425(11)	74(9)	23(3)
C(21)	1733(5)	6970(13)	1708(10)	42(4)
C(22)	2352(4)	6730(12)	873(11)	39(4)
C(23)	1593(6)	6927(13)	-139(10)	46(4)
O(1)	-118(4)	3852(14)	-911(9)	82(6)
O(2)	-130(3)	941(10)	461(8)	49(3)
O(3)	123(4)	4048(13)	1697(8)	69(4)
O(4)	963(3)	5724(8)	1753(7)	33(2)
O(5)	1952(3)	3404(10)	3036(6)	41(3)
O(6)	845(4)	3008(9)	3030(7)	46(3)
O(7)	1561(3)	4477(9)	-1488(6)	30(2)
O(8)	685(3)	5876(9)	-168(7)	42(3)
O(9)	480(3)	3586(10)	-2000(7)	43(3)
O(10)	33(3)	1217(10)	-1542(7)	45(3)
O(11)	1209(4)	1666(10)	-2116(7)	49(3)
O(12)	969(3)	-1026(9)	-797(7)	39(3)
O(13)	434(3)	829(10)	2387(7)	41(3)
O(14)	1695(3)	727(10)	2915(8)	48(3)
O(15)	910(4)	-1303(9)	958(8)	46(3)
O(16)	2383(3)	1917(9)	1962(6)	30(2)
O(17)	2055(3)	2172(9)	-889(7)	38(3)
O(18)	1762(3)	-396(8)	513(8)	42(3)
O(19)	2547(3)	4416(9)	2277(8)	48(3)
O(20)	2398(3)	4469(9)	-353(7)	37(3)

Crystallographic Data for $Os_7(CO)_{20}[P(OCH_2)_3CMe]$ (7)

Empirical Formula	$C_{31}H_{15}O_{23}Os_7P$
Formula Weight (g mol^{-1})	2117.80
Crystal Description	Red Plates
Crystal System	Orthorhombic
Space Group	Pca2(1)
a (Å)	19.0253(4)
b (Å)	12.1174(4)
c (Å)	17.9746(5)
α (°)	90
β (°)	90
γ (°)	90
Volume ($Å^{-3}$), Z	4143.8(2), 4
D (calculated, Mg m^{-3})	3.395
Absorption Coefficient	21.449
Independent Reflections	43107
R1, Rw ($I \geq 2.0\sigma(I)$)	0.0707, 0.1891

Fractional Atomic Coordinates and Equivalent Isotropic Thermal Parameters (U_{eq} in $Å^2$) for $Os_7(CO)_{20}[P(OCH_2)_3CMe]$ (7)

Atom	X	Y	Z	U_{eq}
Os(1)	8828(1)	3218(1)	259(1)	31(1)
Os(2)	8253(1)	1198(1)	-283(1)	28(1)
Os(3)	9125(1)	1146(1)	988(1)	27(1)
Os(4)	8577(1)	-883(1)	380(1)	30(1)
Os(5)	9704(1)	1664(1)	-429 (1)	28(1)
Os(6)	10066(1)	-356(1)	271(1)	30(1)
Os(7)	9162(1)	-323(1)	-1042(1)	31(1)
P(1)	7956(4)	3995(7)	932(5)	33(2)
O(1)	7198(12)	3480(20)	823(13)	48(5)
O(2)	7867(12)	5290(20)	786(15)	52(5)

O(3)	8080(12)	3930(20)	1800(13)	48(5)
C(1)	6623(17)	4100(30)	1270(20)	48(7)
C(2)	7328(18)	5830(30)	1240(20)	48(6)
C(3)	7495(18)	4400(30)	2230(20)	52(7)
C(4)	6950(16)	4980(30)	1758(17)	37(5)
C(5)	6405(16)	5460(30)	2230(20)	43(8)
C(11)	8703(16)	4240(30)	-415(18)	35(5)
O(11)	8592(13)	4990(20)	-890(14)	53(6)
C(12)	9439(16)	4210(30)	740(20)	37(6)
O(12)	9806(13)	4850(20)	1060(17)	58(7)
C(21)	7430(15)	1170(20)	415(16)	27(4)
O(21)	7022(12)	1102(17)	798(14)	42(6)
C(22)	7935(15)	2410(30)	-788(17)	35(5)
O(22)	7615(13)	3090(20)	-1177(16)	56(7)
C(23)	7663(16)	380(30)	-1007(18)	35(5)
O(23)	7339(10)	30(19)	-1449(13)	40(9)
C(31)	9739(17)	2090(30)	1480(17)	33(5)
O(31)	10066(17)	2730(20)	1806(15)	64(8)
C(32)	8356(17)	1420(30)	1660(17)	34(5)
O(32)	7921(13)	1590(20)	2098(13)	51(6)
C(33)	9428(16)	160(20)	1683(16)	26(4)
O(33)	9593(12)	-470(20)	2211(13)	43(6)
C(41)	7655(17)	-1240(30)	21(19)	41(6)
O(41)	7136(12)	-1640(20)	-158(15)	50(6)
C(42)	8200(20)	-970(30)	1315(19)	46(7)
O(42)	7918(15)	-1130(30)	1931(13)	65(8)
C(43)	8921(16)	-2370(30)	300(20)	42(6)
O(43)	9089(12)	-3200(20)	263(17)	54(7)
C(51)	10369(15)	2610(30)	23(18)	34(5)
O(51)	10809(10)	3206(19)	256(15)	45(6)
C(52)	10464(15)	1170(30)	-1026(19)	34(5)
O(52)	10965(11)	910(20)	-1338(12)	48(6)
C(53)	9440(16)	2590(30)	-1251(18)	33(4)
O(53)	9303(14)	3040(20)	-1776(16)	65(8)
C(61)	10767(15)	530(30)	800(20)	42(6)
O(61)	11160(12)	950(20)	1151(13)	46(6)
C(62)	10723(17)	-960(30)	-230(20)	47(6)
O(62)	11239(13)	-1460(30)	-640(16)	61(7)
C(63)	10163(18)	-1540(30)	899(18)	38(5)
O(63)	10245(11)	-2350(18)	1313(14)	42(5)
C(71)	8609(17)	-1630(30)	-1275(18)	39(6)
O(71)	8319(15)	-2355(19)	-1437(17)	60(7)
C(72)	8955(16)	530(30)	-1909(17)	36(5)
O(72)	8814(13)	890(30)	-2492(13)	49(6)
C(73)	9911(15)	-1120(30)	1498(19)	41(6)
O(73)	10288(15)	-1630(30)	-1846(15)	72(9)

C(81)	8915(18)	6420(40)	2880(20)	122(14)
C(82)	8333(18)	6720(30)	3290(20)	113(14)
C(83)	8109(16)	6060(40)	3889(20)	125(15)
C(84)	8470(20)	5090(40)	4040(20)	121(14)
C(85)	9050(20)	4780(30)	3630(30)	136(16)
C(86)	9273(14)	5450(40)	3040(20)	127(15)

REFERENCES

1. Cotton, F.A.; Wilkinson, G.; Murillo, C.A.; Bochmann, M., *Advanced Inorganic Chemistry*. 6th ed; Wiley: New York, 1999.

2. Gonzalez–Moraga, G., *Cluster Chemistry*. 1st ed; Springer–Verlag: Germany, 1993.

3. Dyson, P.J.; McIndoe, *Transition Metal Carbonyl Cluster Chemistry*; Gordon and Science Publishers: Singapore, 2000.

4. Shriver, D.F.; Atkins, P., *Inorganic Chemistry*. 3rd ed; W. H. Freeman and Company: New York, 1999.

5. Vargas, M.D.; Nicholls, J.N., *Advances in Inorganic Chemistry and Radiochemistry*, Emeleus, H.J.;Sharpe, A.G.; Academic Press: New York, 1986.

6. Wong, J.S.-Y.; Lin, Z.-Y.; Wong, W.-T. *Organometallics*, **2003**, *22*, 4798.

7. *Comprehensive Organometallic Chemistry II*, Wilkinson, G.; Stone, F.G.A.;Abel, E.W.; Pergamon: New York, 1995.

8. *The Chemistry of Metal Cluster Complexes* Shriver, D.F.; Kaesz, H.D.;Adams, R.D.; VCH: New York, 1990.

9. Sanchez-Cabrera, G.; Zuno-Cruz, F.J.; Rosales-Hoz, M.J.; Bakhmutov, V.I. *J. Organomet. Chem.*, **2002**, *660*, 153.

10. Eady, C.R.; Johnson, B.F.G.; Lewis, J. *J. Chem. Soc., Dalton Trans.*, **1975**, 2606.

11. Nicholls, J.N.; Vargas, M.D., *Inorganic Syntheses*, Kaesz, H.D.; Wiley-Interscience: New York, 1989.

12. Jackson, P.F.; Johnson, B.F.G.; Lewis, J. *J. Chem. Soc., Chem. Commun.*, **1980**, 224.

13. Ditzel, E.J.; Johnson, B.F.G.; Lewis, J.; Raithby, P.R.; Taylor, M.J. *J. Chem. Soc., Dalton Trans.*, **1985**, 555.

14. Deeming, A.J., *Advances in Organometallic Chemistry*, Stone, F.G.A.;West, R.; Academic: New York, 1986.

15. Johnston, V.J.; Einstein, F.W.B.; Pomeroy, R.K. *J. Am. Chem. Soc.*, **1987**, *109*, 7220.

16. Johnston, R.D.; Einstein, F.W.B.; Pomeroy, R.K. *J. Am. Chem. Soc.*, **1987**, *109*, 8111.

17. Johnston, V.J.; Einstein, F.W.B.; Pomeroy, R.K. *Organometallics*, **1988**, *7*, 1867.

18. Wang, W.; Einstein, F.W.B.; Pomeroy, R.K. *J. Chem. Soc., Chem. Commun.*, **1992**, 1737.

19. Mingos, D.M.P.; Wales, D.J., *Introduction to Cluster Chemistry*; Prentice-Hall: Englewood Cliffs: New Jersey, 1990.

20. Martin, L.R.; Einstein, F.W.B.; Pomeroy, R.K. *Organometallics*, **1988**, *7*, 294.

21. (a) *Metal Clusters in Chemistry*, Braustein, P.; Oro, L.;Raithby, P.R.; Wiley-VCH: Weinheim, Germany,1999; (b) Elschenbroicg, C.; Salzer, A., *Organometallics: A Concise Introduction*; VCH: New York,1989; (c) Cotton, F.A.; Wilkinson, G., *Advanced Inorganic Chemistry*. 5th ed; Wiley: New York,1988; (d) *Metal Clusters*, Moskovits, M.; Wiley: New York,1986.

22. *Transition Metal Clusters*, Johnson, B.F.G.; Wiley: New York, 1980.

23. Canal, J.P.; Yap, G.P.A.; Pomeroy, R.K. *Organometallics*, **2003**, *22*, 3439.

24. Higgins, J. *Chemical and Engineering News*, **1987**, 31.

25. Blake, A.J.; Johnson, B.F.G.; Nairn, J.G.M. *Acta. Cryst., Sect. C*, **1994**, *50*, 1052.

26. Elschenbroich, C.; Salzer, A., *Organometallics: A Concise Introduction*. 2nd ed; VCH: New York, 1992.

27. *The Chemistry of Metal Cluster Complexes*, Shiver, D.; Kaesz, H.D.;Adams, R.D.; VCH: New York, 1990.

28. Housecroft, C.E.; Sharpe, A.G., *Inorganic Chemistry*; Prentice-Hall: Englewoof Cliffs: New Jersey ,2001.

29. Nicholls, J.N.; Farrar, D.H.; Jackson, P.F.; Johnson, B.F.G.; Lewis, J. *J. Chem. Soc., Dalton Trans.*, **1982**, 1395.

30. Eady, C.R.; Johnson, B.F.G.; Lewis, J.; Mason, R.; Hitchcock, P.B.; Thomas, K.M. *J. Chem. Soc., Chem. Commun.*, **1977**, 385.

31. Johnson, B.F.G.; Lewis, J.; Luniss, J.; Braga, D.; Grepioni, F. *J. Organomet. Chem.*, **1991**, *401*, C46.

32. Luh, T.-Y. *Coordination Chemisry Reviews*, **1984**, *60*, 255.

33. Bruce, M.I.; Liddell, M.J.; Hughes, C.A.; Skelton, B.W.; White, A.H. *J. Organomet. Chem.*, **1988**, *347*, 157.

34. Biradha, K.; Hansen, V.M.; Leong, W.K.; Pomeroy, R.K.; Zaworotko, M.J. *J. Cluster Sci.*, **2000**, *11*, 285.

35. Johnson, B.F.G.; Lewis, J.; Pearsall, M.-A.; Scott, L.G. *J. Organomet. Chem.*, **1991**, *413*, 337.

36. Davis, H.B.; Einstein, F.W.B.; Glavina, P.G.; Jones, T.; Pomeroy, R.K.; Rushman, P. *Organometallics*, **1989**, *8*, 1030.

37. Einstein, F.W.B.; Johnston, R.D.; Ma, A.K.; Pomeroy, R.K. *Organometallics*, **1990**, *9*, 52.

38. Wilcox, C.T.; Jennings, M.C.; Pomeroy, R.K. *J. Cluster Sci.*, **2004**, *15*, 107.

39. Johnson, B.F.G.; Bott, A.W.; Hugh-Jones, D.; Rodger, A. *Polyhedron*, **1990**, *9*, 1769.

40. Cotton, F.A.; Wilkinson, G.; Gaus, P.L., *Basic Inorganic Chemistry*. 3rd ed; John Wiley & Sons: New York, 1995.

41. Orpen, A.G.; Sheldrick, G.M. *Acta. Cryst.*, **1978**, *B34*, 1989.

42. Rushman, P.; van Buuren, G.N.; Shiralian, M.; Pomeroy, R.K. *Organometallics*, **1983**, *2*, 693.

43. Drake, S.R.; Loveday, P.A., *Inorganic Syntheses*, Angelici, R.J.; Wiley: New York, 1990.

44. Hayward, C.T.; Shapley, J.R. *Inorg. Chem.*, **1982**, *21*, 3816.

45. Corrigan, J.F.; Doherty, S.; Taylor, M.J.; Carty, A.J. *J. Am. Chem. Soc.*, **1994**, *116*, 9799.

46. Eady, C.R.; Johnson, B.F.G.; Lewis, J. *J. Organomet. Chem.*, **1972**, *37*, C39.

47. Johnson, B.F.G.; Johnston, R.D.; Lewis, J. *J. Chem. Soc. (A)*, **1968**, 2865.

48. Canal, J.P., Ph.D. Thesis, Simon Fraser University, 2004.

49. Jiang, F., Ph.D. Thesis, Simon Fraser University, 1999.

50. Martin, L.R.; Einstein, F.W.B.; Pomeroy, R.K. *Inorg. Chem.*, **1985**, *24*, 2777.

51. L'Eplattenier, F.; Calderazzo, F. *Inorg. Chem.*, **1968**, *7*, 1290.

52. Shipley, J.A.; Batchelor, R.J.; Einstein, F.W.B.; Pomeroy, R.K. *Organometallics*, **1991**, *10*, 3620.

53. Darensbourg, D.J.; Nelson, H.H.; Hyde, C.L. *Inorg. Chem.*, **1974**, *13*, 2135.

54. (a) Albers, M.O.; Coville, N.J.; Singleton, E. *J. Chem. Soc., Dalton Trans.*, **1982**, 1069; (b) Cotton, F.A.; Parish, R.V. *J. Chem. Soc.*, **1960**, 1440; (c) Reckziegel, A.; Bigorgne, M. *J. Organomet. Chem.*, **1965**, *3*, 341.

55. Cobbledick, R.E.; Einstein, F.W.B.; Pomeroy, R.K.; Spetch, E.R. *J. Organomet. Chem.*, **1980**, *195*, 77.

56. (a) Tachikawa, M.; Shapley, J.R. *Organomet. Chem.*, **1977**, *124*, C19; (b) Johnson, B.F.G.; Khattar, R.; Lewis, J.; McPartlin, M.; Morris, J.; Powell, G.L. *J. Chem. Soc., Chem. Commun.*, **1986**, 507; (c) Johnson, B.F.G.; Lewis, J.; McPartlin, M.; Morris, J.; Powell, G.L.; Raithby, P.R.; Vargas, M.D. *J. Chem. Soc., Chem. Commun.*, **1986**, 429; (d) Johnson, B.F.G.; Lewis, J.; Pippard, D.A. *J. Chem. Soc., Dalton Trans.*, **1981**, 407; (e) Churchill, M.R.; Hollander, F.J.; Shapley, J.R.; Foose, D.S. *J. Chem. Soc., Chem. Commun.*, **1978**, 534; (f) Couture, C.; Farrar, D.H. *J. Chem. Soc., Dalton Trans.*, **1986**, 1395; (g) Freeman, M.J.; Miles, A.D.; Murray, M.; Orpen, A.G.; Stone, F.G.A. *Polyhedron*, **1984**, *3*, 1093.

57. (a) Vargas, M.D.; Nicholls, J.N. *Adv. Inorg. Chem. Radiochem.*, **1986**, *30*, 123; (b) Bott, A.W.; Jeffery, J.G.; Johnson, B.F.G.; Lewis, J. *J. Organomet. Chem.*, **1990**, *394*, 533; (c) Cox, D.J.; John, G.R.; Johnson, B.F.G.; Lewis, J. *J. Organomet. Chem.*, **1980**, *186*, C69.

58. Johnson, B.F.G.; Lewis, J.; Pearsall, M.A.; Scott, L.G. *J. Organomet. Chem.* , **1991**, *402*, C27.

59. Tolman, C.A. *Chem. Rev.*, **1977**, *77*, 313.

60. Deeming, A.J.; Smith, M.B. *J. Chem. Soc., Chem. Commun.*, **1993**, 844.

61. Yamamoto, Y.; Aoki, K.; Yamazaki, H. *Inorg. Chem.*, **1979**, *18*, 1681.

62. Churchill, M.R.; DeBoer, B.G. *Inorg. Chem.*, **1977**, *16*, 878.

63. (a) Orpen, A.G.; Sheldrick, G.M. *Acta Cryst.*, **1978**, *B* 1989; (b) Eady, C.R.; Gavens, P.D.; Johnson, B.F.G.; Lewis, J.; Malatesta, M.C.; Mays, M.J.; Orpen, A.G.; Rivera, A.V.; Sheldrick, G.M.; Hursthouse, M.B. *J. Organomet. Chem.*, **1975**, *149*, C43.

64. Wang, W.; Einstein, F.W.B.; Pomeroy, R.K. *Organometallics*, **1994**, *13*, 1114.

65. Wang, W.; Batchelor, R.J.; Lu, C.-Y.; Einstein, F.W.B.; Pomeroy, R.K. *Organometallics*, **1993**, *12*, 3598.

66. Einstein, F.W.B.; Johnston, V.J.; Pomeroy, R.K. *Organometallics*, **1990**, *9*, 2754.

67. Jiang, F.; Jenkins, H.A.; Biradha, K.; Davis, H.B.; Pomeroy, R.K.; Zaworotko, M.J. *Organometallics*, **2000**, *19*, 5049.

68. (a) Plastas, H.J.; Stewart, J.M.; Grim, S.O. *Inorg. Chem.*, **1973**, *12*, 265; (b) Wovkulich, M.J.; Atwood, J.L.; Canada, L.; Atwood, J.D. *Organometallics*, **1985**, *4*, 867; (c) Cotton, F.A.; Darensbourg, D.J.; Kolthammer, W.S. *Inorg. Chem.*, **1981**, *20*, 4440.

69. de Lange, P.P.; Fruhauf, H.-W.; Kraakman, M.J.; Van Wijnkoop, M.; Kranenburg, M.; Groot, A.H.; Vrieze, K.; Fraanje, J.; Wang, Y.; Numan, M. *Organometallics*, **1993**, *12*, 417.

70. Appleton, T.G.; Clark, H.C.; Manzer, L.E. *Coord. Chem. Rev.*, **1973**, *10*, 335.

71. Baslol, F.; Pearsall, R.G., *Mechanisms of Inorganic Reactions*. 2nd ed; Wiley: New York, 1967.

72. Hansen, V.M.; Ma, A.K.; Biradha, K.; Pomeroy, R.K.; Zaworotko, M.J. *Organometallics*, **1998**, *17*, 5267.

73. Craig, J.C.; Purushothaman, K.K. *J. Org. Chem.*, **1970**, *35*, 1721.

74. Alex, R.F.; Pomeroy, R.K. *Organometallics*, **1987**, *6*, 2437.

75. Ditzel, E.J.; Holden, H.D.; Johnson, B.F.G.; Lewis, J.; Saunders, A.; Taylor, M.J. *J. Chem. Soc., Chem. Commun.* , **1982**, 1373.

76. Heitsch, C.W.; Verkade, J.G. *Inorg. Chem.*, **1962**, *1*, 392.

77. Johnson, B.F.G.; Kamarudin, R.A.; Lahoz, F.J.; Lewis, J.; Raithby, P.R. *J. Chem. Soc., Dalton Trans.*, **1988**, 1205.

78. Urbanic, M.A.; Shapley, J.R., *Inorganic Synthesis*, Angelici, R.J.; Wiley: New York, 1990.

79. Byers, B.H.; Brown, T.L. *J. Am. Chem. Soc*, **1977**, *99*, 2527.

80. (a) Fischer, E.O.; Brenner, K.S.Z. *Naturforsch., Teil B*, **1962**, *17*, 774; (b) Garder, S.A.; Andrews, P.S.; Rausch, M.R. *Inorg. Chem.*, **1973**, *12*, 2396.

81. Davis, H.B., Ph.D. Thesis, Simon Fraser University, 1991.

82. L'Eplattenier, F.; Calderazzo, F. *Inorg. Chem.*, **1967**, *6*, 2092.

83. (a) Kubas, G.J.; Larson, A.C.; Ryan, R.R. *J. Org. Chem.*, **1979**, *44*, 3867; (b) Hartmuth, C.K.; Anderson, P.G.; Sharpless, K.B. *J. Am. Chem. Soc*, **1994**, *116*, 1278.

84. (a) Mann, B.E., *Comprehensive Organometallic Chemistry*, Wilkinson, G.; Stone, F.G.A.;Abel, E.W.; Wiley: New York, 1982; (b) Mann, B.E.; Taylor, B.F., *^{13}C NMR Data for Organometallic Compounds*; Academic New York, 1981.

85. Johnson, B.F.G.; Benfield, R.E., *Transition Metal Clusters*, Johnson, B.F.G.; Wiley: Chichester, England, 1980.

86. (a) Band, E.; Muetterties, E.L. *Chem. Rev.*, **1978**, *78*, 639; (b) Geoffroy, G.L. *Acc. Chem. Res.*, **1980**, *13*, 469.

87. (a) Haruta, M. *J. New Mat. Electrochem. Systems*, **2004**, *7*, 163; (b) Hutchings, G.J.; Carrettin, S.; Landon, P.; Edwards, J.K.; Enache, D.; Knight, D.K.; Xu, Y.-I.; Carley, A.F. *Topics in Catalysis*, **2006**, *38*, 223; (c) Pattrick, G.; vander Lingen, E.; Corti, C.W.; Holliday, R.J.; Thompson, D.T. *Topics in Catalysis*, **2004**, *30/31*, 273.

88. Mann, B.E. *J. Chem. Soc., Dalton Trans.*, **1997**, 1457.

89. Aime, S.; Gambino, O.; Milone, L. *Inorg. Chem. Acta*, **1975**, *15*, 53.

90. (a) Johnson, B.F.G.; Roberts, Y.V. *Polyhedron*, **1993**, *12*, 977; (b) Farrugia, L.J.; Senior, A.M.; Braga, D.; Grepioni, F.; Orpen, A.G.; Crossley, J.G. *J. Chem. Soc., Dalton Trans.*, **1996**, 631; (c) Johnson, B.F.G.; Roberts, Y.V.; Parisini, E. *J. Chem. Soc., Dalton Trans.*, **1992**, 2573; (d) Johnson, B.F.G. *J. Chem. Soc., Dalton Trans.*, **1997**, 1473; (e) Johnson, B.F.G.; Tay, S. *Inorg. Chim. Acta*, **2002**, *332*, 201; (f) Forster, A.; Johnson, B.F.G.; Lewis, J.; Matheson, T.W.; Robinson, B.H.; Jackson, G. *J. Chem. Soc., Chem. Commun.*, **1974**, 1042.

91. Li, J.; Jug, K. *Inorg. Chim. Acta*, **1992**, *196*, 89.

92. Eady, C.R.; Jackson, W.G.; Johnson, B.F.G.; Lewis, J.; Matheson, T.W. *J. Chem. Soc., Chem. Commun.*, **1975**, 958.

93. Bodner, G.M.; May, M.P.; McKiney, L.E. *Inorg. Chem.*, **1980**, *19*, 1951.

94. Sandstrom, J., *Dynamic NMR Spectrscopy*; Academic Press: Toronto, 1982.